Technical Report
for
NASA Grant NAG 1-1087

Fourier Functional Analysis for Unsteady Aerodynamic Modeling

KU-FRL-872-2

By

Suei Chin and C. Edward Lan

Flight Research Laboratory
The University of Kansas Center for Research, Inc.
Lawrence, Kansas 66045-2969

February 1991

Abstract

In the current study, a method based on Fourier analysis is developed to analyze the force and moment data obtained in large amplitude forced oscillation tests at high angles of attack. The aerodynamic models for normal force, lift, drag and pitching moment coefficients are built up from a set of aerodynamic responses to harmonic motions at different frequencies. Based on the aerodynamic models of harmonic data, the indicial responses are formed. The final expressions for the models involve time integrals of the indicial type advocated by Tobak and Schiff. Results from linear two- and three- dimensional unsteady aerodynamic theories as well as test data for a 70-deg delta wing are used to verify the models. It is shown that the present modeling method is accurate in producing the aerodynamic responses to harmonic motions and the ramp type motions. The model also produces correct trend for a 70-deg delta wing in harmonic motion with different mean angles-of-attack. However, the current model cannot be used to extrapolate data to higher angles-of-attack than that of the harmonic motions which form the aerodynamic model. For linear ramp motions, a special method is used to calculat the corresponding frequency and phase angle at a given time. The calculated results from modeling show higher lift peak for linear ramp motion than for

harmonic ramp motion. The current model also shows resonably good results for the lift responses at different mean angles of attack.

Contents

Nomenclature

A_j	coefficient of cosine Fourier series
B_j	coefficient of sine Fourier series
C_{ave}	the average value of the constant terms in the harmonic oscillation responses
C_j	reference values
c_ℓ	2-D lift coefficient
C_D	3-D drag coefficient
C_L	3-D lift coefficient
C_{L_α}	variation of lift coefficient with respect to angle of attack
C_{L_q}	variation of lift coefficient with respect to pitch rate
C_m	3-D pitching moment coefficient
C_N	3-D normal force coefficient
d	a constant
E_{ij}	constants associated with the virtual mass effect
H_{ij}	constants in amplitude function to be determined
i	imaginary part of a complex number
j	index
k	reduced frequency ($=\omega\ell/v_\infty$)
M	Mach number

n	index for reduced frequency, also index for the coefficient in Padé approximants
N	the number of frequency
PD_j	Padé approximants
P_{ij}	coefficients for Padé approximants
t	time
t'	nondimensional time ($=tv_\infty/\ell$)
UQVLM	unsteady quasi-vortex lattice method program
v_∞	free stream velocity
Greek:	
α	angle of attack ($=\alpha_0$ coskt')
α_1	defined as $\alpha_m+\alpha$
α_0	amplitude of angle of attack
α_m	mean angle of attack
$\dot{\alpha}$	time rate of change in angle of attack
α	time rate of change in $\dot{\alpha}$
ℓ	reference length
τ	dummy time integration variable
ξ	running variable in time
θ	defined as θ=kt'
ϕ	phase angle

Chapter 1

Introduction

Due to the requirement of increased performance and maneuverability, the flight envelope of a modern fighter is frequently extended to the high angle-of-attack regime. Vehicles maneuvering in this regime are subjected to nonlinear aerodynamic loads. The nonlinearities are due mainly to three-dimensional separated flow and concentrated vortex flow that occur at large angles of attack. Accurate prediction of these nonlinear airloads is of great importance in the analysis of a vehicle's flight motion and in the design of its flight control system. As Tobak and Schiff mentioned in ref. 1, the main difficulty in determining the relationship between the instantaneous aerodynamic load on a maneuvering vehicle and the motion variables is that this relationship is determined not only by the instantaneous values of motion variables but also by all of the prior states of the motion up to the current state. Due to advanced computer techniques, one straightforward way is to solve the flow-field problem and the dynamic equation together. For example, a CFD method can be used to solve the Navier-Stokes equations governing the separated flow field. Then the calculated forces and moments are used in the dynamic equations governing the vehicle's motion to calculate motion variables. The motion

variables will change the vehicle's attitude, and thus the forces and moments. Results of repeatedly calculating these coupled equations would be the complete time histories of the aerodynamic response and of the vehicle's motion. Although solving these coupled equations is the exact way to account for the time-history effects in predicting the aerodynamic response to arbitrary maneuvers, this is obviously a very costly approach. In particular, at high angles of attack, the aerodynamic loads depend nonlinearly on the motion variables. Under such conditions, even if the vehicles start from closely similar initial conditions, they can experience widely varying motion histories. Thus, a satisfactory evaluation of the performance envelope of the aircraft may require a large number of coupled computations, one for each change in initial conditions. Further, since the motion and the aerodynamic response are linked together in this approach, there can be no reutilization of the previously obtained aerodynamic reactions.

To avoid the disadvantage of solving the coupled flow- field equations and aircraft's motion equations, an alternate approach is to use a mathematical modeling to describe the steady and unsteady aerodynamics for the aircraft's equations of motion. Ideally, with a mathematical model, an evaluation of the aerodynamic terms specified by the model would be required only once. The specified model can be reutilized to solve the

aircraft's equations of motion over a range of motion variables and flight conditions.

In the classical linear potential flow theory (refs. 2 and 3), researchers in the field of aeroelasticity used the Fourier transform to relate the aerodynamic response of step change in angle of attack of a wing to that of harmonic oscillatory motions. The transient aerodynamic reaction to a step change is termed the "indicial function" and has been calculated for several classes of isolated wings (refs. 2-5). By a suitable superposition (ref. 6) of these results, the aerodynamic forces and moments induced in any maneuvers can be studied (refs. 2 and 3). Tobak has applied the indicial function concept to analyze the motions of wings and wing-tail combinations (ref. 7). Later, based on a consideration of function, Tobak and his colleagues (refs. 1 and 8) have extended the concept of indicial function into the nonlinear aerodynamic regimes. The simplest nonlinear aerodynamic model proposed in ref.1 has been applied by several authors (refs. 9-13) to perform the analysis. However, that simplest model is accurate only to the first order of frequency. It needs to be improved for a more general response.

Aerodynamic forces and moments acting on a rapidly maneuvering aircraft are, in general, nonlinear functions of motion variables, their time rate of change, and the history of maneuvering. How these unsteady aerodynamic forces and moments may be represented becomes uncertain,

in particular at high angles of attack. If the response is measured by wind-tunnel dynamic testing, questions arise as to how the measured time-history data can be analyzed and expressed in a form suitable for flight dynamic simulation. For a certain type of nonlinearities produced in a test with small-amplitude oscillation, the analysis has been accomplished by separating the time-history data into in-phase and out-phase components (ref. 14). When large-amplitude forced oscillations are employed in the wind-tunnel testing at a large mean angle of attack, the aerodynamic phenomena may involve dynamic stall and/or strong vortex flow, with or without vortex breakdown. In this case, higher harmonic components in the aerodynamic response are expected to exist (ref. 15) and the phenomenon of aerodynamic lag may be important. Therefore, a more general modeling technique is needed.

In this research, a numerical method will be developed to analyze the nonlinear and time-dependent aerodynamic response to establish the generalized indicial function in terms of motion variables and their time rates of change.

Chapter 2

Mathematical Development

2.1 Aerodynamic Modeling

2.1.1 Historical Review

For the conventional airplanes, linear relationships are used to represent the aerodynamic responses to motion variables (ref. 16). For example, the total lift for an airplane in symmetric steady flight can be written as

$$C_L = C_{L_0} + C_{L_\alpha}\,\alpha_{wb} \tag{1}$$

where α_{wb} is the angle of attack measured with respect to wing-body mean aerodynamic chord and C_{L_0} is the lift when $\alpha_{wb}=0$. C_{L_α} is the lift-curve slope of the whole configuration and α is the angle of attack of the zero lift line of the airplane as shown in figure 1. This relationship is good only for airplanes flying below stalled α. When airplanes fly at high angles of attack, as most modern fighters do, the relationships between the aerodynamic responses and motion variables become nonlinear and are much more difficult to describe. To deal with the aerodynamic responses for helicopters during dynamic stall, Wayne (ref. 17) developed an empirical

model to predict the dynamic stall lift. In flight simulation, two common ways are used to treat high-angle-of attack aerodynamics. One is using the tabulated data (ref. 18) and the other is to use a local linearized model which form a piecewise continuous fit of the nonlinear response (ref. 19).

Based on the functional analysis, Tobak and Schiff (ref. 1) is able to develop a fundamental formulation of aerodynamic response for arbitrary motion. Their methodology is briefly reviewed in the following. By assuming that small step changes of α and $q\ell/v_\infty$ at time τ, the incremental response ΔC_L at time t is written as

$$\begin{aligned} \lim_{\Delta\alpha \to 0} \frac{\Delta C_L(t,\tau)}{\Delta\alpha} &= C_{L_\alpha}[\alpha(\xi),\ q(\xi);\ t,\ \tau] \\ \lim_{\Delta(q\ell/v_\infty) \to 0} \frac{\Delta C_L(t,\tau)}{\Delta(q\ell/v_\infty)} &= C_{L_q}[\alpha(\xi),\ q(\xi);\ t,\ \tau] \end{aligned} \tag{2}$$

where ξ is a running variable in time over the interval zero to τ(see fig. 2), ℓ is a reference length and v_∞ is the free stream velocity. The incremental response ΔC_L due to a step change is called the indicial response. If the variation of variables α and q over the range 0 to t is replaced by the summation of many step changes as shown in figure 3, the summation of incremental responses yields an integral form for C_L at time t as

$$C_L(t) = C_L(0) + \int_0^t C_{L_\alpha}[\alpha(\xi),\, q(\xi);\, t,\, \tau]\, \frac{d\alpha}{d\tau}\, d\tau + \frac{\ell}{V_\infty} \int_0^t C_{L_q}[\alpha(\xi),\, q(\xi);\, t,\, \tau]\, \frac{dq}{d\tau}\, d\tau \tag{3}$$

To have practical applications, this functional integral form needs to be simplified. By assuming that α and q are analytical functions in a neighborhood of $\xi=\tau$, variables α and q can be expanded by their Taylor series at $\xi=\tau$. The indicial responses C_{L_α}, for example can be expressed as

$$C_{L_\alpha}[\alpha(\xi),\, q(\xi);\, t,\, \tau] = C_{L_\alpha}[t,\, \tau;\, \alpha(\tau),\, \dot{\alpha}(\tau), \cdots\cdots, q(\tau),\, \dot{q}(\tau), \cdots\cdots] \tag{4}$$

By further assuming that only the first two coefficients are needed in Taylor expansion of indicial responses, the integral form of eq. (3) becomes

$$C_L(t) = C_L(0) + \int_0^t C_{L_\alpha}[t,\tau;\alpha(\tau),\dot{\alpha}(\tau),q(\tau),\dot{q}(\tau)]\frac{d\alpha}{d\tau}d\tau + \frac{\ell}{V_\infty}\int_0^t C_{L_q}[t,\tau;\alpha(\tau),\dot{\alpha}(\tau),q(\tau),\dot{q}(\tau)]\frac{dq}{d\tau}d\tau \tag{5}$$

Eq. (5) is applicable to the study of rapidly varying maneuvers, where hysteresis phenomena are known to exist. However, it is difficult to implement eq. (5). By introducing the assumption of no hysteresis effect

and a slowly varying motion, Tobak and Schiff neglected the dependence of the indicial response on $\dot{\alpha}$ and $\dot{q}$. By further assuming that the indicial response is a function of elapsed time $t-\tau$ instead of t and τ separately, a much simplified expression of eq. (3) can be written as

$$C_L(t)=C_L(0)+\int_0^t C_{L_\alpha}[t-\tau;\alpha(\tau),q(\tau)]\frac{d\alpha(\tau)}{d\tau}d\tau + \frac{\ell}{v_\infty}\int_0^t C_{L_q}[t-\tau;\alpha(\tau),q(\tau)]\frac{dq(\tau)}{d\tau}d\tau \qquad (6)$$

Although the form of eq. (6) represents a great simplification over that of eq. (3), the equation still includes the full linear form as a special case.

Jenkins (ref. 20) applied a local Taylor expansion to indicial response C_{L_α} and used that Taylor expansion form to fit numerical indicial responses calculated from a program called NLWAKE. By substituting C_{L_α} into eq. (6), Jenkins was able to predict the oscillating motion for airfoil at low frequencies.

2.1.2 Current Development

In the current research, the hysteresis effect is included and the assumption of low frequencies will be removed. Therefore, a form between eq. (5) and eq. (6) is written as

$$C_L(t)=C_L(0)+\int_0^t C_{L_\alpha}[t-\tau;\ \alpha(\tau),\ \dot{\alpha}(\tau),\ q(\tau),\ \dot{q}(\tau)]\ \frac{d\alpha(\tau)}{d\tau}d\tau + \frac{\ell}{V_\infty}\int_0^t C_{L_q}[t-\tau;\ \alpha(\tau),\ \dot{\alpha}(\tau),\ q(\tau),\ \dot{q}(\tau)]\ \frac{dq(\tau)}{d\tau}d\tau \tag{7}$$

In wind-tunnel testing, q is the same as $\dot{\alpha}$. Since the method developed in this study will be used to analyze wind tunnel data, $\dot{\alpha}$ will be used instead of q in the following investigation and the investigation will be focused on lift force. The effect of $\ddot{\alpha}$ (i.e. $\dot{q}$) is included in the virtual mass effect (noncirculatory response). As explained in reference 2 for 2-D incompressible flow, the noncirculatory response is identical in every harmonic motion and therefore, is indepedent of the time history of motion. The same concept is adopted in the present study. Then eq. (7) is rewritten as

$$C_L(t)=C_L(0)+\text{ noncirculatory response} + \int_0^t C_{L_\alpha}[t-\tau;\ \alpha(\tau),\ \dot{\alpha}(\tau)]\ \frac{d\alpha(\tau)}{d\tau}d\tau + \frac{\ell}{V_\infty}\int_0^t C_{L_{\dot{\alpha}}}[t-\tau;\ \alpha(\tau),\ \dot{\alpha}(\tau)]\ \frac{d\dot{\alpha}(\tau)}{d\tau}d\tau \tag{8}$$

The main objective in the present investigation is to find a suitable form for the integrand of eq. (8). Then the time response $C_L(t)$ can be calculated through the integration by substituting the suitable form of C_{L_α} and $C_{L_{\dot{\alpha}}}$.

In the linear theory (refs. 2 and 3) , the aerodynamic response could be separated into a product of an amplitude function and a phase function in harmonic motion. The amplitude function depends on motion variables and their time rate of change. On the other hand, the phase function is a function of frequency and accounts for any phase lag between the response and the excitation. In a two-dimensional linear theory, the phase function is given by Theodorsen's circulation function (refs. 2 and 3). After response has been obtained at different frequencies with the same amplitude in harmonic oscillation, the phase function can be determined numerically. After use of reciprocal relations (ref. 21), the indicial function can be defined by numerical means. This approach has been used for numerical determination of indicial lift for plunging airfoil in ref. 5 and for plunging wings in ref. 22.

The method for the linear theory will be generalized as follows. Instead of assuming that the aerodynamic response is a product of an amplitude function and a phase function as it is in the linear theory, it is taken to be a sum of the products of amplitude functions and phase functions in harmonic motion; i.e.,

$$C_L = C_0 + \sum_j (\text{amplitude function})_j * (\text{phase function})_j$$

In the linear theory, j equals 1 in the equation. To determine what the forms of the amplitude functions and the phase functions are, the aerodynamic response due to harmonic oscillation is assumed to be of the form

$$C_L = F_0 + F(\alpha,\dot{\alpha})\alpha + G(\alpha,\dot{\alpha})\dot{\alpha} \tag{9}$$

and it is defined that

$$\alpha_1 = \alpha_m + \alpha_0 \cos(kt')$$

$$\alpha = \alpha_0 \cos(kt')$$

$$\dot{\alpha} = (-\alpha_0 k) \sin(kt')$$

where k is the reduced frequency, t' is the nondimensionalized time, α_m is the mean angle of attack and α_0 is the amplitude of angle of attack. To find the constant F_0 and functions F and G as functions of $\alpha(t)$ and $\dot{\alpha}(t)$, a functional analysis is needed. However, the following method, "successive Fourier analysis," represents a practical way to accomplish the task. The first step is to Fourier-analyze the response over one period. For simplicity, a Fourier series with three terms will be used to explain the procedure of the modeling. Then

$$C_L = A_0 + A_1 \cos\theta + A_2 \cos 2\theta + A_3 \cos 3\theta + B_1 \sin\theta + B_2 \sin 2\theta + B_3 \sin 3\theta \quad (10)$$

The second step is to split the result into the form of eq. (9) with $F(\alpha,\dot{\alpha})$ and $G(\alpha,\dot{\alpha})$ being Fourier-analyzed again. The result after "successive Fourier Analysis" becomes

$$\begin{aligned} C_L = A_0 &+ \{ CC[0,0] + CC[1,0]\alpha + CC[2,0]\alpha^2 \\ &+ DC[0,1]\dot{\alpha} + DC[1,1]\alpha\dot{\alpha} + CC[0,2]\dot{\alpha}^2 \}\alpha \\ &+ \{ CS[0,0] + CS[1,0]\alpha + CS[2,0]\alpha^2 \\ &+ DS[0,1]\dot{\alpha} + DS[1,1]\alpha\dot{\alpha} + CS[0,2]\dot{\alpha}^2 \}\dot{\alpha} \end{aligned} \quad (11)$$

The detailed procedure of "successive Fourier analysis" is shown in Appendix 1. By collecting the same order terms of α, $\dot{\alpha}$ and their products together, the result of C_L becomes

$$\begin{aligned} C_L = A_0 &+ \{ CC[0,0]\alpha + CS[0,0]\dot{\alpha} \} \\ &+ \{ CC[1,0]\alpha^2 + DC[0,1]\alpha\dot{\alpha} + CS[1,0]\alpha\dot{\alpha} \\ &+ DS[0,1]\dot{\alpha}^2 \} \\ &+ \{ CC[2,0]\alpha^3 + DC[1,1]\alpha^2\dot{\alpha} \\ &+ CC[0,2]\alpha\dot{\alpha}^2 + CS[2,0]\alpha^2\dot{\alpha} \\ &+ DS[1,1]\alpha\dot{\alpha}^2 + CS[0,2]\dot{\alpha}^3 \} \end{aligned} \quad (12)$$

Equation (12) is a useful form for determining stability derivatives based on forced oscillation tests. However, it can be seen that for each different frequency k with the same amplitude, there will be different response C_L and different coefficients CC, DC, CS and DS. To have practical applications, a general representation of these coefficients as a function of reduced frequency at a constant amplitude is needed. For applications to a maneuvering aircraft, the following representation of aerodynamic response based on the generalized indicial lift concept is more convenient.

It is recalled that in the classical airfoil theory the circulatory lift is written as the product of Theodorsen's circulation function (representing the phase lag) and the quasi-steady lift (representing the amplitude function). In the present nonlinear theory, the same form will also be adopted. From the classical potential theory (ref. 23), it has been found that Padé approximants provide an accurate approximation of the theoretical phase function. Therefore, Padé approximants will be used for the present model as phase functions to represent coefficients CC, DC, CS and DS. Question arises as to what the amplitude function would be. Since the quasi-steady lift (lift without lag) represents the amplitude function, one way to find the amplitude function is to extrapolate coefficients CC, CS, DC and DS from very small k values to k=0. However, difficulty may arise in extrapolation as illustrated in the following.

From the classical airfoil theory (ref. 2), the lift coefficient for a flat plate oscillating with one radian amplitude and with respect to midchord in incompressible flow can be written in complex form as

$$c_\ell = 2\pi \left[0.5\ \dot{\alpha}\ + C(k)\ (\alpha + 0.5\ \dot{\alpha}\ )\right] = \bar{c_\ell}\ e^{ikt}$$

and

$$\bar{c_\ell} = 2\pi \left[0.5\ ik + C(k)\ (1 + 0.5\ ik)\right]$$

$$= 2\pi \left[0.5\ ik + (\ F(k) + iG(k)\ )\ (1 + 0.5\ ik)\right] \qquad (13)$$

where the first term inside the brackets is the virtual mass effect. C(k) in the second term is the Theodorsen's function for the phase lag and the term (1 + 0.5 ik) represents the amplitude function or the quasi-steady lift. Therefore, the response c_ℓ can be calculated by taking C(k) value from a table (ref. 24) and substituting k and C(k) into eq. (13). Suppose the responses are known for each k value but not the amplitude function. Then the amplitude function needs to be extrapolated from small k values. Eq. (13) is rewritten for the unknown amplitude function as

$$\bar{c_\ell} = 2\pi \left[0.5\ ik + C(k)\ (1 + H_1\ ik)\right] \qquad (14)$$

Separating eq. (14) into the real and imaginary parts, it is obtained as

$$\bar{c_{\ell}}_R = 2\pi \, (F(k) - H_1 \, G(k) \, k) \tag{15a}$$

and

$$\bar{c_{\ell}}_I = 2\pi \, (0.5 \, k + G(k) + H_1 \, F(k) \, k) \tag{15b}$$

For k=0.01, the exact values of the phase function (ref. 24) are F(k)=0.9824215 and G(k)=-0.0456521. The response c_ℓ is calculated from a very accurate 2-D UQVLM program and $\bar{c_{\ell}}_I$=-0.2245678. Then, H_1 is obtained by dividing the small difference

$$\bar{c_{\ell}}_I/2\pi - (0.5k + G) = 0.0049110$$

by a small value of k and H_1=0.49989. In application to a general problem, G, F and H_1 are all unknowns. Therefore, numerical errors will be exaggerated in predicting H_1 and the result is unpredictable. For nonlinear cases, the phase functions are also unknowns and need to be solved. Therefore, a small error in assuming the phase function will make the prediction of quasi-steady response inaccurate. The numerical solution in a direct optimization method would be difficult to converge as has been

experienced. To avoid this kind of difficulty, a form for the amplitude function is modeled in the present research and to fit the aerodynamic responses at given k values by a one dimensional gradient method. For this purpose, eq. (9) (or the experimental oscillatory results) is rewritten in a complex form, as follows:

$$C_L = A_0 + (A_1 - iB_1)\, e^{ikt'} + (A_2 - iB_2)\, e^{i2kt'} + (A_3 - iB_3)\, e^{i3kt'} \qquad (16)$$

It should be kept in mind that only the real part of the response has a physical meaning. The reason to put in the complex form is to benefit from the great mathematical convenience of the $e^{ikt'}$ notation. If α is rewritten as

$$\alpha = \alpha_0\, e^{ikt'}$$

and

$$\dot{\alpha} = (i\alpha_0 k)\, e^{ikt'}$$

then eqs. (12) and (16) and the classical airfoil theory suggest that the response could be put in the following form involving the products of amplitude functions and phase functions as

$$
\begin{aligned}
C_L = {} & C_0(k) \\
& + E_{11}\dot{\alpha} + E_{21}\ddot{\alpha} + C_1 * (H_{11}\alpha + H_{21}\dot{\alpha}) * (1 - PD_1) \\
& + E_{12}\dot{\alpha}_2 + E_{22}\ddot{\alpha}_2 + C_2 * (H_{12}\alpha^2 + H_{22}\alpha\dot{\alpha} + H_{32}\dot{\alpha}^2) \\
& \qquad * (1 - PD_2) \\
& + E_{13}\dot{\alpha}_3 + E_{23}\ddot{\alpha}_3 + C_3 * (H_{13}\alpha^3 + H_{23}\alpha^2\dot{\alpha} + H_{33}\alpha\dot{\alpha}^2 + H_{43}\dot{\alpha}^3) \\
& \qquad * (1 - PD_3)
\end{aligned}
\tag{17}
$$

where PD is a Padé approximant with order 2 and is defined as

$$PD_j = \frac{P_{1j}\,(ik)^2 + P_{2j}\,(ik)}{P_{3j}\,(ik)^2 + (ik) + P_{4j}}$$

$E_{11}\ \dot{\alpha}_j + E_{21}\ \ddot{\alpha}_j$ etc. are the virtual-mass effect and account for the noncirculatory lift (ref. 2). The variables $\dot{\alpha}_j$ and $\ddot{\alpha}_j$ are defined as

$$\dot{\alpha}_j = ik\ \alpha_0^{\,j}\ e^{ijkt'}$$

and

$$\ddot{\alpha}_j = -k_2 \alpha_0^j e^{ijkt'}$$

to be consistent with higher order terms. When j=1 in the above equations, $\dot{\alpha}_1 = \dot{\alpha}$ and $\ddot{\alpha}_1 = \ddot{\alpha}$. In addition, H_{21}, H_{22}, H_{23}, etc., are related to the pitch-rate effect. It should be noted that those terms inside the parentheses following C_1, C_2, C_3, such as $(H_{11}\alpha + H_{21}\dot{\alpha})$, represent the quasi-steady response and $(1 - PD_j)$ represents the unsteady aerodynamic lag in response. Therefore, the present assumed form for aerodynamic modeling encompasses the classical linear theory.

C_j are the reference values used to normalize the lift given by $A_j - i B_j$ in the least squared-error method. j is the index consistent with the exponent of the exponential term in eq. (16). For example if the j's term in eq. (17) represents the coefficient of $e^{ikt'}$, then j is 1. If the j's term in eq. (17) represents the coefficient of $e^{i2kt'}$ then j is 2, etc. The first term, $C_0(k)$, in eq. (17) is a constant term, supposedly a function of frequency. From available experimental data (ref. 25), it is found that an averaged constant can be used to represent $C_0(k)$ term as shown in Figure 4 for a delta wing. The unknown coefficients P_{1j}, P_{2j}, P_{3j} and P_{4j} are calculated from the least squared-error method. E_{11}, E_{21}, H_{11}, H_{12}, etc., will be obtained separately by minimizing the sum of squares of errors. This is equivalent to a two-level optimization method to determine the unknowns in eq. (17). That is, E, H, etc., are assumed first. Then P_{1j}, etc., are determined by minimizing

the sum of squared errors. The values of E_{11}, H_{11}, etc., are varied next so that the sum of squared errors is minimized. It was found that this approach is more effective in determining a global minimum solution for the unknowns than a straightforward optimization (one level) method because of nonlinearity in the unknowns in the optimization problem. It should be noted that in the literature the phase function has been typically determined by the response to plunging motions. Therefore, those terms associated with $\dot{\alpha}$ in eq. (17) do not appear. This would very much simplify the mathematics of determining the Padé approximants. The details of the present method are discussed in the following.

2.2 Least-Square Method

By choosing proper values of E_{11}, H_{11}, H_{12}, etc., in eq. (17), the corresponding A_j - i B_j term in eq. (16) is then divided by the amplitude function. The result will appear as

$$V_j + iW_j = 1 - \frac{A_j - iB_j - E_{1j}\, ik - E_{2j}\,(-k^2)}{(\text{amplitude function})_j} = \frac{P_{1j}\,(ik)^2 + P_{2j}\,(ik)}{P_{3j}\,(ik)^2 + (ik) + P_{4j}} \tag{18}$$

If both sides of eq. (18) are multiplied by the denominator of the Padé approximant and separated into real and imaginary parts, then

$$Re \equiv P_{1j}k^2 - P_{3j}V_jk^2 + P_{4j}V_j - W_j k = 0 \tag{19a}$$

and

$$Im \equiv P_{2j}k + P_{3j}W_jk^2 - P_{4j}W_j - V_jk = 0 \tag{19b}$$

The sum of squared errors is defined as

$$Err = \Sigma\, Re(k_i)^2 + \Sigma\, Im(k_i)^2 \tag{20}$$

By equating the first derivatives of squared errors (eq. 20) with respect to variables P_{1j}, P_{2j}, P_{3j} and P_{4j} to zero, the unknown coefficients P_{1j}, P_{2j}, P_{3j} and P_{4j} can be determined by

$$\begin{bmatrix} \Sigma k_i^4 & 0 & -\Sigma V_i k_i^4 & \Sigma V_i k_i^2 \\ 0 & \Sigma k_i^2 & \Sigma W_i k_i^3 & -\Sigma W_i k_i \\ -\Sigma V_i k_i^4 & \Sigma W_i k_i^3 & \Sigma(V_i^2 k_i^4 + W_i^2 k_i^4) & -\Sigma(V_i^2 k_i^2 + W_i^2 k_i^2) \\ \Sigma V_i k_i^2 & -\Sigma W_i k_i & \Sigma(V_i^2 k_i^2 + W_i^2 k_i^2) & \Sigma(V_i^2 + W_i^2) \end{bmatrix} \begin{bmatrix} P_{1j} \\ P_{2j} \\ P_{3j} \\ P_{4j} \end{bmatrix} = \begin{bmatrix} \Sigma W_i k_i^3 \\ \Sigma V_i k_i^2 \\ 0 \\ 0 \end{bmatrix} \tag{21}$$

where i varies over the range of input frequencies, and the mode subscript j on V and W has been omitted.

2.3 Gradient Method

After the unknown coefficients P_{1j}, P_{2j}, P_{3j} and P_{4j} have been found, a one-dimensional gradient method is used to find E and H values which will make the sum of the squared errors minimum. The E or H value is perturbed first by a small amount ΔE or ΔH to find the gradient of the sum of squared errors. If the gradient tends to reduce the error, then the E or H value is perturbed further until several iterations has been reached (it is set to be 5 iterations in the current program). After that, the same procedure is applied to other E or H. Then the whole procedure is repeated again until several iterations has been reached (it is set to be 10 in the current program).

Finally, the response of C_L is written as

$$
\begin{aligned}
C_L = {} & C_{ave} \\
& + E_{11}\dot{\alpha} + E_{21}\ddot{\alpha} + C_1 * (H_{11}\alpha + H_{21}\dot{\alpha}) * (1 - PD_1) \\
& + E_{12}\dot{\alpha}_2 + E_{22}\ddot{\alpha}_2 + C_2 * (H_{12}\alpha^2 + H_{22}\alpha\dot{\alpha} + H_{32}\dot{\alpha}^2) * (1 - PD_2) \\
& + E_{13}\dot{\alpha}_3 + E_{23}\ddot{\alpha}_3 \\
& + C_3 * (H_{13}\alpha^3 + H_{23}\alpha^2\dot{\alpha} + H_{33}\alpha\dot{\alpha}^2 + H_{43}\dot{\alpha}^3) * (1 - PD_3)
\end{aligned}
\qquad (22)
$$

It is easily seen that each term in the above equation is a product of an amplitude function and a phase function. The procedure to put oscillating response data into the form of eq. (22) is summarized in the next section.

2.4 Summary of Numerical Procedure

Step 1. Unsteady-response analysis:

Use Fourier analysis to analyze the harmonic motion responses for different frequencies over one period. For each frequency, the responses should be in the same form as in eq. (16).

Step 2. Constant-term analysis:

From step 1, if constant terms appear in the Fourier analysis then C_{ave} is calculated from each constant term due to different frequencies as

$$C_{ave} = \frac{\sum_{n=1}^{N} A_0(k_n)}{N} \tag{24}$$

where N is the number of frequencies used in step 2 and $A_0(k_n)$ are the constant terms due to different frequencies k_n in Fourier analysis.

Step 3. Amplitude-phase identification:

In this step, the coefficients A_j and B_j calculated from step 1 are put into the form of a product of amplitude functions and phase functions as in eq. (22). The procedure is as follows:

3-a Set the reference values C_j

3-b Set the initial guess for E or H values.

3-c Use the least-square method to find unknown coefficients P_{1j}, P_{2j}, P_{3j} and P_{4j}.

3-d Use the gradient method to find better E or H values.

Repeat steps 3-b to 3-d until the sum of square errors reached minimum or the iteration limit is reached.

Although three-term Fourier series are used in the above, the procedure is applicable to any number of Fourier terms.

2.5 Indicial Formulation

In linear theory, the reciprocal relations (or Fourier summation) (ref. 21) has been used to calculate the indicial response. However, in nonlinear theory those relations can not be applied. As Tobak (ref. 7) mentioned in his paper, the aerodynamic response due to a step change should reach steady-state value asymptotically at subsonic speeds. In linear theory, these asymptotic relations are represented by exponential functions (refs. 2 and 5), and these exponential functions are calculated through the phase function. Therefore, the phase function in the current nonlinear modeling will be converted into exponential function in time domain but the amplitude function is kept unchanged. If eq. (21) is rewritten for m-terms Fourier series as

$$
\begin{aligned}
C_L = C_{ave} & \\
& + E_{11}\dot{\alpha} + E_{21}\ddot{\alpha} + C_1 * (H_{11}\alpha + H_{21}\dot{\alpha}) * (1 - PD_1) \\
& + E_{12}\dot{\alpha}_2 + E_{22}\ddot{\alpha}_2 + C_2 * (H_{12}\alpha^2 + H_{22}\alpha\dot{\alpha} + H_{32}\dot{\alpha}^2) * (1-PD_2) \\
& + E_{13}\dot{\alpha}_3 + E_{23}\ddot{\alpha}_3 + C_3 * (H_{13}\alpha^3 + H_{23}\alpha^2\dot{\alpha} + H_{33}\alpha\dot{\alpha}^2 + H_{43}\dot{\alpha}^3) \\
& \qquad * (1-PD_3) \\
& + \cdots\cdots\cdots\cdots \\
= C_{ave} & + \\
& + \sum_{j=1}^{m} E_{1j}\dot{\alpha}_j + E_{2j}\ddot{\alpha}_j \\
& \qquad + (\text{amplitude function})_j * (\text{phase function})_j
\end{aligned}
\tag{25}
$$

where the phase functions represented by the Padé approximants are defined as

$$
\begin{aligned}
1 - \frac{P_{1j}(ik)^2 + P_{2j}(ik)}{P_{3j}(ik)^2 + ik + P_{4j}} &= 1 - \frac{ik\, a_{1j}}{ik + a_{3j}} + \frac{ik\, a_{2j}}{ik + a_{4j}} \\
&= 1 - \frac{i(jk)\, a_{1j}}{i(jk) + ja_{3j}} + \frac{i(jk)\, a_{2j}}{i(jk) + ja_{4j}}
\end{aligned}
\tag{26}
$$

By applying the Fourier integral to the phase function, the corresponding expression in time domain is calculated as

$$\frac{1}{2\pi\, i(jk)} \int_{-\infty}^{\infty} \left[1 - \frac{P_{1j}(ik)^2 + P_{2j}(ik)}{P_{3j}(ik)^2 + ik + P_{4j}}\right] e^{ijkt'} d\,(jk)$$
$$= 1 - a_{1j}\, e^{-a_{3j}t'} - a_{2j}\, e^{-a_{4j}t'} \tag{27}$$

the detailed derivation is in appendix B. Then, the indicial response C_L for the circulatory lift is written as

$$\begin{aligned} C_{L_{\text{indicial}}} = {} & C_1 * (H_{11}\alpha + H_{21}\dot{\alpha}) * (1 - a_{11}\, e^{-a_{31}t'} - a_{21}\, e^{-a_{41}t'}) \\ & + C_2 * (H_{12}\alpha^2 + H_{22}\alpha\dot{\alpha} + H_{32}\dot{\alpha}^2) \\ & \quad * (1 - a_{12}\, e^{-a_{32}2t'} - a_{22}\, e^{-a_{42}2t'}) \\ & + \cdots\cdots\cdots \\ = {} & \sum_{j=1}^{m} (\text{amplitude function})_j \\ & * (1 - a_{1j}\, e^{-a_{3j}jt'} - a_{2j}\, e^{-a_{4j}jt'}) \end{aligned} \tag{28}$$

In the current research, five terms Fourier series is used to analyze the experimental data. Therefore, the response can be written as

$$\begin{aligned} C_{L_{\text{indicial}}} = {} & C_1 * (H_{11}\alpha + H_{21}\dot{\alpha}) * (1 - \exp_1) \\ & + C_2 * (H_{12}\alpha^2 + H_{22}\alpha\dot{\alpha} + H_{32}\dot{\alpha}^2) * (1 - \exp_2) \\ & + C_3 * (H_{13}\alpha^3 + H_{23}\alpha^2\dot{\alpha} + H_{33}\alpha\dot{\alpha}^2 + H_{43}\dot{\alpha}^3) * (1 - \exp_3) \\ & + C_4 * (H_{14}\alpha^4 + H_{24}\alpha^3\dot{\alpha} + H_{34}\alpha^2\dot{\alpha}^2 + H_{44}\alpha\dot{\alpha}^3 + H_{54}\dot{\alpha}^4) \\ & \quad * (1 - \exp_4) \\ & + C_5 * (H_{15}\alpha^5 + H_{25}\alpha^4\dot{\alpha} + H_{35}\alpha^3\dot{\alpha}^2 + H_{45}\alpha^2\dot{\alpha}^3 + H_{55}\alpha\dot{\alpha}^4 \\ & \quad + H_{65}\dot{\alpha}^5) * (1 - \exp_5) \end{aligned} \tag{29}$$

By differentiating with α and $\dot{\alpha}$, $(C_{L_{indicial}})_{\alpha}$, $(C_{L_{indicial}})_{\dot{\alpha}}$ are obtained as follows:

$$
\begin{aligned}
(C_{L_{indicial}})_{\alpha} = {} & C_1 * H_{11} * (1 - \exp_1) \\
& + C_2 * (2H_{12}\alpha + H_{22}\dot{\alpha}) * (1 - \exp_2) \\
& + C_3 * (3H_{13}\alpha^2 + 2H_{23}\alpha\dot{\alpha} + H_{33}\dot{\alpha}^2) \\
& \quad * (1 - \exp_3) \\
& + C_4 * (4H_{14}\alpha^3 + 3H_{24}\alpha^2\dot{\alpha} + 2H_{34}\alpha\dot{\alpha}^2 + H_{44}\dot{\alpha}^3) \\
& \quad * (1 - \exp_4) \\
& + C_5 * (5H_{15}\alpha^4 + 4H_{25}\alpha^3\dot{\alpha} + 3H_{35}\alpha^2\dot{\alpha}^2 + 2H_{45}\alpha\dot{\alpha}^3 + H_{55}\dot{\alpha}^4) \\
& \quad * (1 - \exp_5)
\end{aligned}
\tag{30}
$$

$$
\begin{aligned}
(C_{L_{indicial}})_{\dot{\alpha}} = {} & C_1 * H_{21} * (1 - \exp_1) \\
& + C_2 * (H_{22}\alpha + 2H_{32}\dot{\alpha}) * (1 - \exp_2) \\
& + C_3 * (H_{23}\alpha^2 + 2H_{33}\alpha\dot{\alpha} + 3H_{43}\dot{\alpha}^2) * (1 - \exp_3) \\
& + C_4 * (H_{24}\alpha^3 + 2H_{34}\alpha^2\dot{\alpha} + 3H_{44}\alpha\dot{\alpha}^2 + 4H_{54}\dot{\alpha}^3) \\
& \quad * (1 - \exp_4) \\
& + C_5 * (H_{25}\alpha^4 + 2H_{35}\alpha^3\dot{\alpha} + 3H_{45}\alpha^2\dot{\alpha}^2 + 4H_{55}\alpha\dot{\alpha}^3 + 5H_{65}\dot{\alpha}^5) \\
& \quad * (1 - \exp_5)
\end{aligned}
\tag{31}
$$

By substituding these derivatives into equation (8), the integrand can be determined. The initial condition $C_L(0)$ is calculated by setting the

variable τ to zero in the indicial response $C_{L_{indicial}}$. Since the noncirculatory lift is identical in every harmonic motion, it must be excluded from the integral. Then the generalized response for arbitrary motion is obtained by substituted the noncirculatory lift and the derivatives of the indicial response to eq. (8). Therefore, the final form of time integration for arbitrary motion is written as

$$C_L(t') = C_{L_{indicial}}[t'-\tau,\ \alpha(\tau),\ \dot{\alpha}(\tau)]_{\tau=0} + C_{ave} + \sum_{j=1}^{m} (E_{1j}\dot{\alpha}_j + E_{2j}\ddot{\alpha}_j)$$
$$+ \sum_{j=1}^{m}\int_0^{t'} \frac{d\ (\text{amplitude function})_j}{d\alpha} * (1 - a_{1j}e^{-a_{3j}(t'-\tau)} - a_{2j}e^{-a_{4j}(t'-\tau)})\ \frac{d\alpha(\tau)}{d\tau}\ d\tau$$
$$+ \frac{\ell}{V_\infty}\sum_{j=1}^{m}\int_0^{t'} \frac{d\ (\text{amplitude function})_j}{d\ \dot{\alpha}} * (1 - a_{1j}e^{-a_{3j}(t'-\tau)} - a_{2j}e^{-a_{4j}(t'-\tau)})\ \frac{d\dot{\alpha}(\tau)}{d\tau}\ d\tau \qquad (32)$$

2.6 Arbitrary motions

In the current research, the indicial responses are derived from data of harmonic motions. Therefore, to have a correct representation, an arbitrary motion must be represented locally by a cosine function. Since the values of α_1 and $\dot{\alpha}$ are usually given at a certain time, they can be described by the cosine and sine function as

$$\alpha_1 = \alpha_m + \alpha_0 \cos(\phi + kt') = \alpha_m + \alpha$$

$$\dot{\alpha} = -\alpha_0 k \sin(\phi + kt') \tag{33}$$

By defining a mean angle-of-attack(α_m) and amplitude(α_0), the above equations can be rewritten as

$$F_1 = \alpha - \alpha_0 \cos(\phi + kt') = 0$$

$$F_2 = \dot{\alpha} + \alpha_0 k \sin(\phi + kt') = 0 \tag{34}$$

the unknowns, the reduced frequency k and phase function angle ϕ at a given time t', can be solved by Newton's method(see Appendix C for a detailed derivation)

Chapter 3

Results and Discussion

3.1 Linear Results

Because appropriate high-alpha experimental data to apply the present modeling method are limited, the present method will first be tested with linear theoretical results. Several cases in the two-dimensional and three-dimensional linear flow have been studied to verify the proposed method of aerodynamic modeling.

3.1.1 Two-Dimensional Flow

The first case studied is a 2-D flat plate oscillating in the incompressible flow. The amplitude is 57.3 degree (one radian) in angle of attack for the airfoil. Therefore it oscillates from 57.3 degree of angle of attack to -57.3 degree of angle of attack then back to 57.3 degree of angle of attack for one cycle with respect to midchord. i.e.

$\alpha_1 = 0.0 + 1.0 \cos(kt')$ (in radian)

The steady lift is already known from the linear theory (ref. 2) as $2\pi\alpha$, and the oscillating complex lift is taken from a 2-D unsteady QVLM

program (ref. 26) as input data for the current model and for comparison. Through numerical experimentation, it is found that only six frequencies are needed to have accurate results. Through the modeling procedure as summarized in section 2.4, the lift can be written as

$$c_\ell = E_{11}\,\dot{\alpha} + E_{21}\,\ddot{\alpha} + 2\pi\,(H_{11}\alpha + H_{21}\dot{\alpha})\,(1.0 - PD_1)$$

and the values of coefficients E_{11}, E_{21}, H_{11}, H_{21} and P_{i1}(for padé approximant PD_1) are listed in Table 1. The results for the lift coefficients are plotted in Figure 5 for different numbers of frequencies used. Compared with the aerodynamic responses by the 2-D UQVLM program, the numerical results from modeling show excellent agreement.

Two Mach numbers, 0.2 and 0.4, are chosen in the 2-D compressible flow to verify the current model. A two-dimensional unsteady QVLM (ref. 26) program is again used to calculate the complex lift as input data for the current model and for comparison. The same frequencies as in the incompressible flow are used as input also. The results for coefficients E_{11}, E_{21}, H_{11}, H_{21} and P_{i1} are listed in Table 1. The aerodynamic responses c_ℓ calculated by the model are plotted in Figures 6 and 7 to compare the results from 2-D unsteady QVLM. These figures show that the numerical results by modeling are very accurate.

3.1.2 Three-Dimensional Flow

The same Mach numbers (includes 0) in the 2-D flow are used in 3-D attached flow to verify the current model. The geometry is a 70 degree delta wing which oscillate from zero degree angle of attack to twenty degree angle of attack with respect to mid root chord. i.e.

$\alpha_1 = 0.1745329 + 0.1745329 \cos kt'$ (in radian)

This means that the mean angle of attack is ten degree (0.1745329 radian) and the amplitude of the oscillation is ten degree (0.1745329 radian). The input aerodynamic responses are calculated from a 3-D unsteady QVLM program (ref. 27). In the program, the total lift is the sum of steady lift at the mean angle-of-attack plus unsteady lift. Since the steady lift is the same for every term, only the unsteady lift is used in the modeling and for comparison. Through numerical experimentation, it is found that the responses at low frequencies do not change significantly, which results in inaccurate modeling. To have accurate approximation, high frequency responses are needed. Seven reduced frequencies (k = 0.01, 0.1, 0.2, 0.6, 1.0, 2.0, 2.5) are used as input data in the 3-D attached flow cases. The results for the coefficients of the modeling are listed in Table 1. The responses C_L from modeling are plotted in Figures 8 to 10 to compare

with the results from 3-D unsteady QVLM program. All of these figures show very good agreement.

3.2 Nonlinear Results

The experimental data (ref. 25) for a 70-degree delta wing in pitching oscillation is used to validate the current aerodynamic model. The angle of attack which describes the pitching motion with respect to the 57% root chord is given as

$$\alpha_1 = 27.5 + 27.5 \cos(180 + kt') \text{ (in degree)}$$

which means the delta wing oscillates from zero degree angle of attack to 55-degree angle of attack then back to zero degree angle of attack for one cycle. The reduced frequency k is nondimensionalized based on wing's root chord and the pitching moment is measured with respect to quarter root chord. Five sets of data corresponding to five different frequencies are available and they will be used as the input data to calculate the coefficients for the current aerodynamic model. Five terms in the Fourier series are employed for the calculation. The calculated coefficients for the current aerodynamic model are listed in Table 2 to Table 5 for C_L, C_D, C_m and C_N.

The lift coefficients obtained from the aerodynamic model(eq. 29) are compared with the original test data in Fig. 11 with good agreement. Experessions for C_D, C_m and C_N are obtained with the same procedures as those used for C_L. The modeled harmonic results are compared with data in Figs. 12 to 14 respectively. Again, the good agreement indicates that the present aerodynamic model is accurate in representing the experimental harmonic data.

3.2.1 Indicial Formulation

Note that eq. (8) is valid for arbitrary motion. To check its range of validity in the nonlinear theory, extensive study has been conducted. Because the indicial responses consist of oscillatory responses, two oscillatory lift cases in the last section are used to verify the indicial integration first. That is, by assuming oscillatory motion in eq. (8), the time-integrated lift response should agree with the forced-oscillation data. Since the angle of attack is set to be a complex number (cos(kt')+i sin(kt')) in oscillating cases, only the real part of the integrated lift is taken. The lift by integrating eq. (8) for a 70-deg. oscillating delta wing with frequencies k=0.098 and k=0.165 are plotted in Figure 15. Compared with the lift from aerodynamic modeling(eq. 25), the integrated lift shows good agreement. Which confirms that at least the current methodology of indicial integration works for harmonic oscillations.

The experimental data(ref. 26) available for more general motion is for harmonic ramp motion. That is, the 70-deg. delta wing model undergoes a harmonic pitching motion(with respect to the 57% root chord) to a certain angle-of-attack and then stops there. To verify the aerodynamic models further, these harmonic ramp responses are applied. Note that the experimental harmonic ramp motion is described by the following pitching motion until reaching a certain angle-of-attack. i.e.

$\alpha_1 = 27.5 + 27.5 \cos(180 + kt')$ (in degree)

The results calculated from indicial integration for C_L in ramp motion up to 55 deg. angle-of-attack at two different frequencies are plotted in figure 16. Compared with experimental data for the 70-deg. delta wing(ref. 28), the C_L responses show good agreement for frequencies 0.0926 and 0.0714. The results for C_L in ramp motion up to α=35,45 and 55 deg at a frequency equal to 0.0714 are ploted in figure 17. It is seen that the present aerodynamic model is fairly accurate if the harmonic ramp motion is from α = 0 to 55 deg. However, the final C_L is overpredicted if the ramp motion stops at an α less than 55 deg, even though the peak C_L is still well predicted. A possible reason for this is that the harmonic data based on α = 0 - 55 deg. contain dynamic effect on vortex-breakdown characteristics at

$\alpha < 55$ deg. The results for C_L at a steady $\alpha = 35$ or 45 deg. should be higher than the static values.

The corresponding drag and pitching moment coefficients at reduced frequencies 0.0926 and 0.0714 are presented in figure 18 and figure 19. For the C_m responses, the result is well predicted except at small time. However, the drag coefficient is not as well predicted in ramp motions as in harmonic motions(see Fig. 12). The same descrepancy in predicted drag coefficients is also found in figure 20 for a harmonic ramp motion with α = 0 to 35 and 45 deg at a frequency eaual to 0.0714. It is not known whether this is caused by differences in the test models and test Reynolds numbers. The test model for the harmonic motions(ref. 25) has two-sided chamfered leading edges with a thickness of 0.5 inch at a Reynolds number of 1.64×10^6 based on the root chord. The model for the ramp motions(ref. 28) is chamfered only on the lower surface of the leading edge and has a thickness of 0.25 inch, and tested at a Reynolds number of 1.54×10^6. The effect of Reynolds number on the static lift coefficient for two different delta wing models is taken from ref. 29 and reploted in figure 21. As shown in the figure, the effect of Reynolds number for the one-side chamfered delta wing appears to be confined to angle of attack above 28 deg and much less than for the two-side chamfered delta wing. The effect of Reynolds number on dynamic lift is reploted as figure 22. As the Reynolds number is increased, the maximun lift tends to decrease. The similar effect of Reynolds number

to other dynamic responses of the two-sided chamfered delta wing can be found in ref. 25. Therefore, using the harmonic motion data of one model to predict the ramp motion of another model may cause discrepancy in drag coefficients.

To illustrate the application of the present aerodynamic model(eq. 30) for arbitrary motions, a linear ramp motion is assumed in the integration. As described in section 2.6, the linear ramp motion is represented by an equivant local harmonic motion using a cosine function. However, from numerical experimentation it is found out that due to the discontinuity in slope($\dot{\alpha}$), if the mean angle and amplitude are set to have the same value, then the calculated responses will have discontinuity there. To avoid the discontinuity of the responses, the amplitude must be set larger than the mean angle of attack. Three values of the amplitude have been tested for the linear ramp motion from α = 0 to 55 deg. and the calculated lift responses are plotted in figure 23. It can be seen from the figure that a 2.5 deg increase in amplitude will smooth out the response. Therefore, in calculating the linear ramp response the amplitude will be set 2.5 deg. larger than the mean angle-of-attack. The lift coefficient for the linear ramp motion for α = 0 to 55 deg is compared with that in a harmonic ramp motion in figure 24. It is seen that the linear ramp motion tends to produce higher C_L beyond the peak value because it has a higher value in

$\dot{\alpha}$. Similar results can be found in figure 25 for lift coefficients corresponding to the linear ramps for α = 0 to 35 and 45 deg.

The indicial lift responses consist of harmonic data which are based on α = 0 to 55 deg are now used to calculate the lift responseto a linear ramp motion up to α = 76 deg. As shown in figure 26, the trend is predicted but the magnitude is over-predicted. Therefore, it may be concluded that the harmonic data based on α = 0 to 55 deg. may not be used to extrapolate the data to higher angles of attack.

The last case is to test the mean angle-of-attack effect. That is, using the harmonic data(ref. 25) at $\alpha_m = \alpha_0$ = 27.5 deg., harmonic responses under different mean angles-of-attack are calculated. From numerical experimentation, it is found that to have correct trend in the prediction, if the mean angle of attack is greater than 27.5 deg, it is set to 27.5 deg. The results from indicial integration are plotted in figure 27. Compared with experimental data taken in a different tunnel with different instrumentation(ref. 31), these numerical results show correct trend. Note that the experimental data are taken under Re = 1.64×10^6 based on the root chord(4.166 ft) for a 70-deg delta wing. The Reynolds number is the same as that of the harmonic data with 27.5 deg. mean angle-of-attack for the aerodynamic model but based on a larger size model and smaller free stream velocity. In addition, the larger 70-deg model is oscillating with

respect to the 40% mean aerodynamic chord(60% root chord) instead of 57% root chord. Therefore, it is difficult to assess the accuracy of the present aerodynamic model.

Chapter 4

Conclusions and Recommendations

4.1 Conclusions

In the current study, a method based on Fourier analysis is developed to analyze the force and moment data obtained in large-amplitude forced oscillation tests at high angle-of-attack. Results from linear two- and three- dimensional unsteady aerodynamic theories as well as test data for a 70-deg delta wing are used to verify the models. It is shown that the present modeling method is accurate in producing the aerodynamic responses in C_L, C_D, C_m and C_N to harmonic motions and the ramp-type motions. The model also produces a correct trend for a 70-deg delta wing in harmonic motion with different mean angles-of-attack. To deal with the linear ramp type motions, a local harmonic motion representation is used in the current model. However, the current model failed to predict the response to a ramp motion which has larger angles-of-attack than that of the harmonic motions which form the aerodynamic model.

4.2 Recommendations

In the current model, the effects of Reynolds number and Mach number are not included in the modeling. The main reason is that not enough experimental data or theoretical results are available to support the study. Therefore, the recommendations for the future work are

(i) A consistent experimental work or numerical calculation for unsteady longitudinal aerodynamics should include Reynolds number and Mach number effects for each reduced frequencies in harmonic motions.

(ii) Modify the current mathematical model to include the Reynolds number and Mach number effects based on the results from (i).

References

1. Tobak, M.; and Schiff, L. B. "Aerodynamic Mathematical Modeling-Basic Concepts." Dynamic Stability Parameters, AGARD-LS-114, 1981.

2. Bisplinghoff, Raymond L.; Ashley, Holt; and Halfman, Robert L. Aeroelasticity. Addison-Wesly Publishing Company, Cambridge, Mass., 1955.

3. Dowell, Earl H. (editor). A Modern Course in Aeroelasticity. Sijthoff & Noordhoft International Publishers, Rockville, Maryland, 1980.

4. Heaslet, M. A.; and Lomax, H. "Two-Dimensional Unsteady Lift Problems in Supersonic Flight." NACA Rep. 945, 1949.

5. Mazelsky, B. "Numerical Determination of Indicial Lift of a Two-Dimensional Sinking Airfoil at Subsonic Mach Numbers from Oscillatory Lift Coefficients with Calculations for Mach Number 0.7." NACA TN 2562, December, 1951.

6. Hildebrand, Francis B. Advanced Calculus for Application. Prentice-Hall, Inc., Englewood Cliff, New Jersey, 1976.

7. Tobak, M. "On the Use of the Indicial Function Concept in the Analysis of Unsteady Motions of Wings and Wing-Tail Combination." NASA Rep. 1188, 1954.

8. Tobak, M.; and Pearson, W. E. "A Study of Nonlinear Logitudinal Dynamic Stability." NASA TR R-209, September, 1964.

9. Katz, J.; and Schiff, L. B. "Modeling Aerodynamic Responses to Aircraft Maneuvers--A Numerical Validation." J.Aircraft, Vol. 23, No. 1, January, 1986, pp. 19-25.

10. Chyu, W. J.; and Schiff, L. B. "Nonlinear Aerodynamic Modeling of Flap Oscillation in Transonic Flow--A Numerical Validation." AIAA Journal, Vol. 21, Jan. 1983, pp. 106-113.

11. Levy, L. L.; and Tobak, M. "Nonlinear Aerodynamics of Bodies of Revolution in Free Flight." AIAA Journal, Vol. 8, Dec. 1970, pp. 2168-2171.

12. Tobak, M.; and Schiff, L. B. "Generalized Formulation of Nonlinear Pitch-Yaw-Roll Coupling, Part 1: Nonlinear Coning-Rate Dependence." AIAA Journal, Vol. 13, March, 1975, pp. 323-326.

13. Tobak, M.; and Schiff, L. B. "Generalized Formulation of Nonlinear Pitch-Yaw-Roll Coupling, Part 2: Nonlinear Coning-Rate Dependence." AIAA Journal, Vol. 13, March, 1975, pp. 327-332.

14. Chambers, J. R.; and Grafton, S. B. "Static and Dynamic Longitudinal Stability Derivatives of a Powered 1/9-Scale Model of a Tilt-Wing V/Stol Transport." NASA TN D-3591, September 1966.

15. Hanff, E. S. "Determination of Non-linear Loads on Oscillating Models in Wind Tunnels." IEEE 10th International Congress on Instrumentation in Aerospace Simulation Facilities, September 1983.

16. Etkin, B. Dynamics of Atmospheric Flight, John Wiley & Sons, Inc. 1972.

17. John, Wayne "A Comprehensive Analytical Model of Rotorcraft Aerodynamics and Dynamics." NASA TM 81182, June 1980.

18. Nguyen, L. T.; Ogburn, M. E.; Gilbert W. P.; Kibler K. S.; Brown , P. W.; and Deal, P. L. "Simulator Study of Stall/Post-Stall Characteristics of a Fighter Airplane With Relaxed Longitudinal Static Stability." NASA TP 1538, December 1979.

19. Linse, D. J. "The Design and Analysis of A High Angle of Attack Fighter Control System." University of Kansas Flight Research Laboratory, Report No. KU-FRL-776-1, 1987.

20. Jenkins, J. E. "Relationships Among Nonlinear Aerodynamic Indicial Response Models, Oscillatory Motion Data, And Stability Derivatives." AIAA Paper 89-3351, Aug. 1989.

21. Garrick, I. E. "Nonsteady Wing Characteristics." High Speed Aerodynamics and Jet Propulsion, Vol. 7, Princeton, New Jersey, 1957.

22. Chao, C. D.; and Lan, C. E. "Calculation of Wing Response to Gusts and Blast Waves with Vortex Lift Effect." NASA CR-172232, October 1983.

23. Vepa, R. "Finite State Modeling of Aeroelastic Systems." NASA CR 2779, Feb. 1977.

24. Luke, Y. L. "Tables of Coefficients for Compressible Flutter Calculations." AF TR No. 6200, August 1950.

25. Soltani, M. R.; Bragg, M. B.; and Brandon, J. M. "Experimental Measurements on an Oscillating 70-Degree Delta Wing in Subsonic Flow." AIAA Paper No. 88-2576, 1988.

26. Lan, C. E. "The Induced Drag of Oscillating Airfoils in Linear Subsonic Compressible Flow." University of Kansas Flight Research Laboratory, Report No. KU-FRL-400, 1975.

27. Lan, C. E. "The Unsteady Suction Analogy and Applications." AIAA Journal, Vol. 20, No. 12 Dec. 1982, pp. 1647-1656.

28. Bragg, M. B. and Soltani, M. R.,"Measured Forces and Moments on a Delta Wing during Pitch-Up," Journal of Aircraft, Vol. 27, March 1990, pp. 262 - 267.

29. Soltani, M. R. and Bragg M. B.,"Measurements on an Oscillating 70-Deg Delta Wing in Subsonic Flow," Journal of Aircraft, Vol. 27, March 1990, pp. 211-217.

30. Private communication with Jay M. Brandon.

31. Brandon M. J. and Shah H. G.,"Effect of Large Amplitude Pitching Motions on The Unsteady Aerodynamic Characteristics of Flat-Plate Wings," AIAA Paper No. 88-4331.

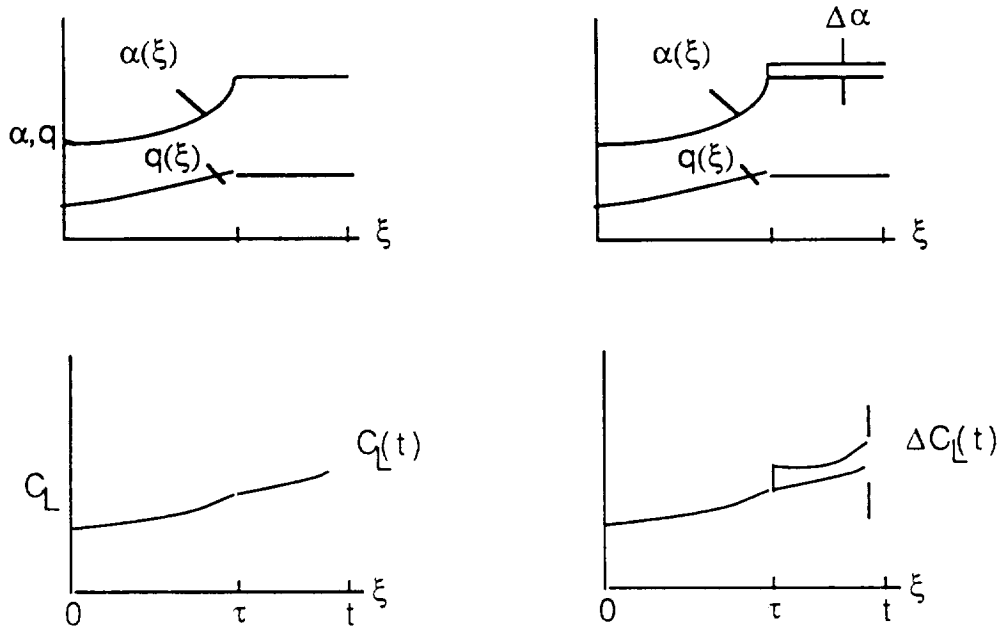

Fig. 2 Indicial response

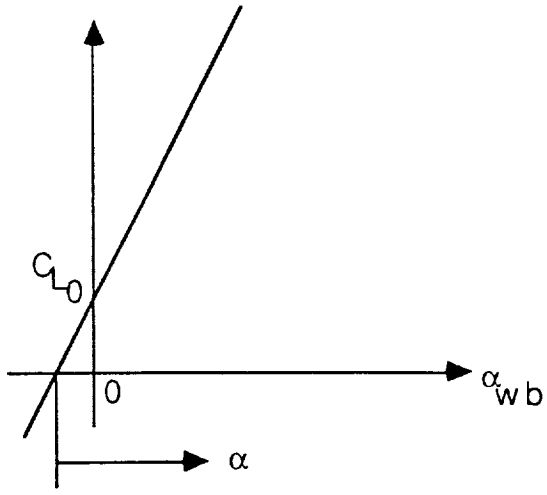

Fig. 1 Graph of total lift

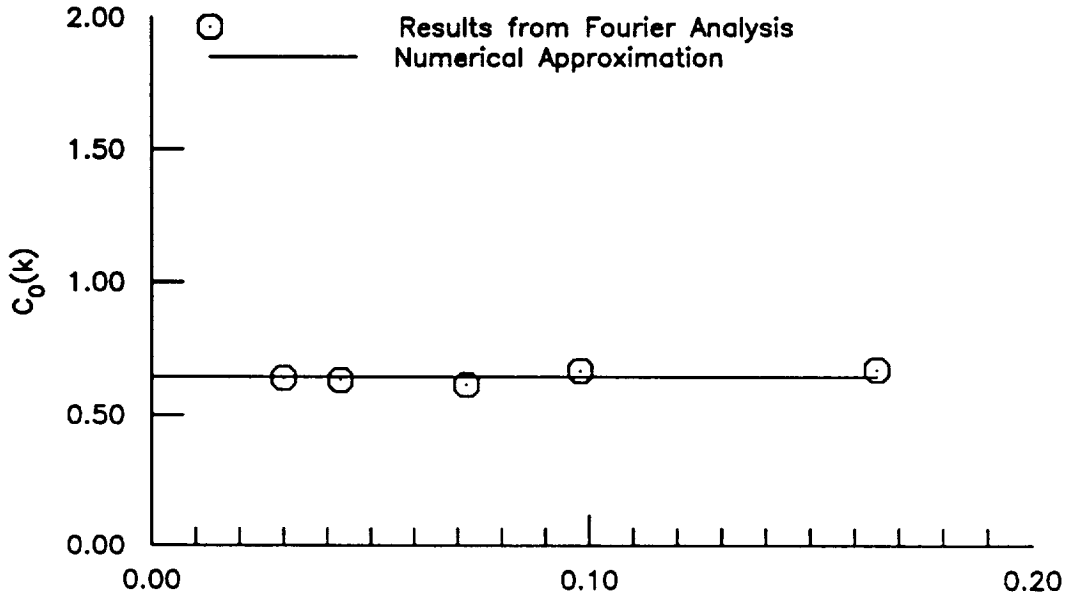

Figure 4 Comparison of Numerically Approximated Constant Terms with Results from Fourier Analysis for The lift of an Oscillating 70–Deg. Delta Wing

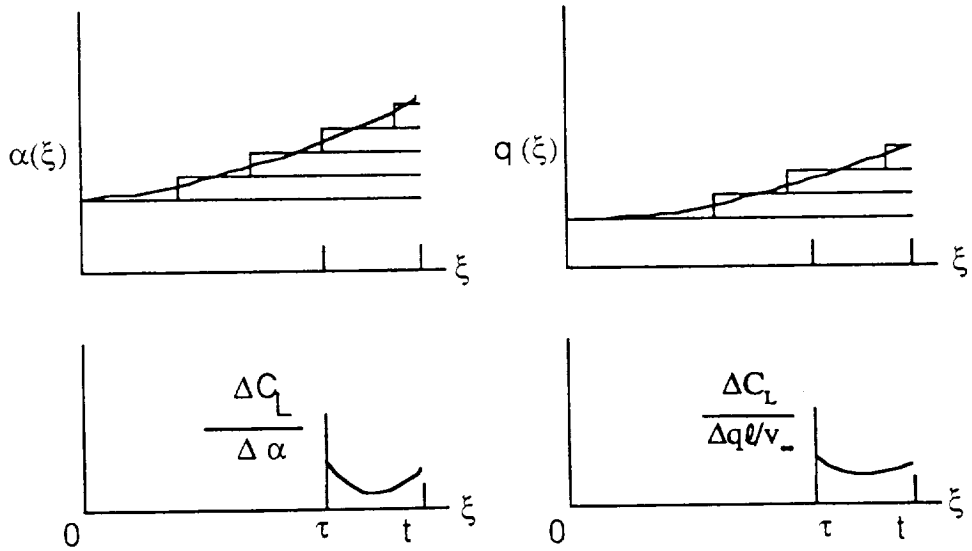

Fig. 3 Summation of incremental response

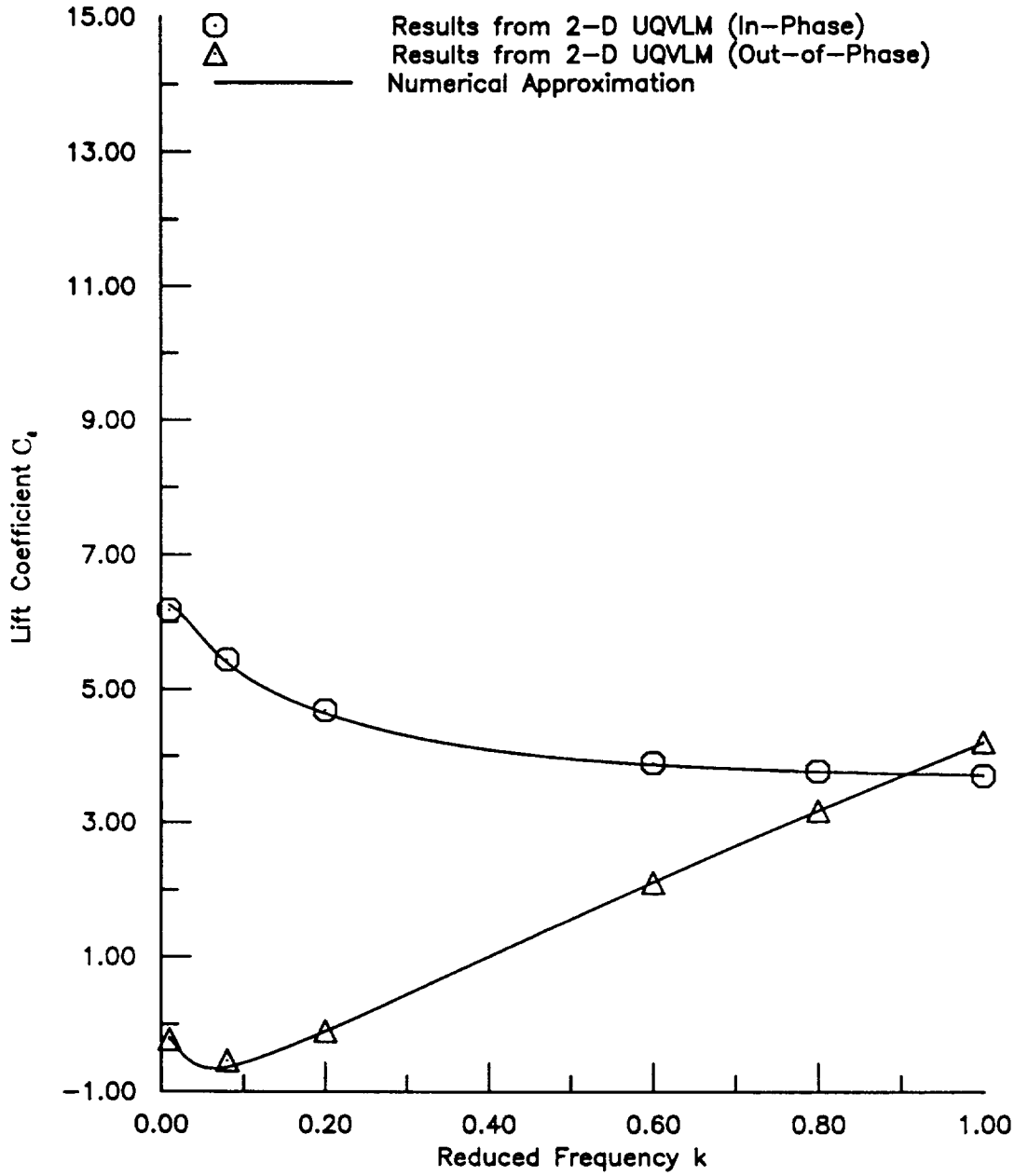

Figure 5 Unsteady Lift Coefficient For a 2-D Flat Plat Pitching about Midchord at M = 0.0

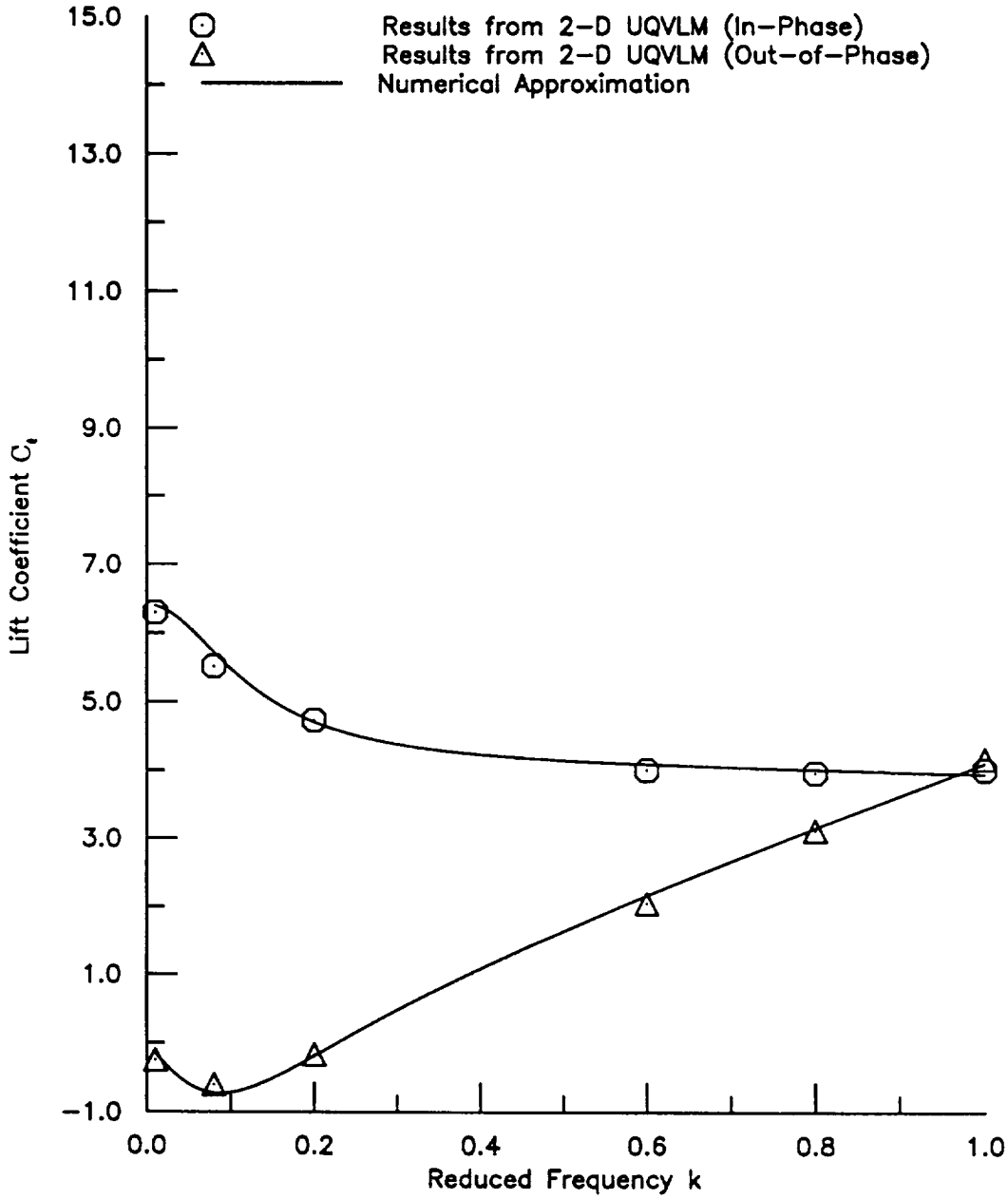

Figure 6 Unsteady Lift Coefficient For a 2-D Flat Plat Pitching about Midchord at M = 0.2

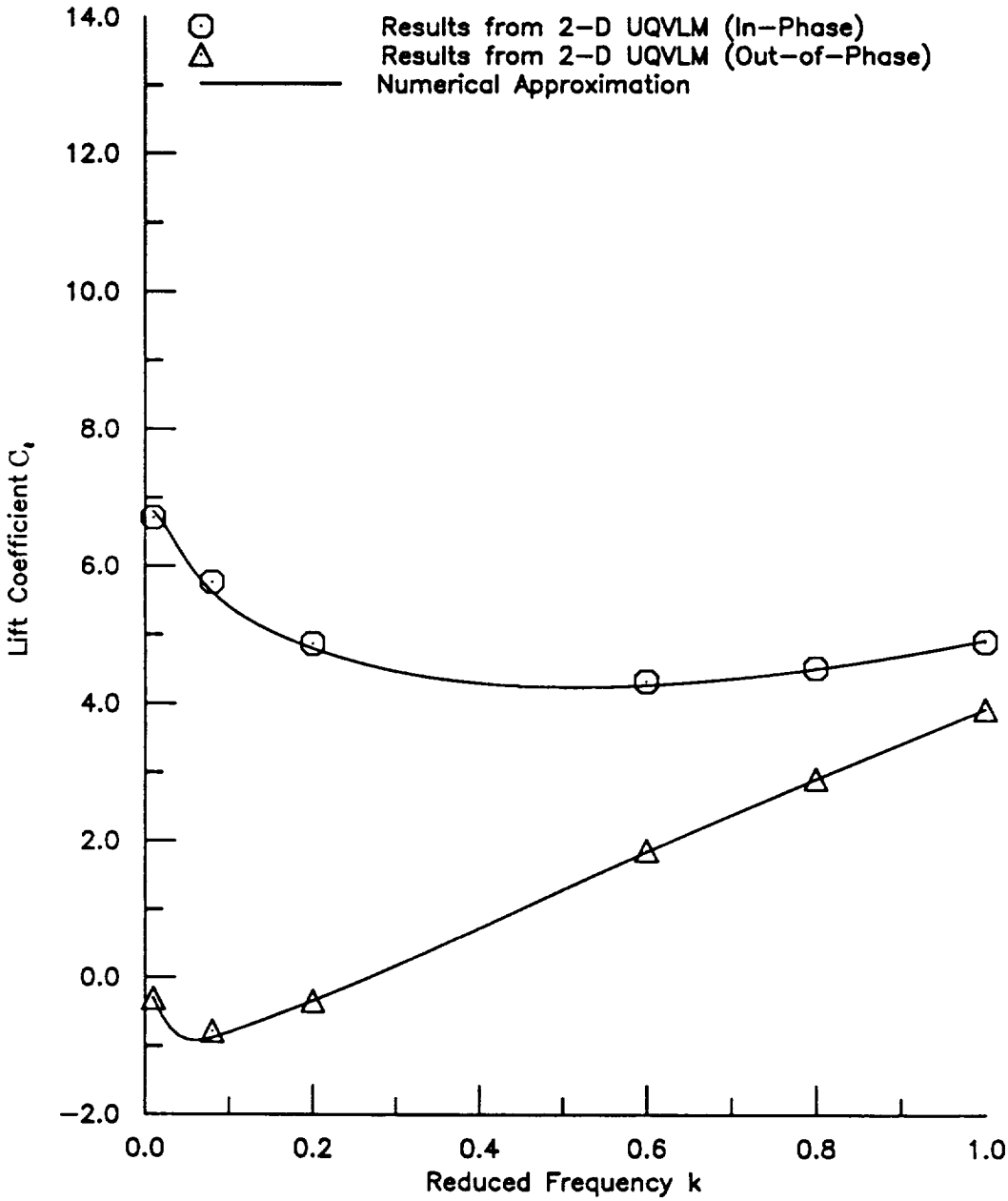

Figure 7 Unsteady Lift Coefficient For a 2–D Flat Plat Pitching about Midchord at M = 0.4

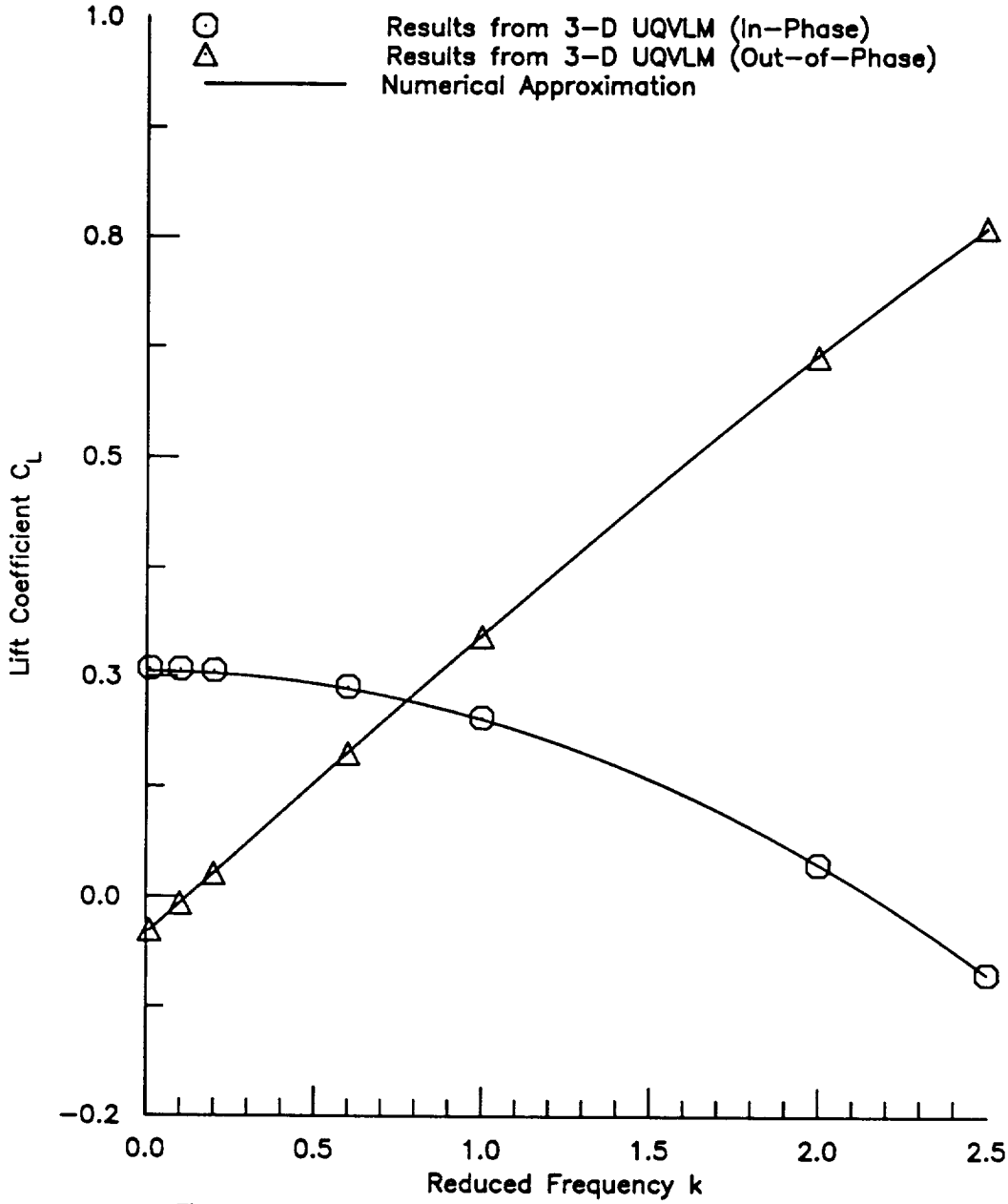

Figure 8 Unsteady Lift Coefficient For a 70-deg Delta Wing Pitching about Mid-Root chord at M = 0.0

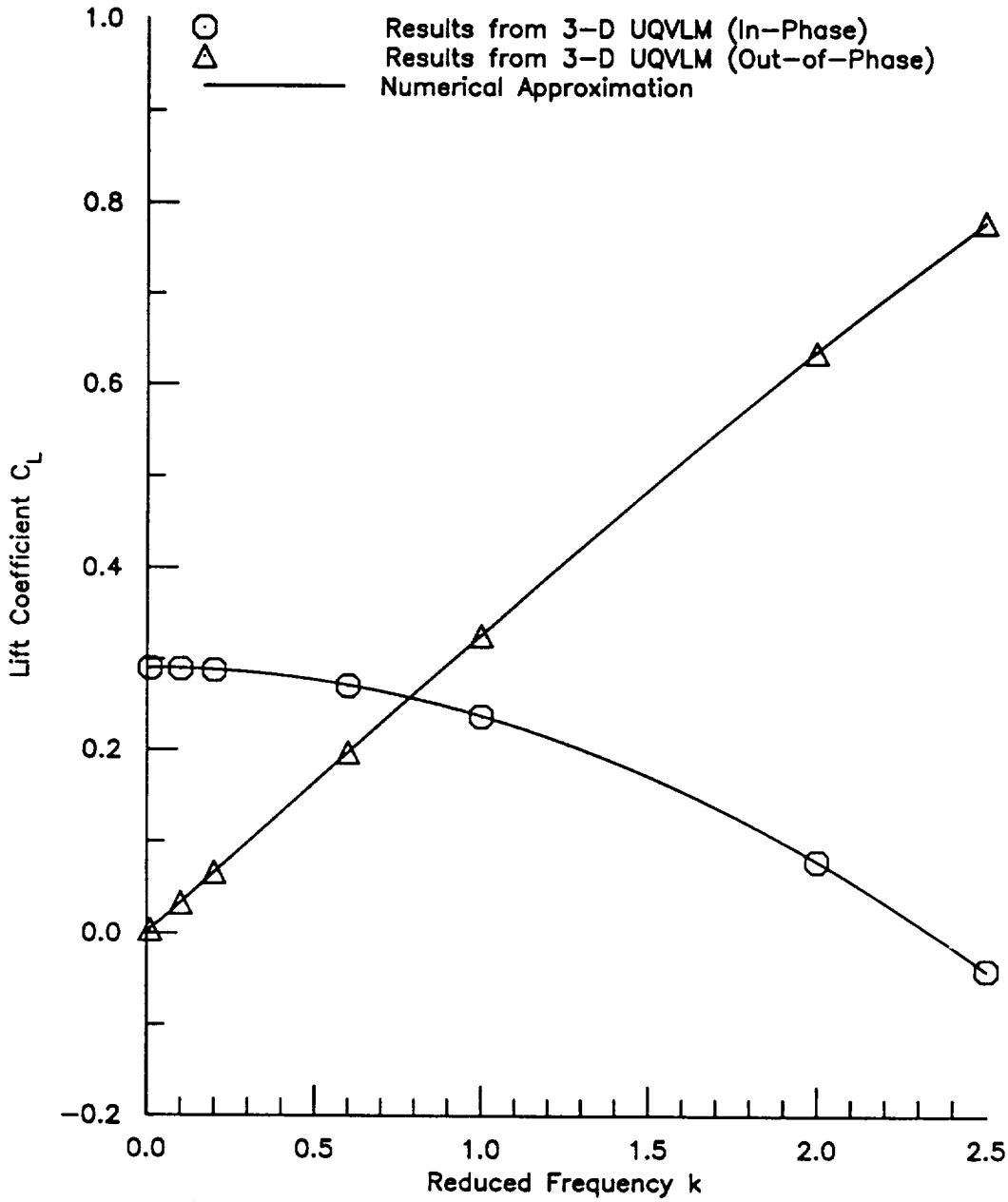

Figure 9 Unsteady Lift Coefficient For a 70-deg Delta Wing Pitching about Mid-Root chord at M = 0.2

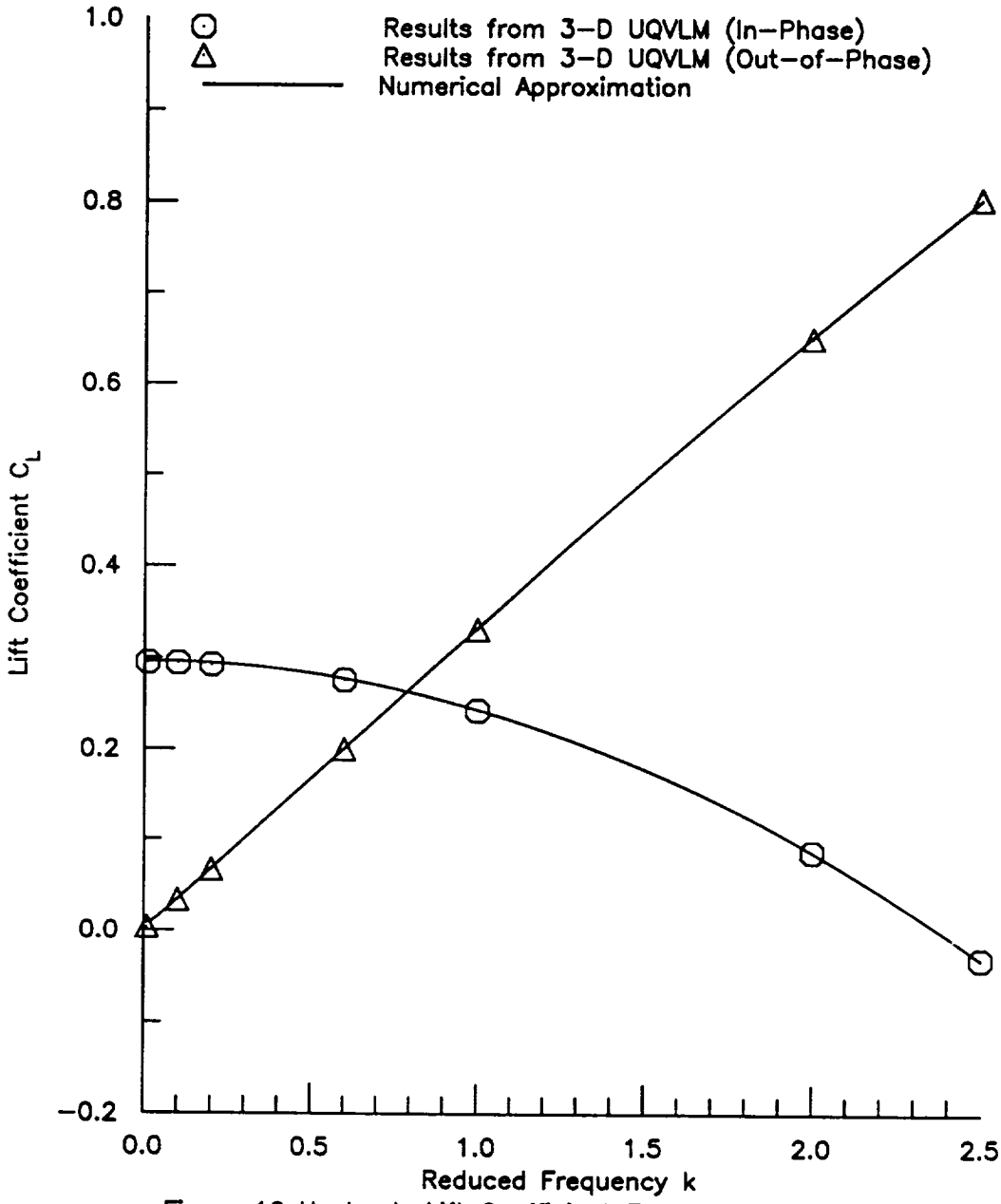

Figure 10 Unsteady Lift Coefficient For a 70-deg Delta Wing Pitching about Mid-Root chord at M = 0.4

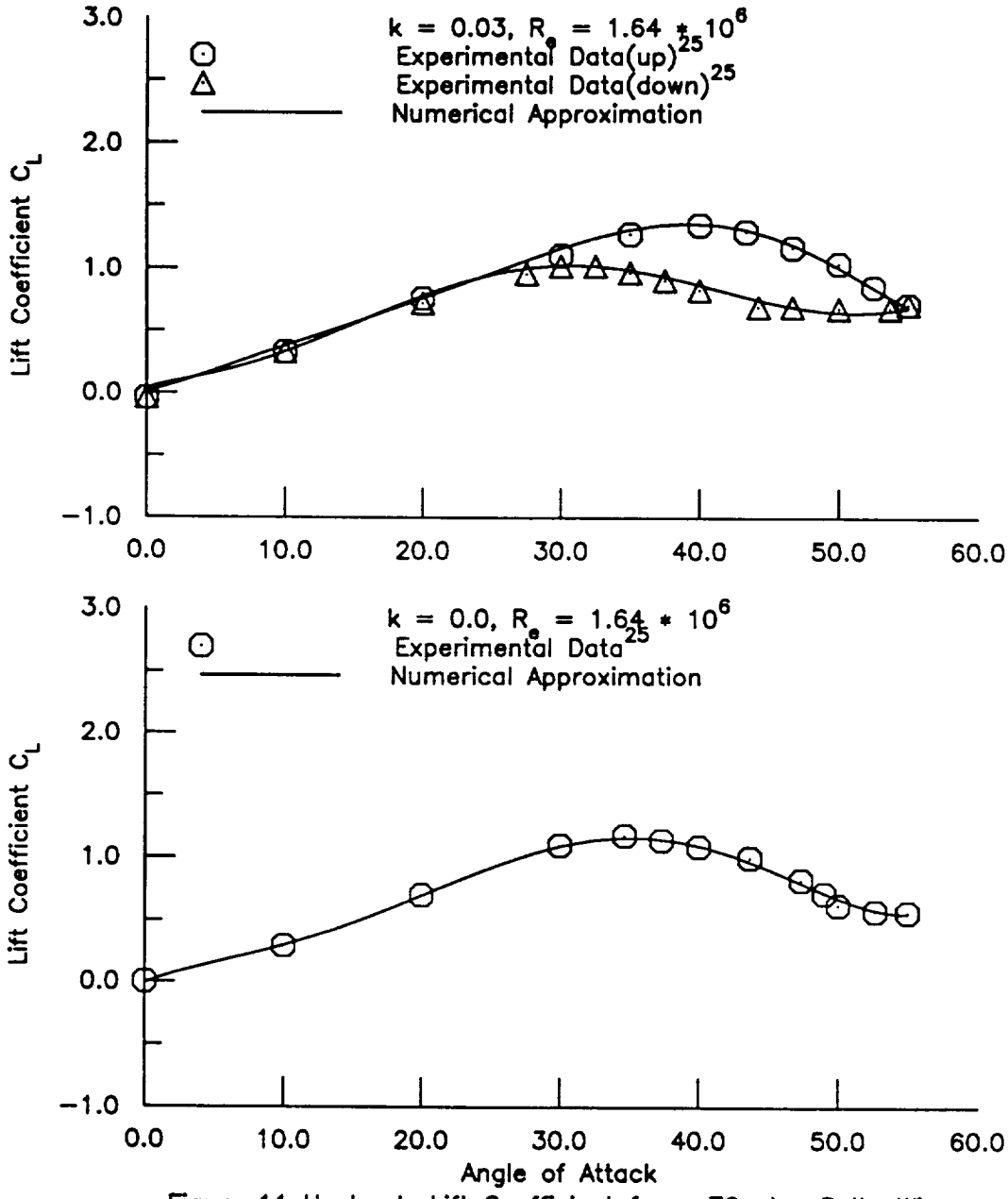

Figure 11 Unsteady Lift Coefficient for a 70–deg Delta Wing Pitching about 57% of Root Chord at Low Speed and Various Frequencies

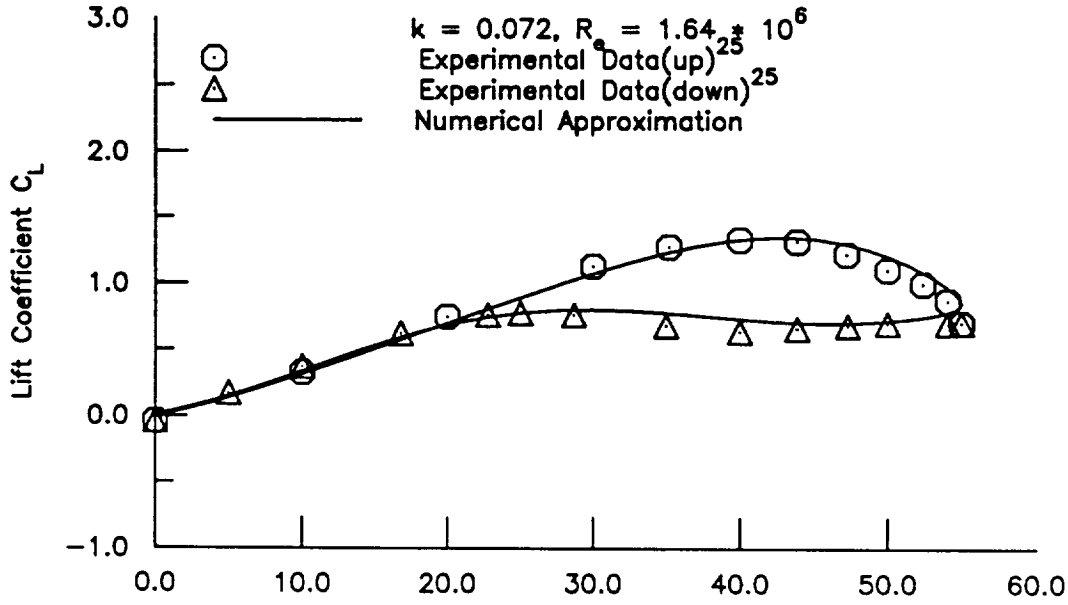

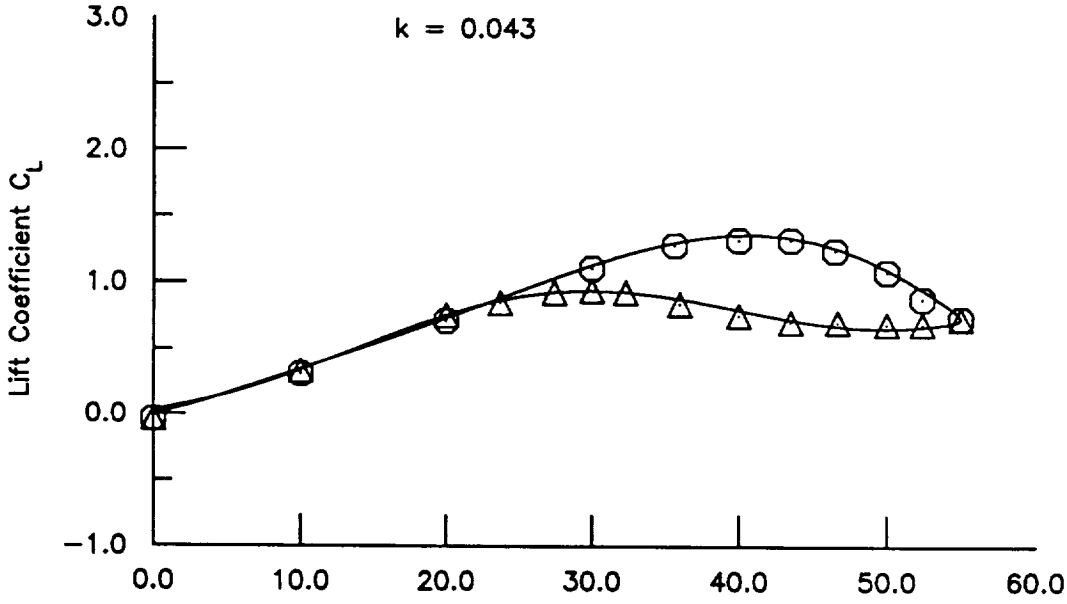

Figure 11 Continued.

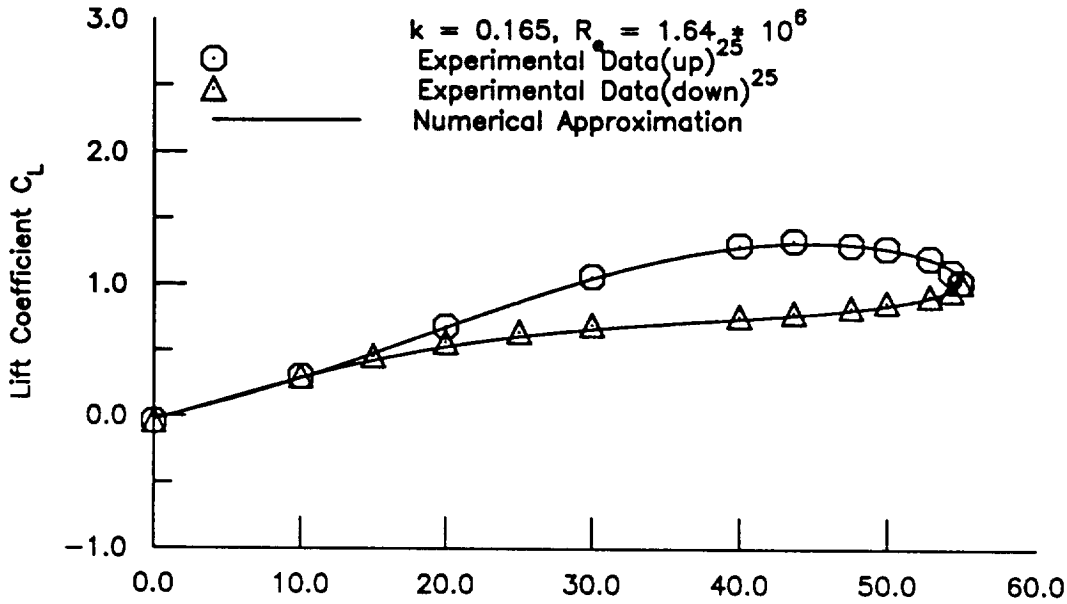

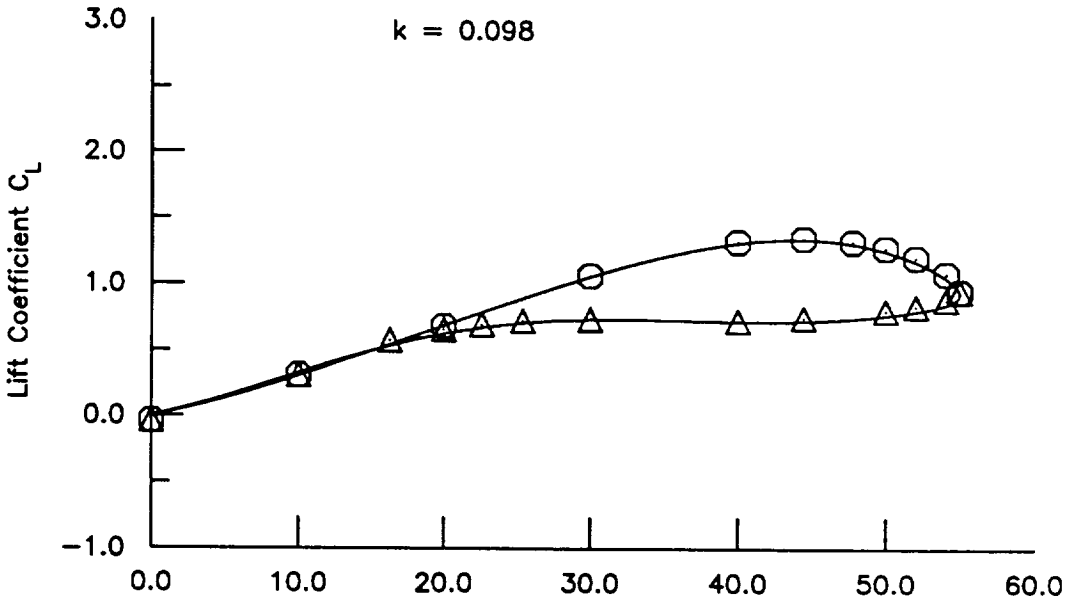

Figure 11 Concluded.

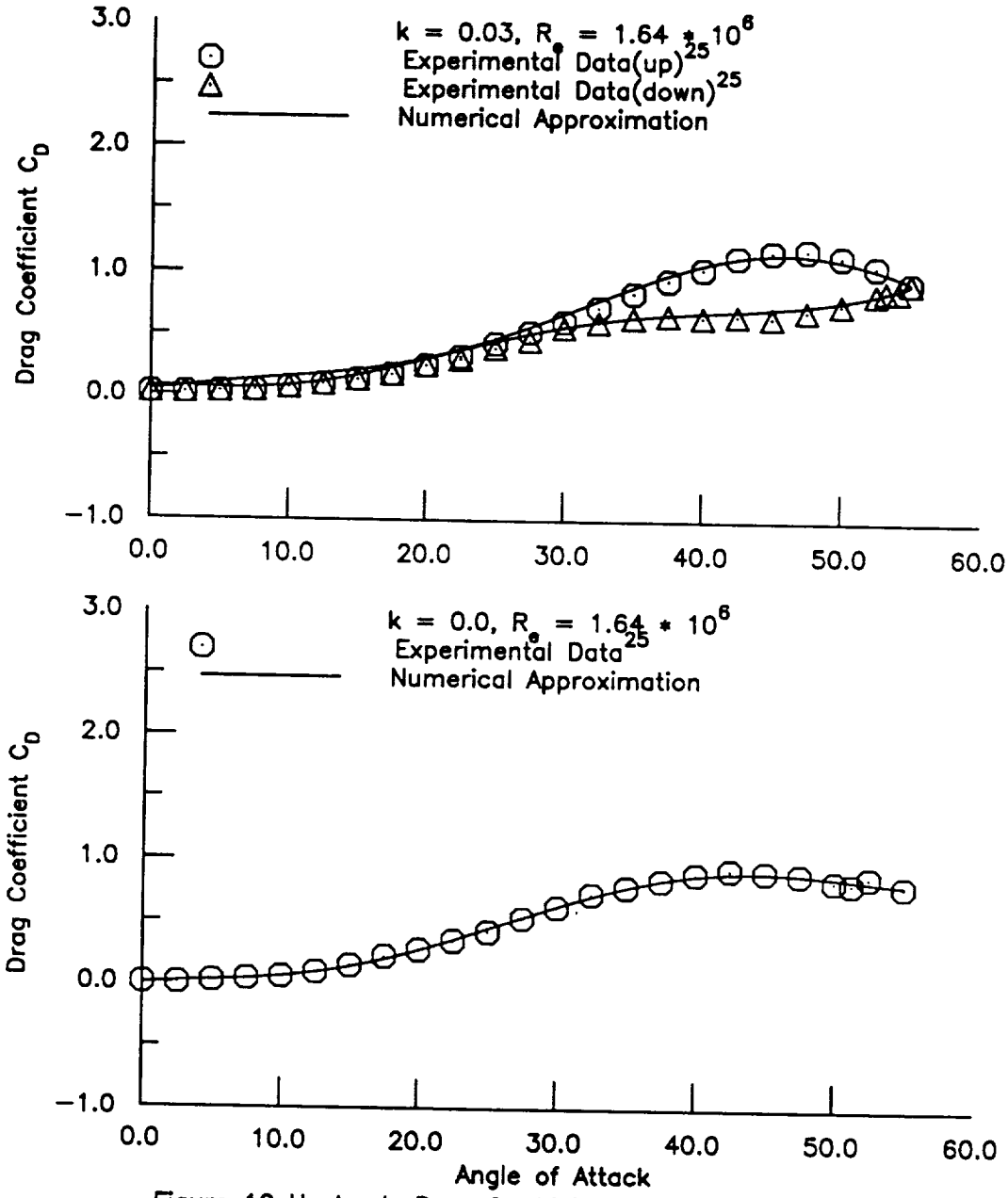

Figure 12 Unsteady Drag Coefficient for a 70−deg Delta Wing Pitching about 57% of Root Chord at Low Speed and Various Frequencies

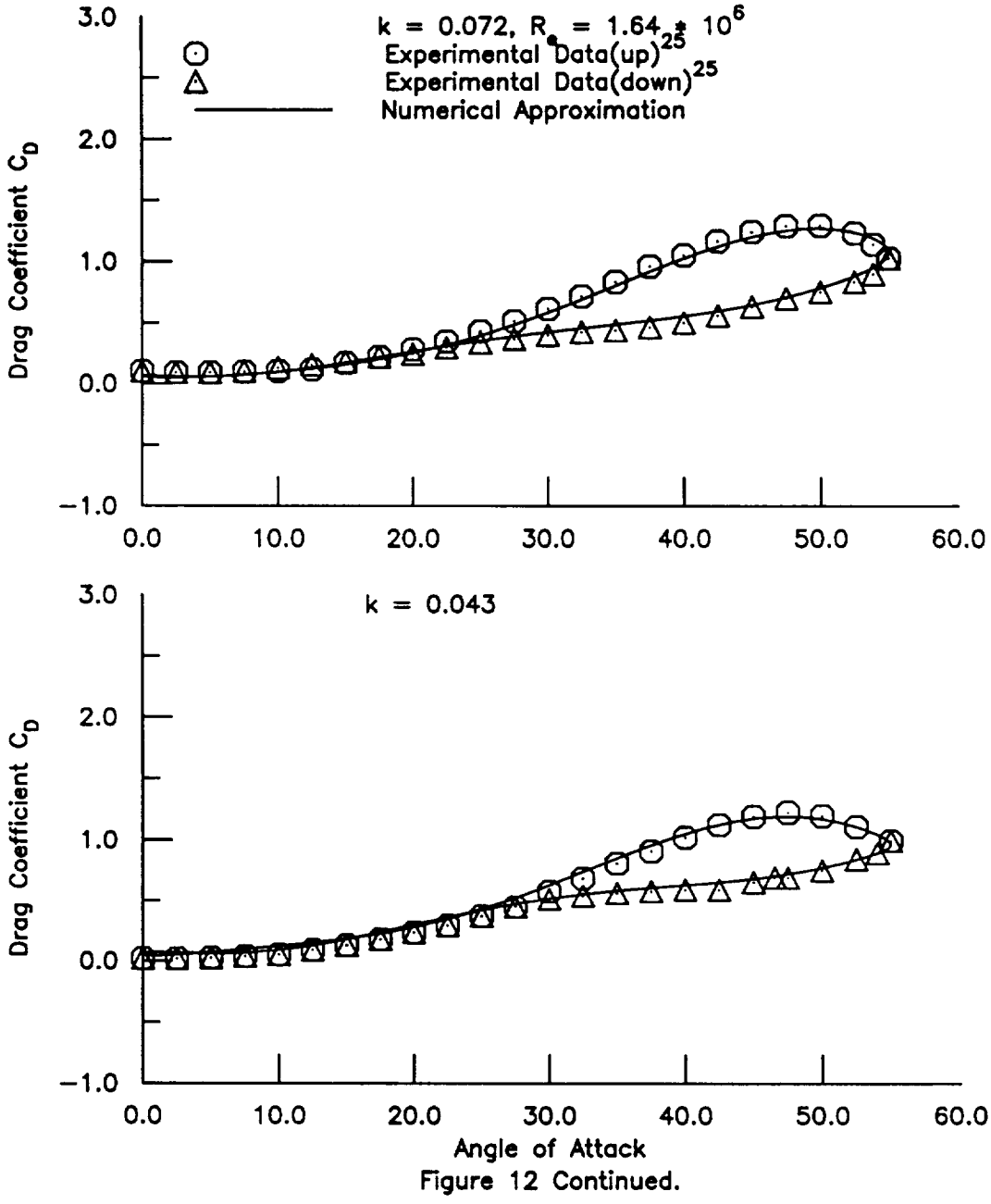

Figure 12 Continued.

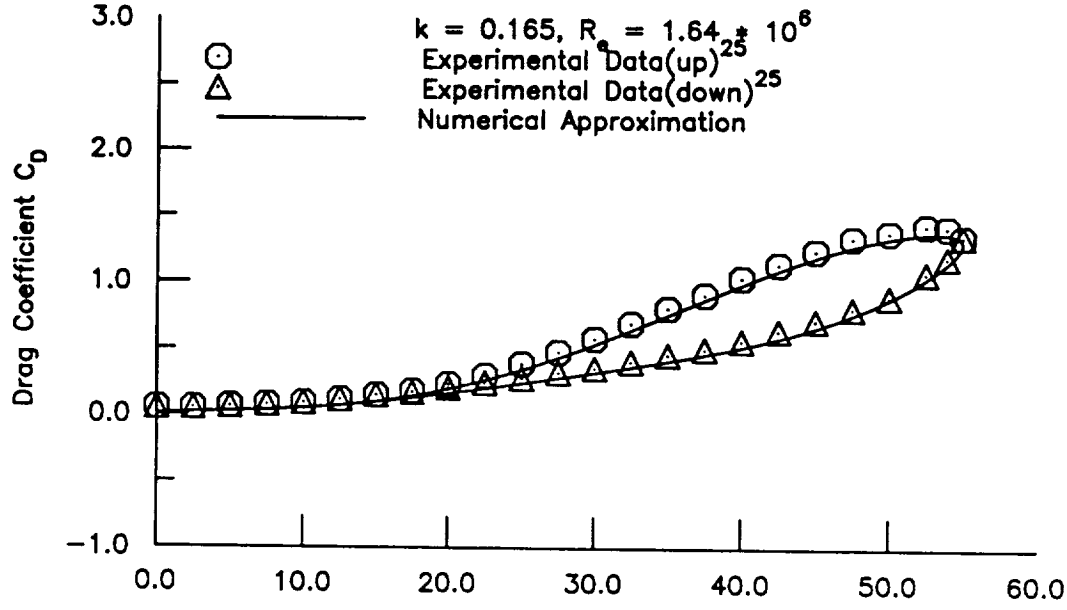

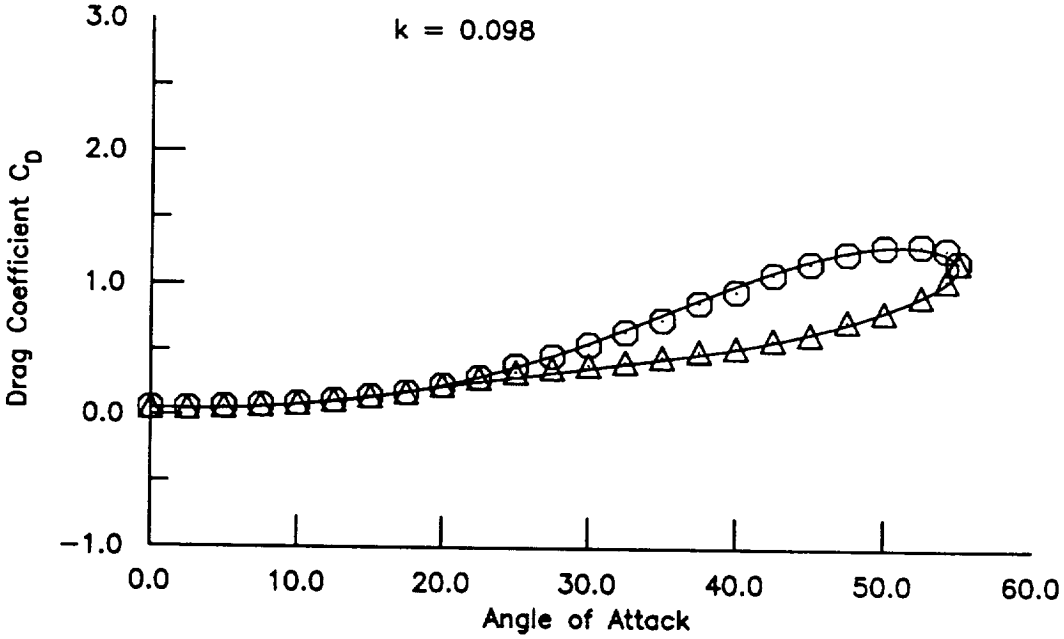

Figure 12 Concluded.

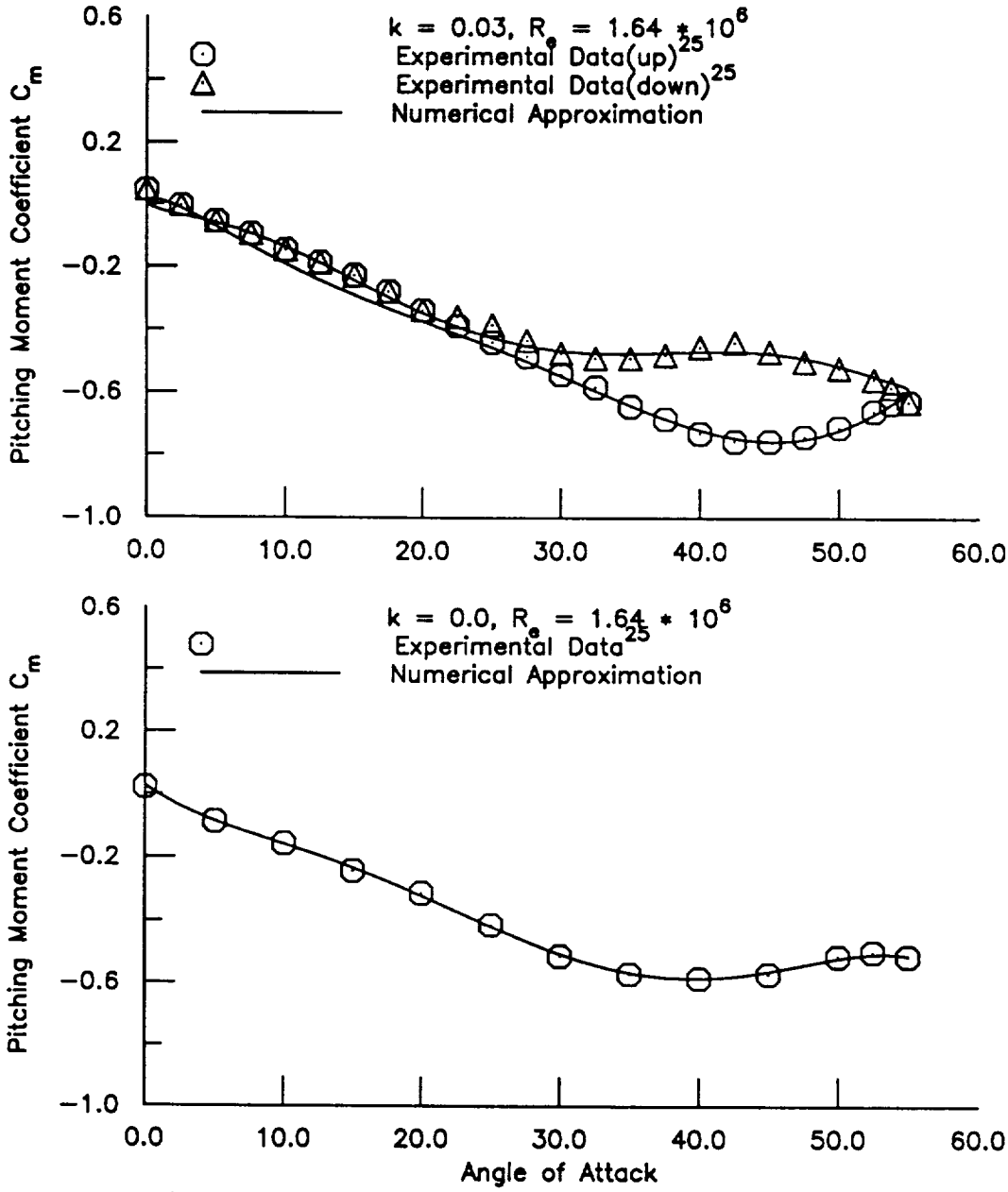

Figure 13 Unsteady Pitching Moment Coefficient for a 70−deg Delta Wing Pitching about 57% of Root Chord at Low Speed and Various Frequencies. Moment Center at 25% of Root Chord

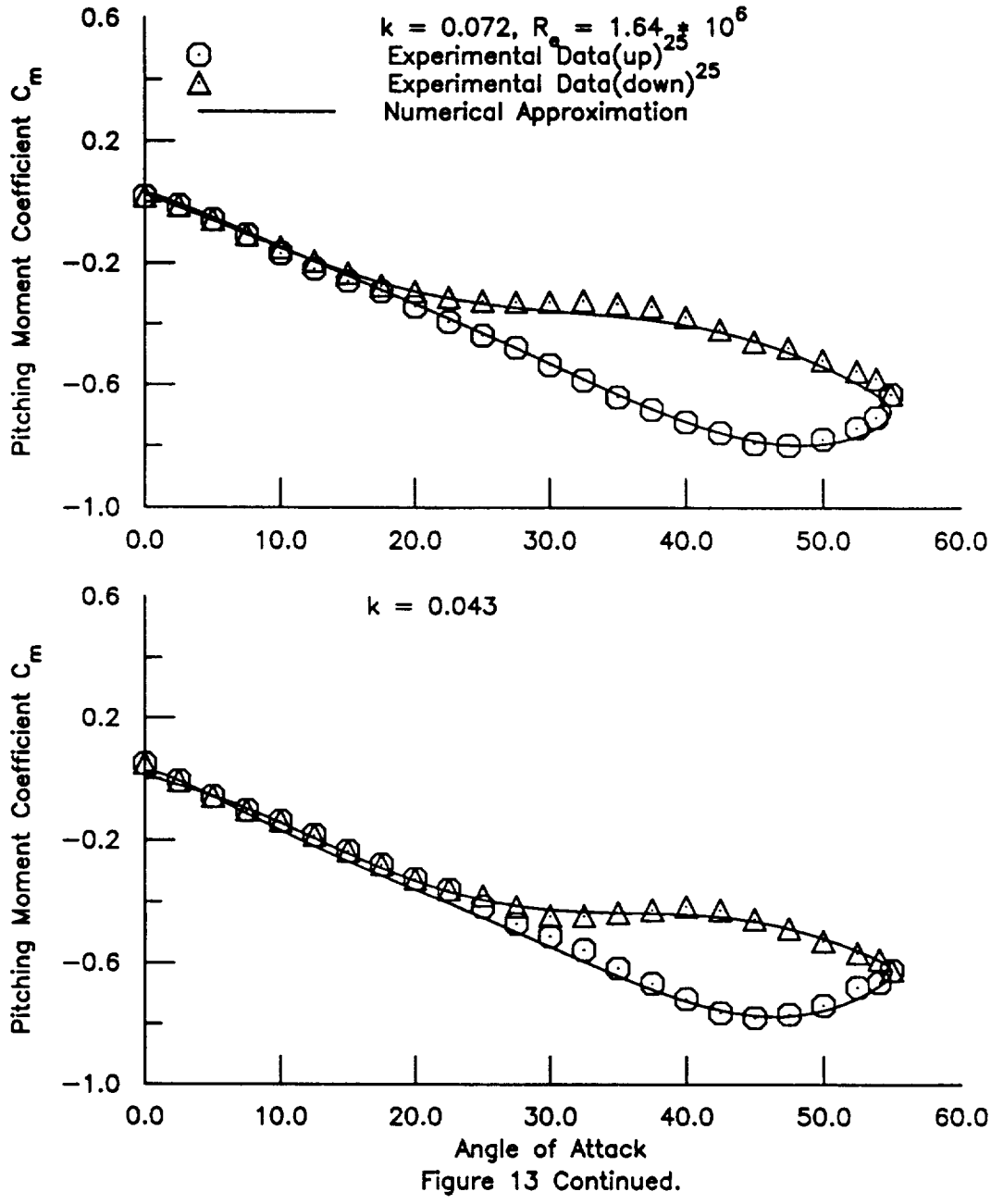

Figure 13 Continued.

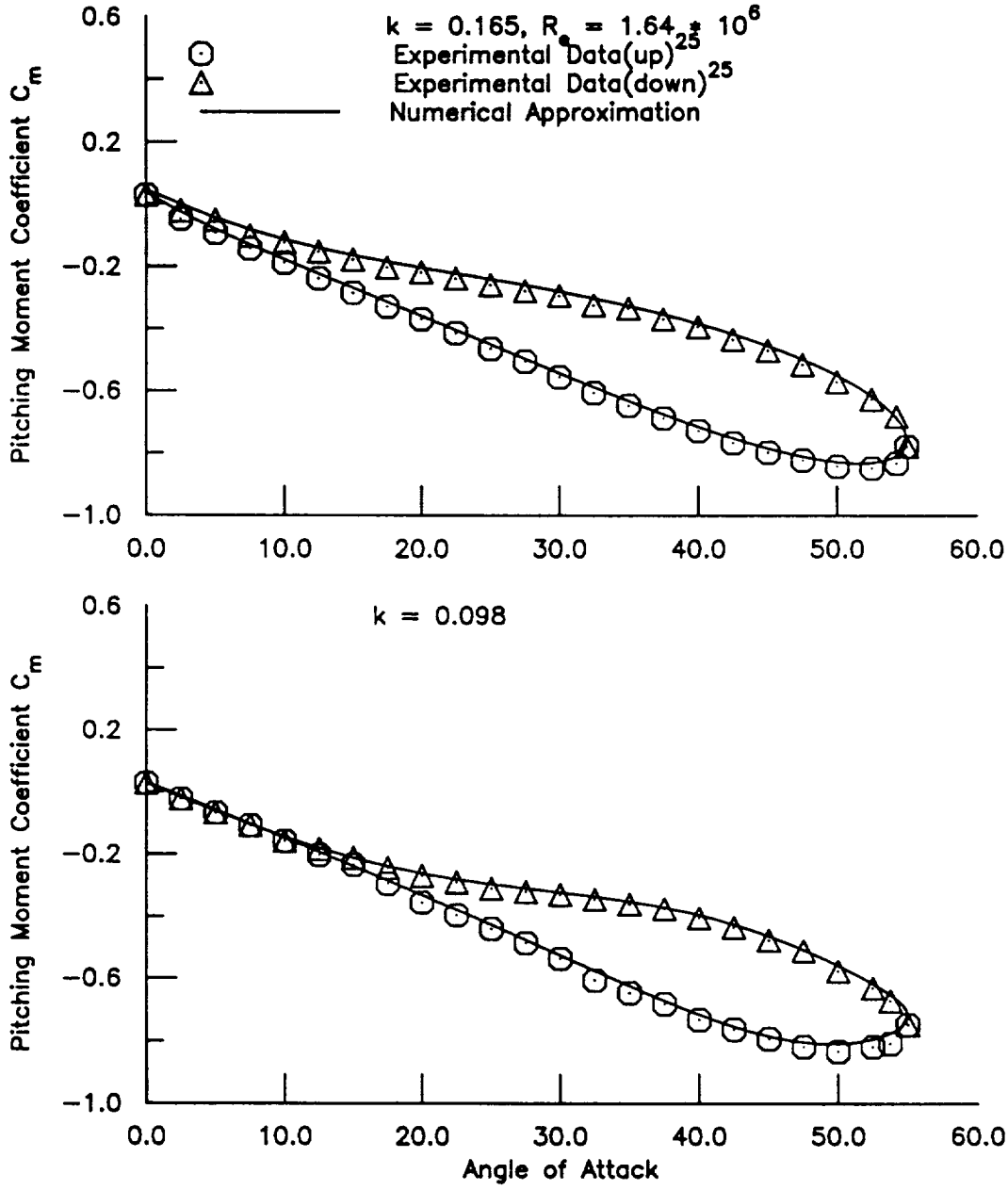

Figure 13 Concluded.

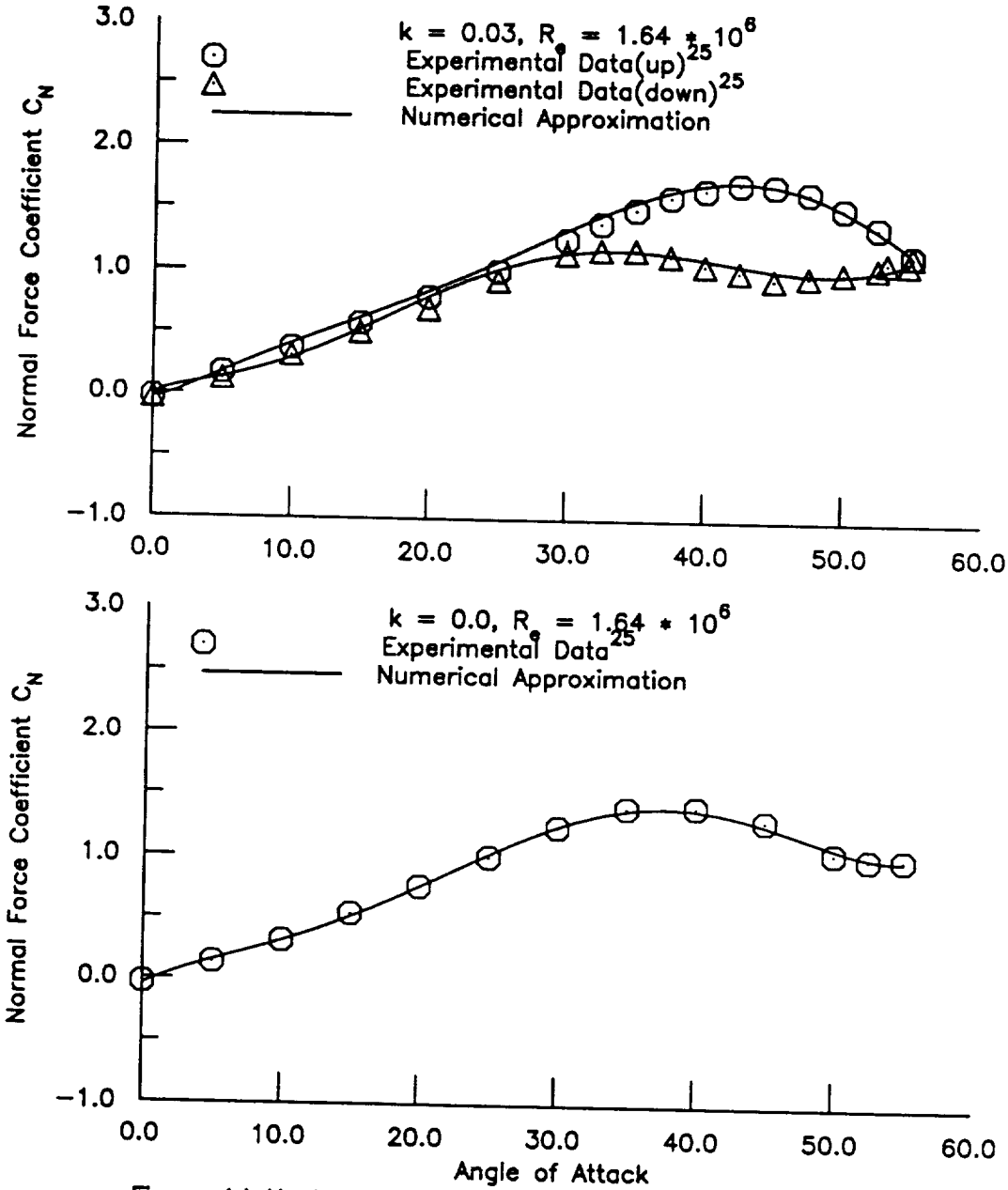

Figure 14 Unsteady Normal Force Coefficient for a 70–deg Delta Wing Pitching about 57% of Root Chord at Low Speed and Various Frequencies

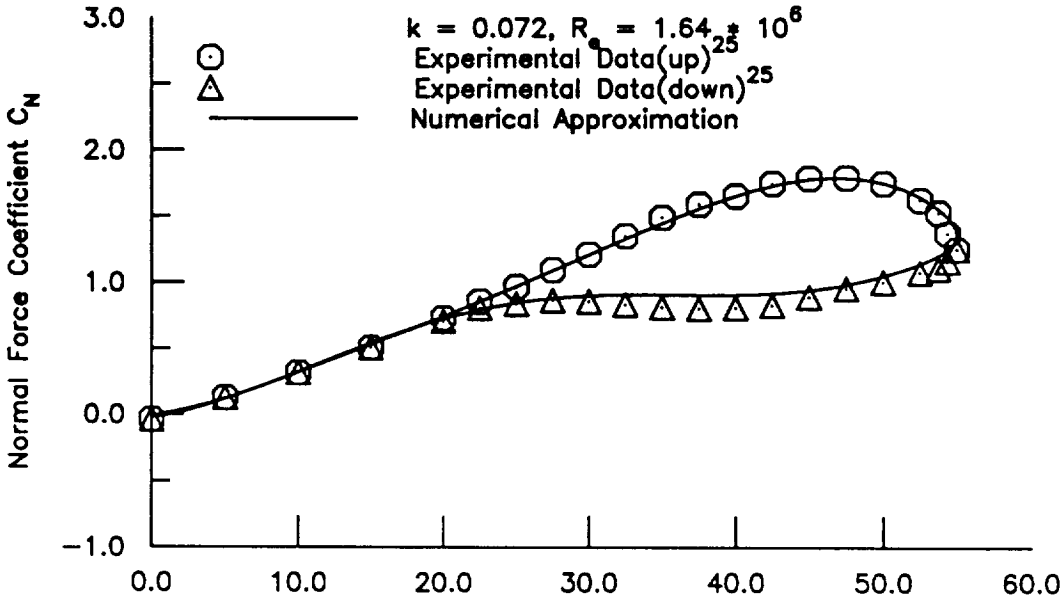

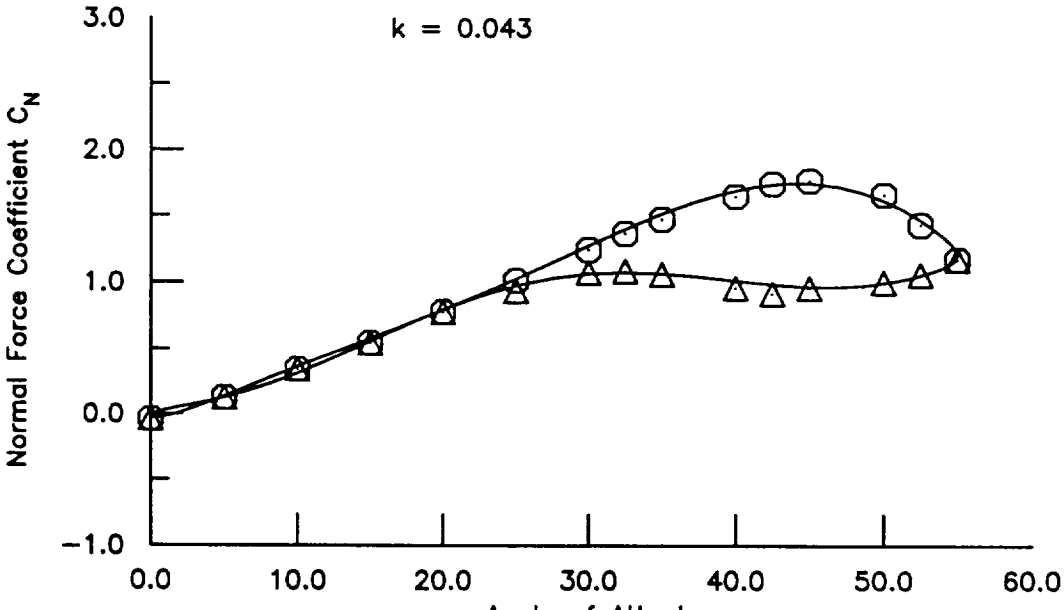

Figure 14 Continued.

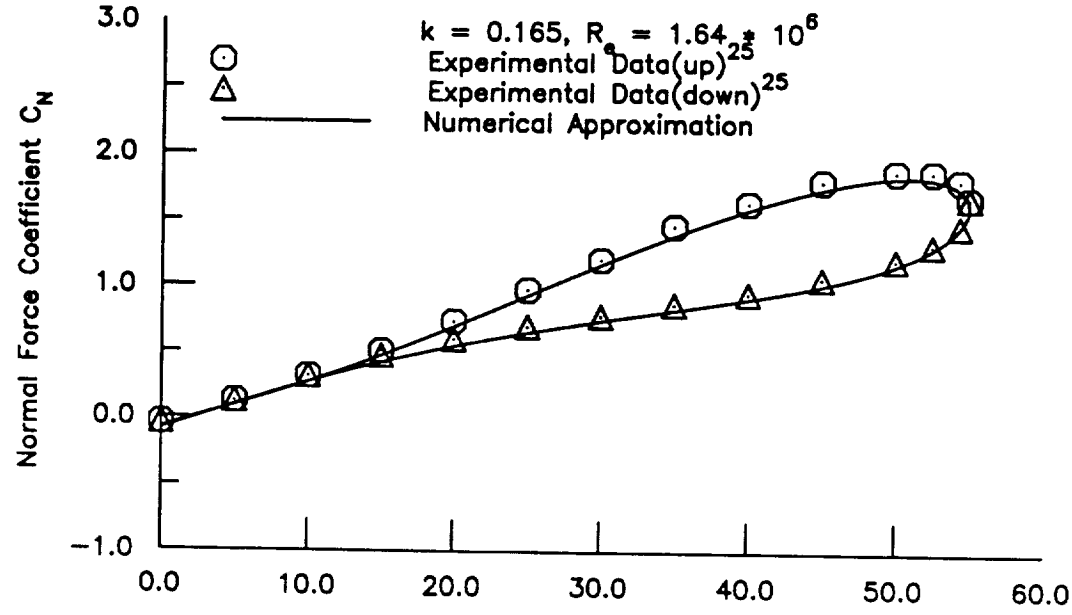

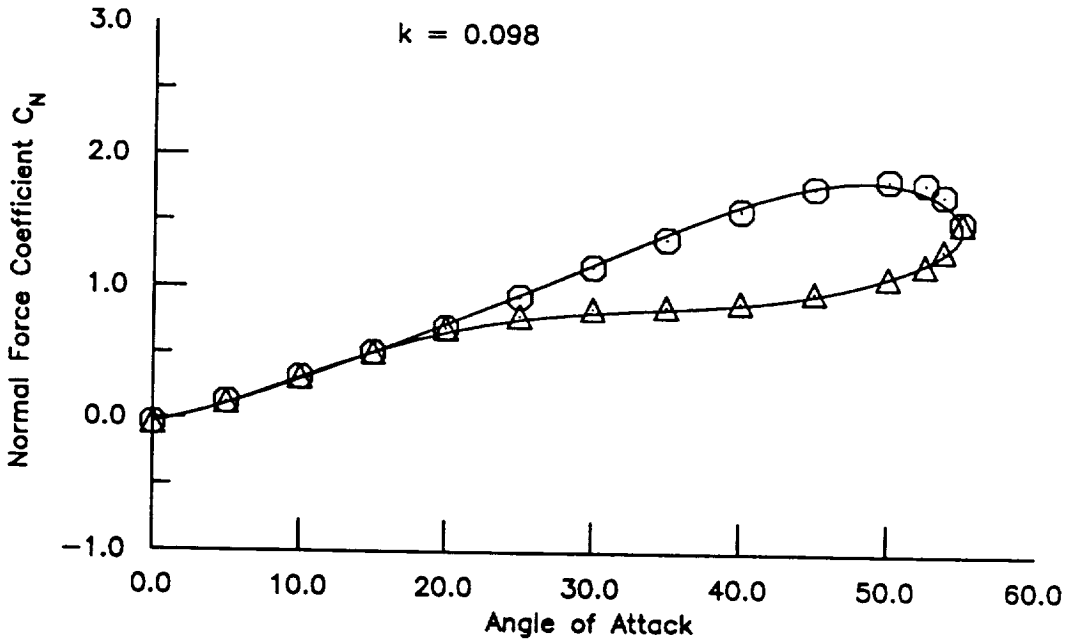

Figure 14 Concluded.

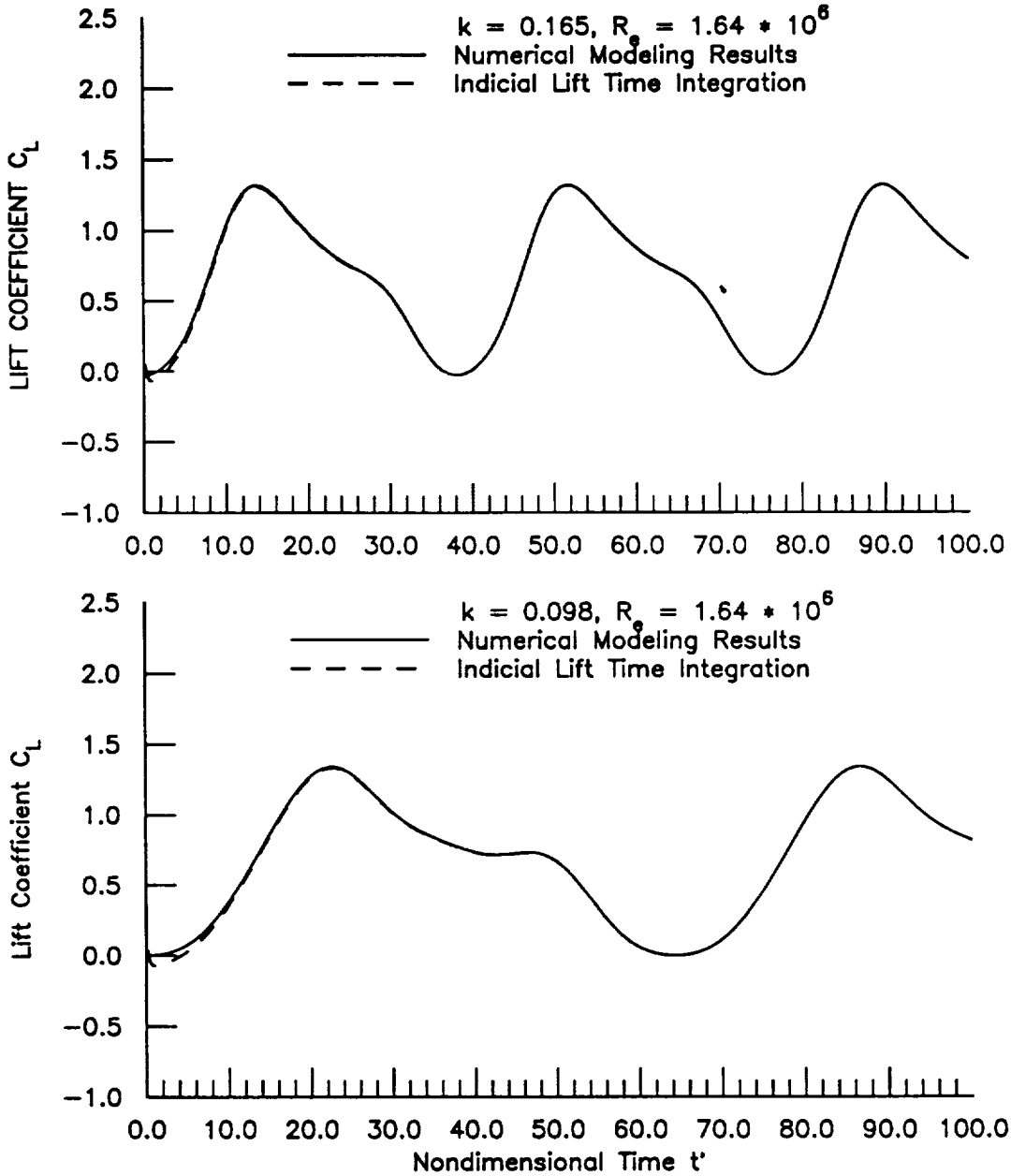

Figure 15 Unsteady Lift Coefficients from Numerical Modeling and Indicial Time Integration for a 70–deg Delta Wing in Harmonic Pitching Oscillation about 57% of Root Chord at Low Speed

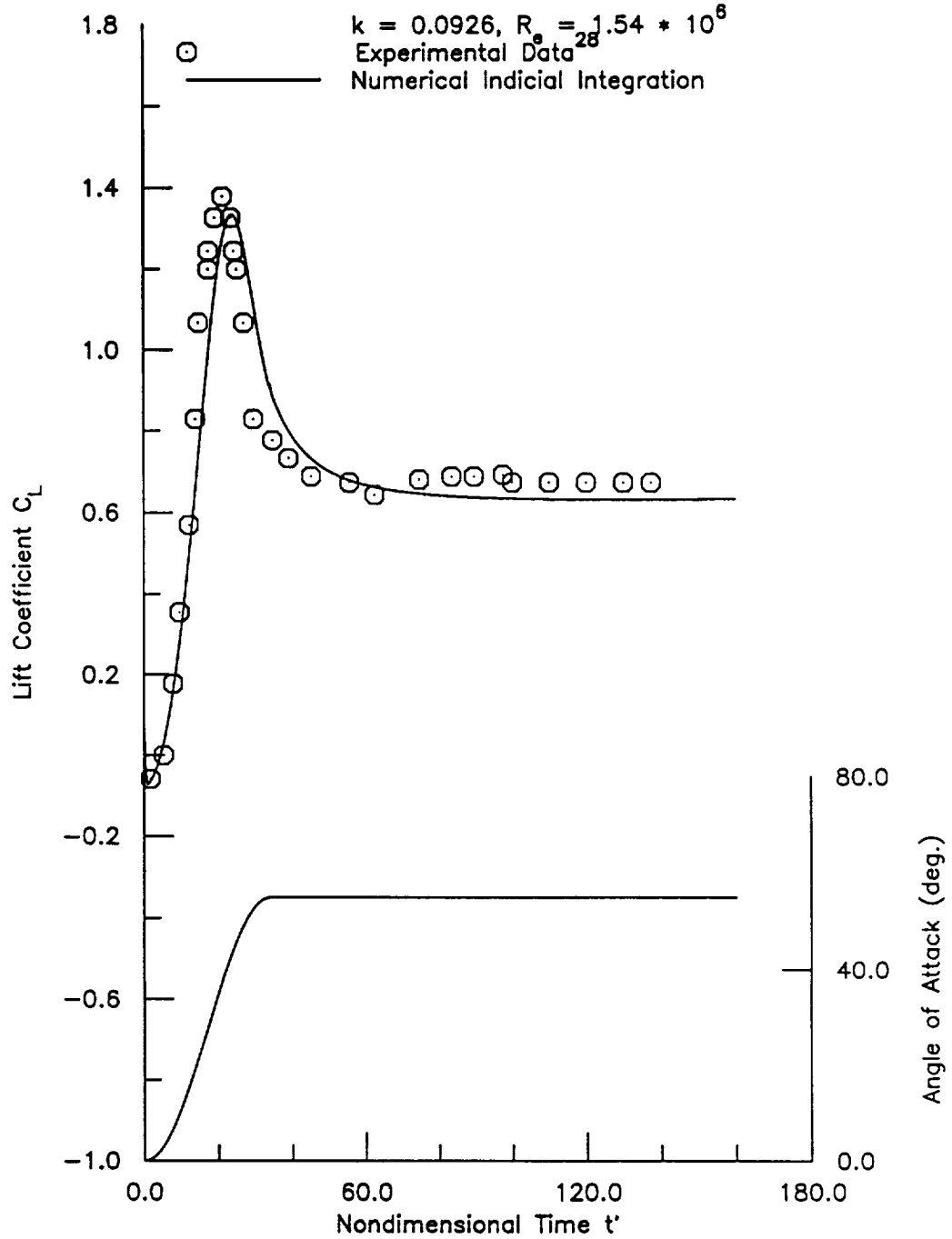

Figure 16 Unsteady Lift Coefficients from Indicial Lift Model and Experiment for a 70−deg Delta Wing in Harmonic Ramp Motion at Low Speed

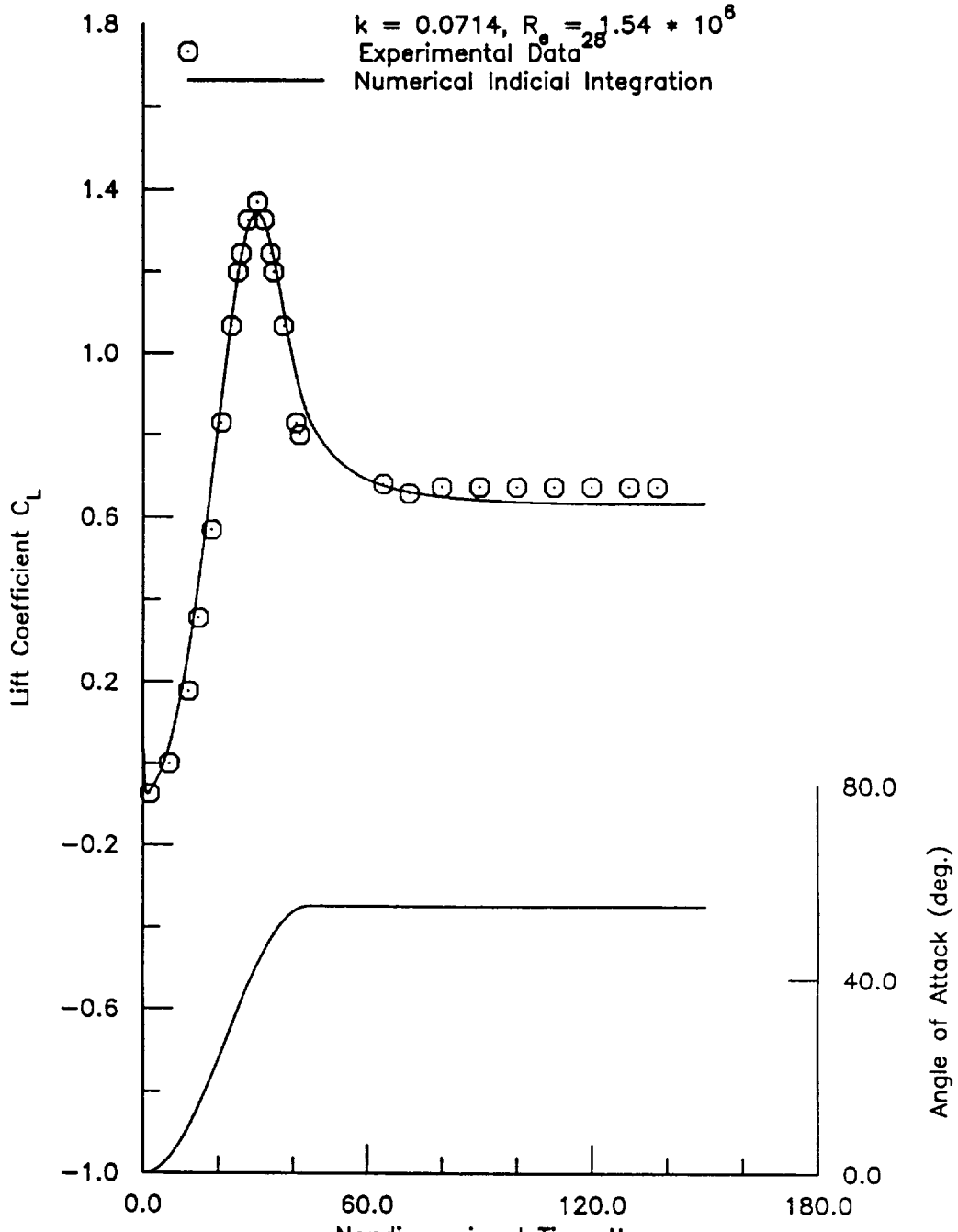

Figure 16 Concluded.

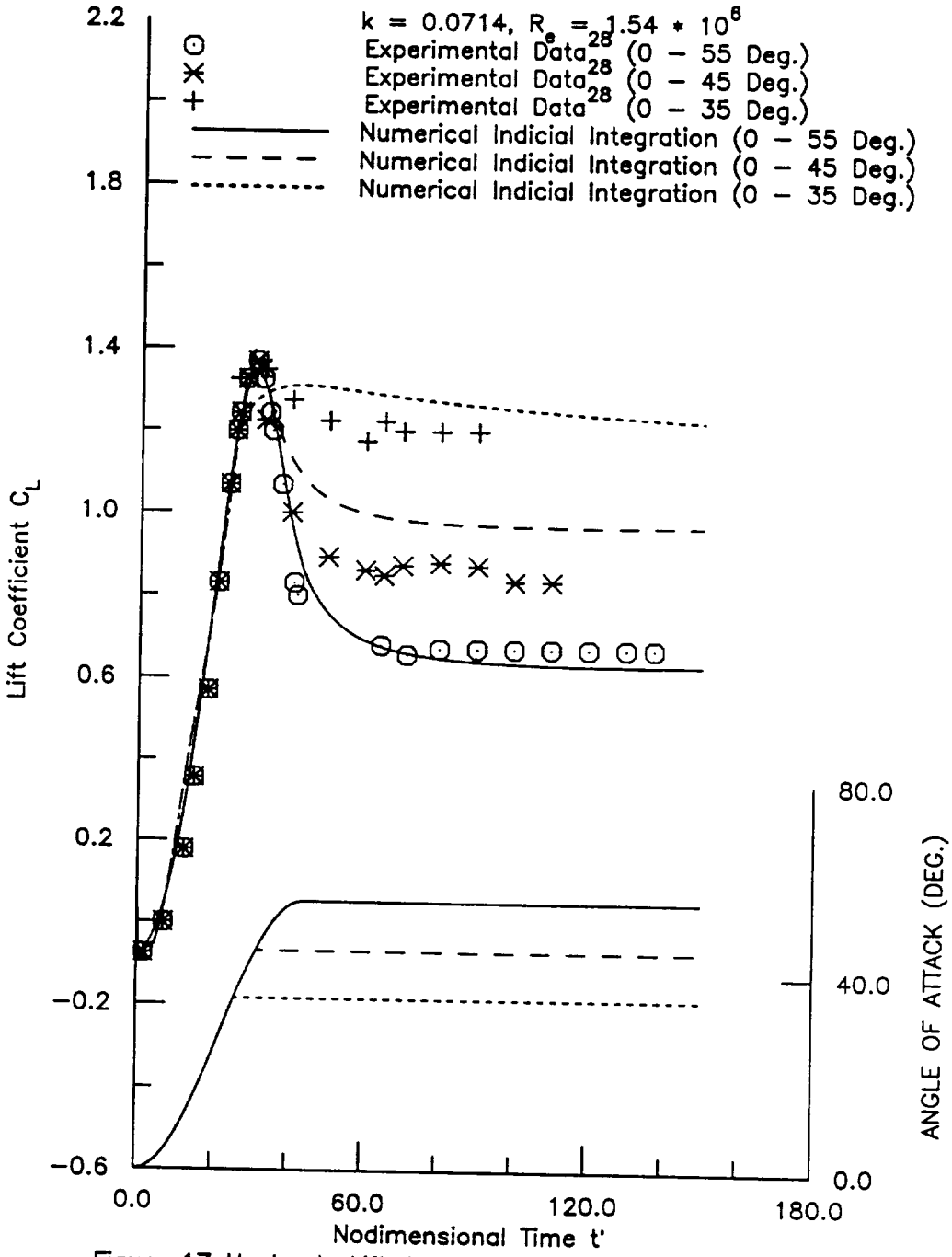

Figure 17 Unsteady Lift Coefficients from Indicial Lift Model and Experiment for a 70–deg Delta Wing in Harmonic Ramp Motion at Low Speed

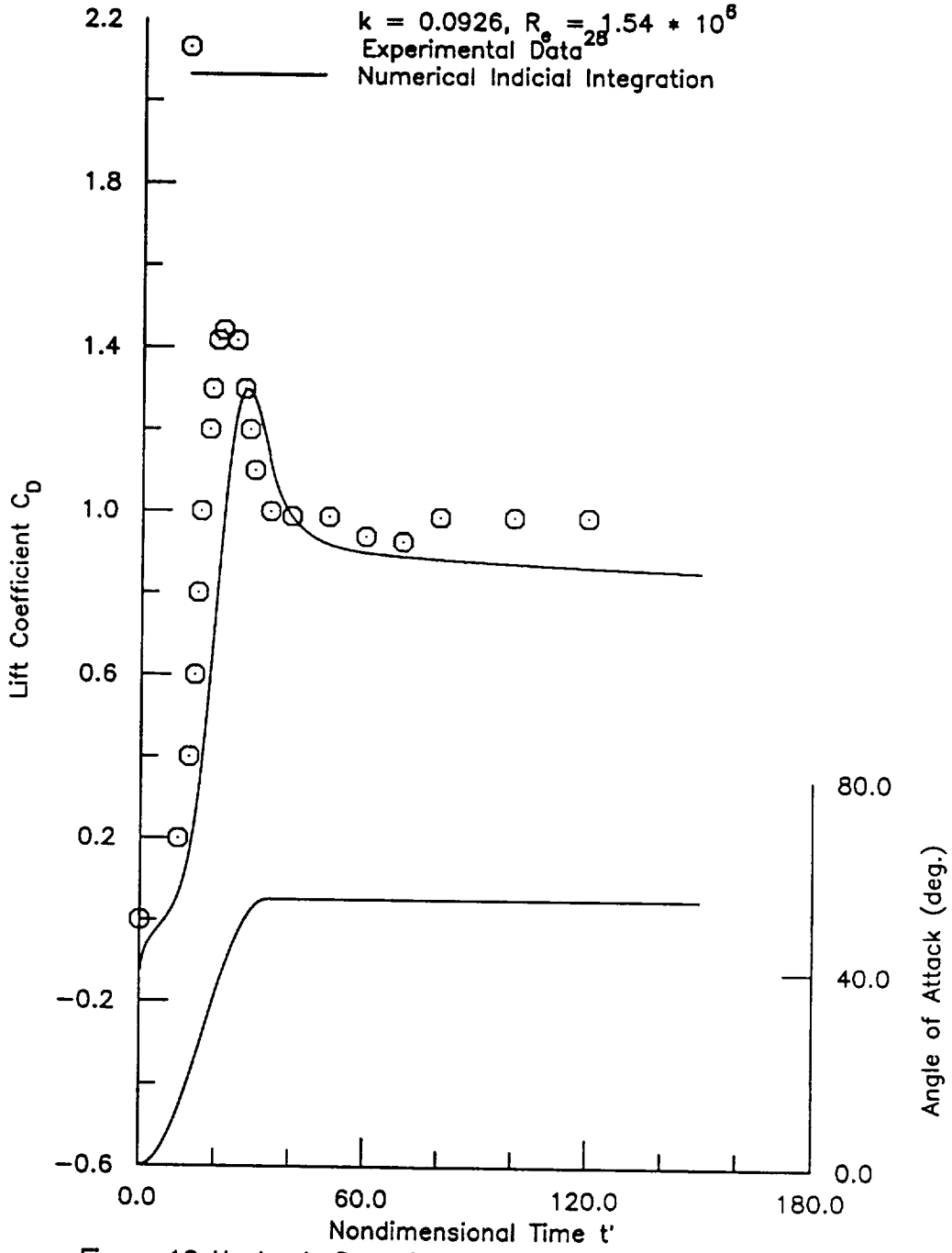

Figure 18 Unsteady Drag Coefficients from Indicial Drag Model and Experiment for a 70−deg Delta Wing in Harmonic Ramp Motion at Low Speed

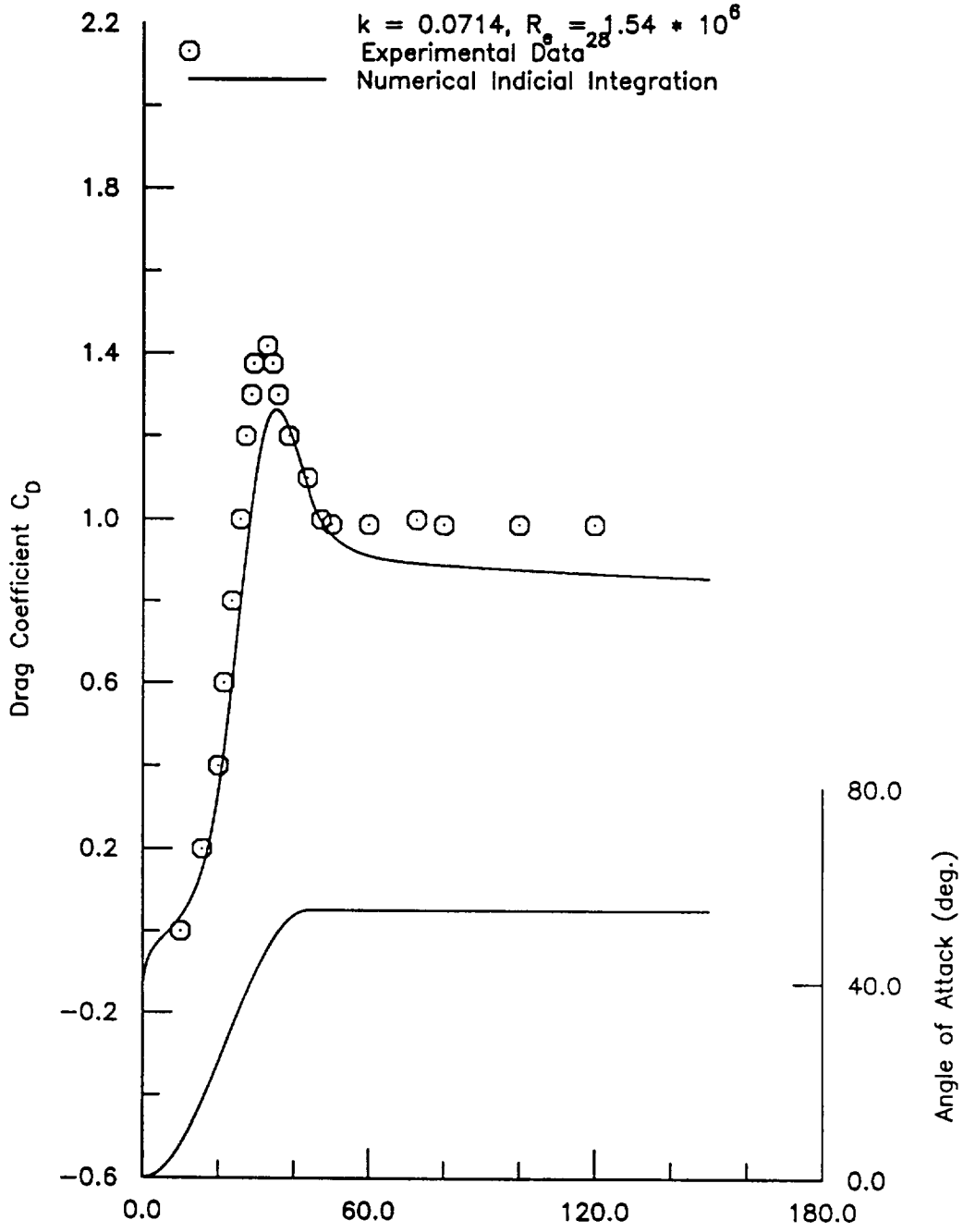

Figure 18 Concluded.

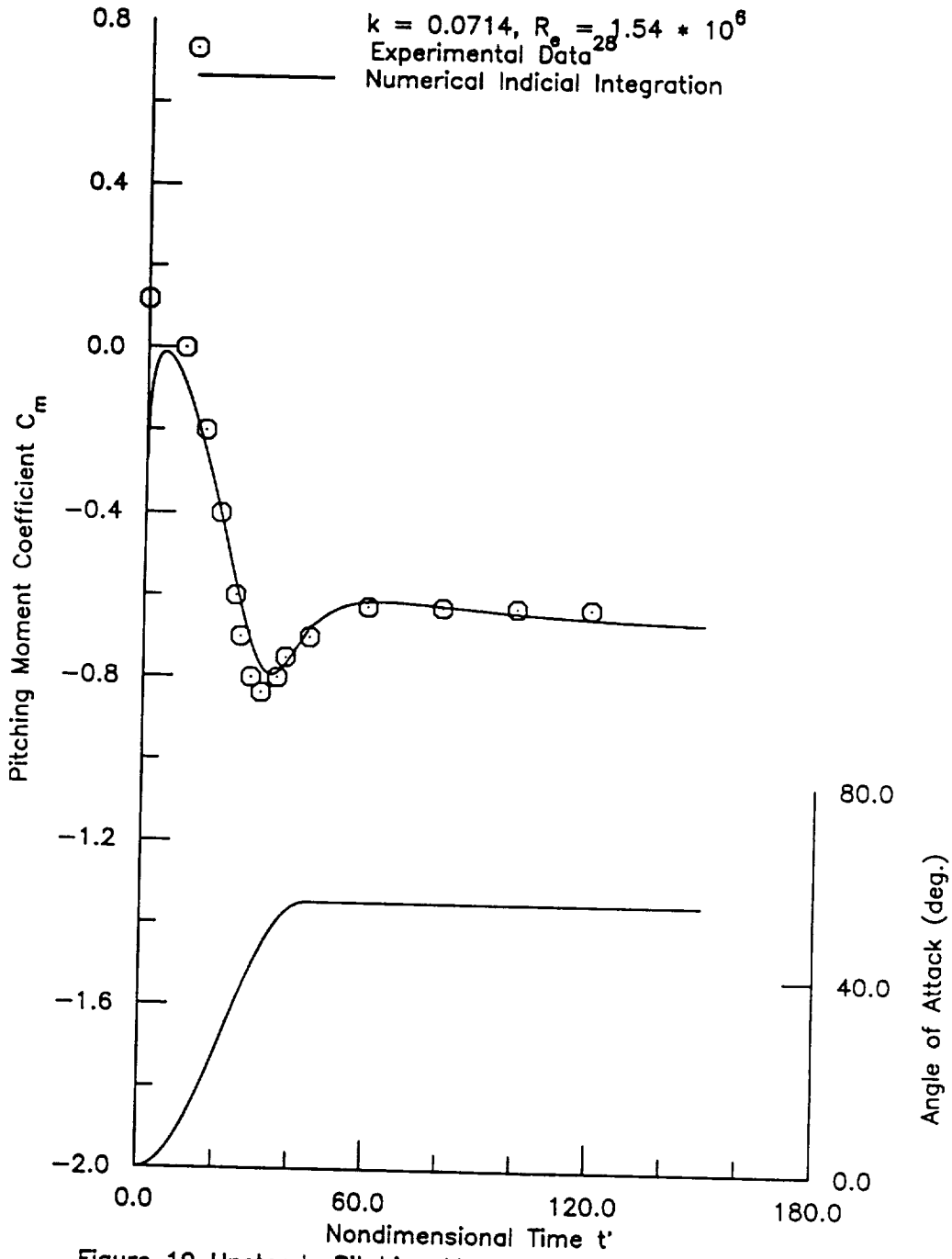

Figure 19 Unsteady Pitching Moment Coefficients from Indicial Pitching Model and Experiment for a 70−deg Delta Wing in Harmonic Ramp Motion at Low Speed. Moment Center at 25% of Root Chord

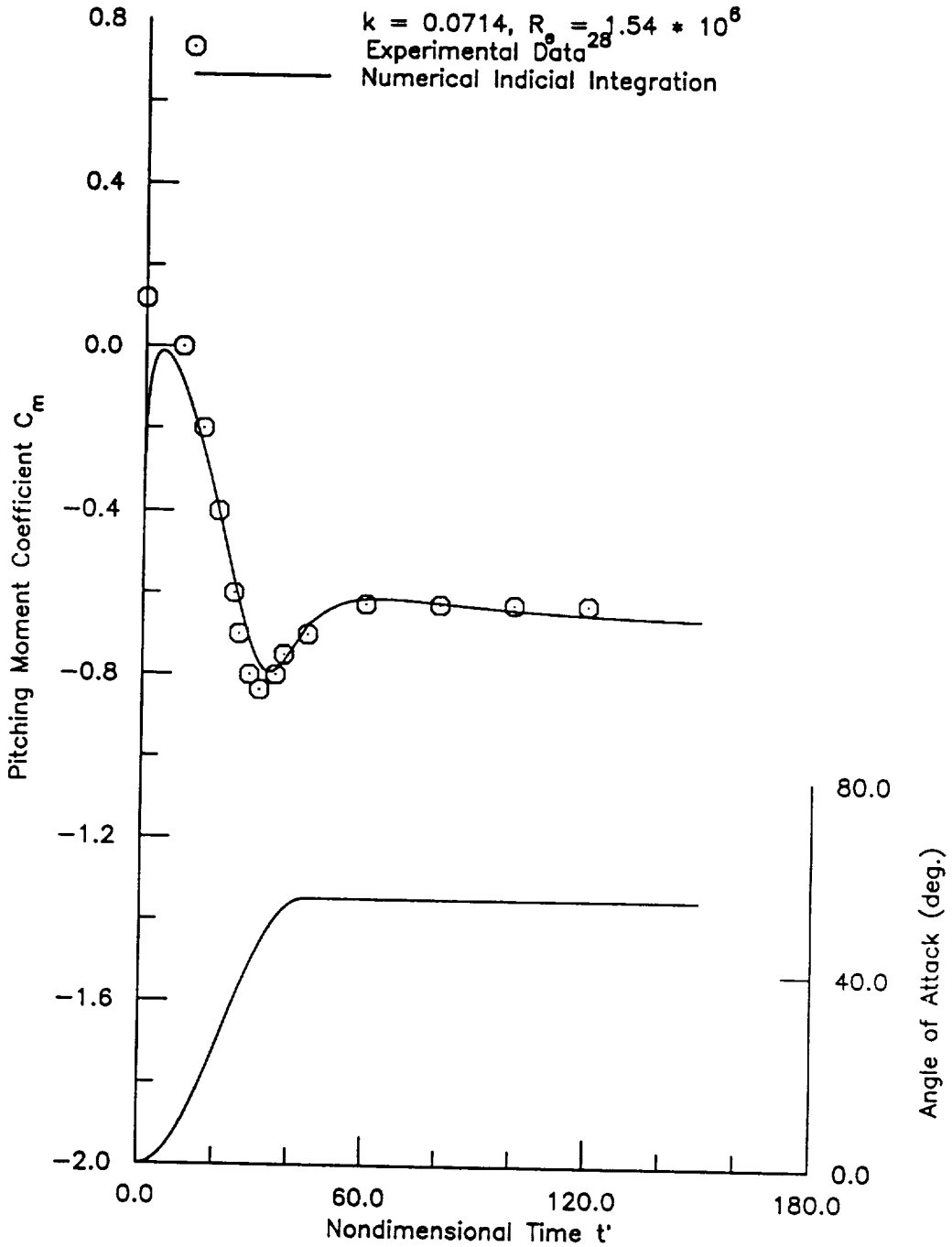

Figure 19 Concluded.

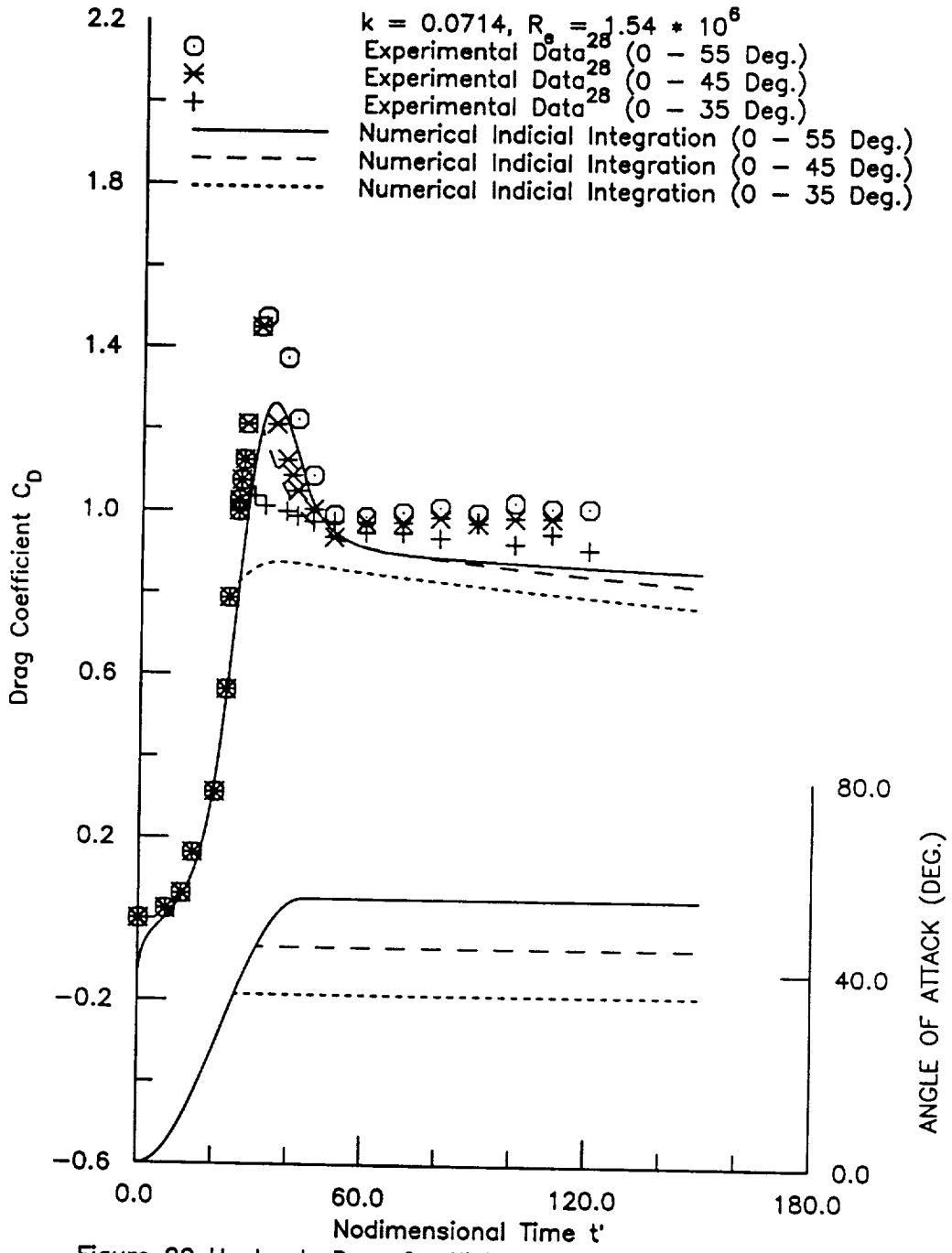

Figure 20 Unsteady Drag Coefficients from Indicial Drag Model and Experiment for a 70–deg Delta Wing in Harmonic Ramp Motion at Low Speed

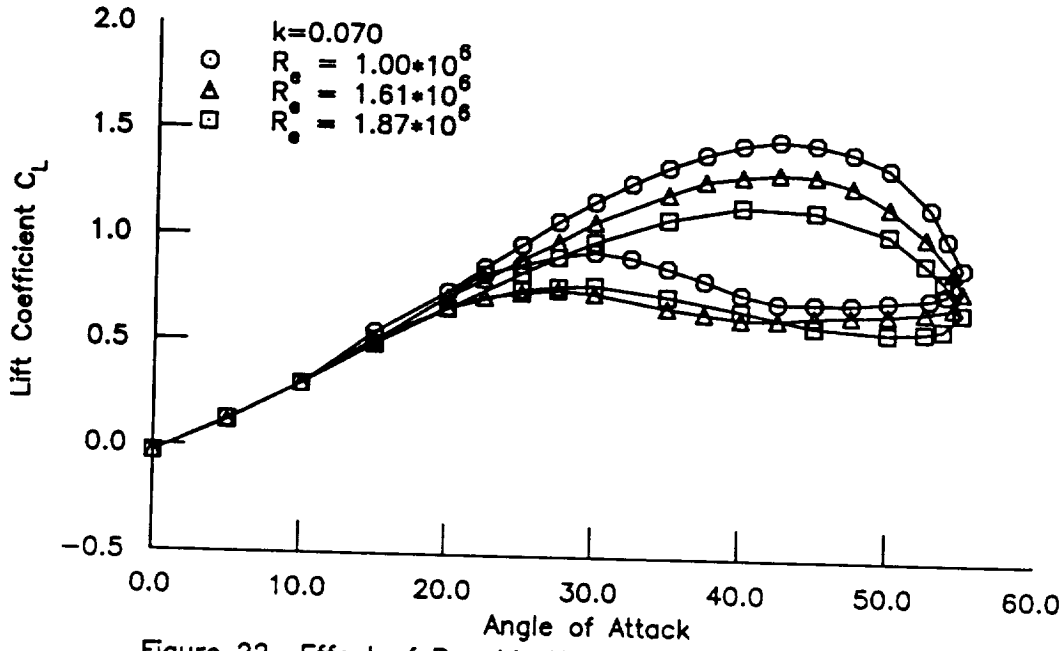

Figure 22 Effect of Renolds Number on Dynamic Lift Coefficient

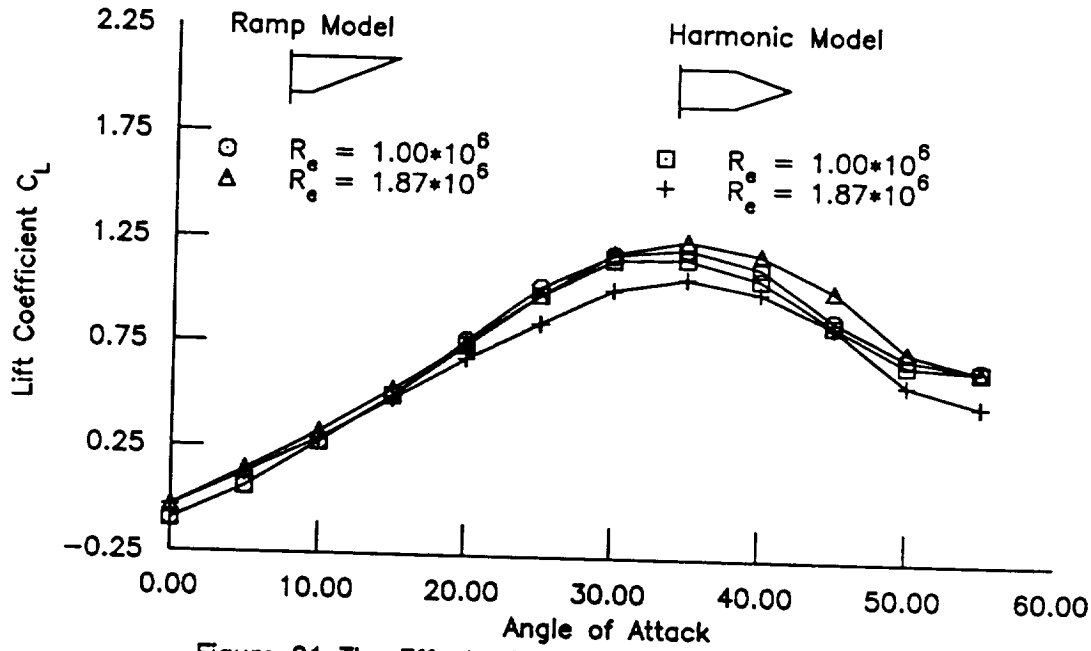

Figure 21 The Effect of Reynolds Number on The Static Lift Coefficient for Two Different Delta Wing Models

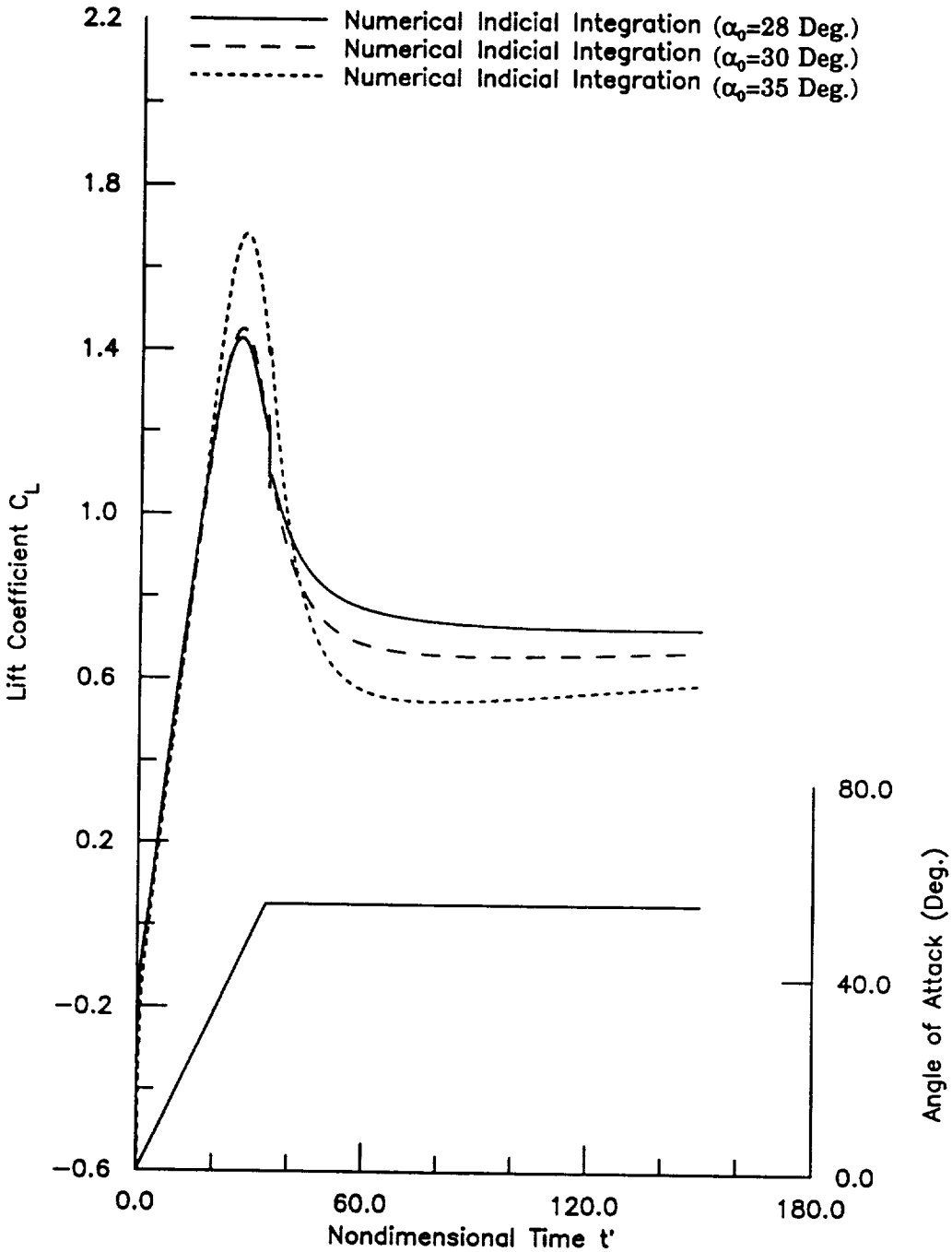

Figure 23 Unsteady Lift Coefficients from Indicial Lift Model for a 70–deg Delta Wing in Linear Ramp Motion

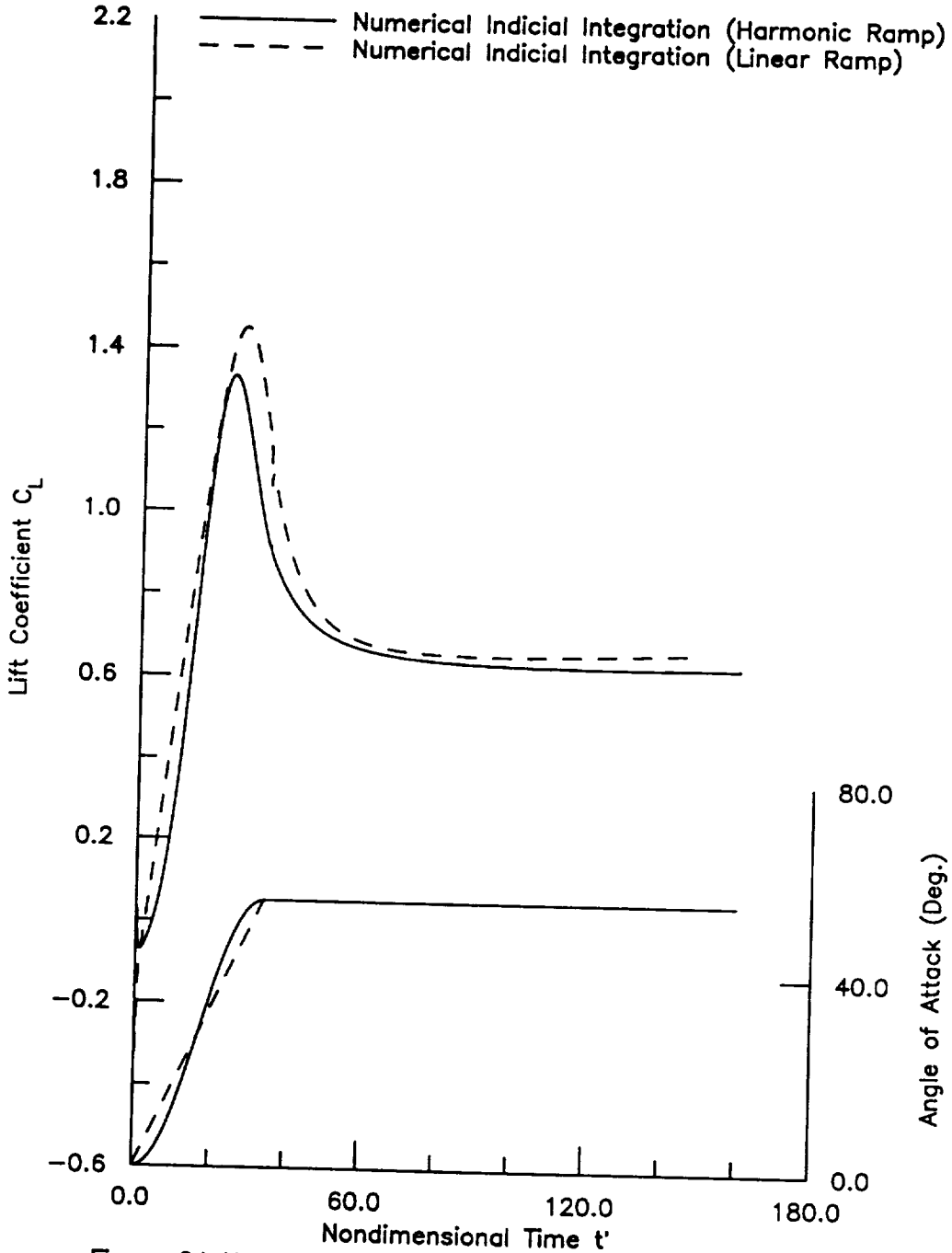

Figure 24 Unsteady Lift Coefficients from Indicial Lift Model for a 70–deg Delta Wing in Both Linear and Harmonic Ramp Motion

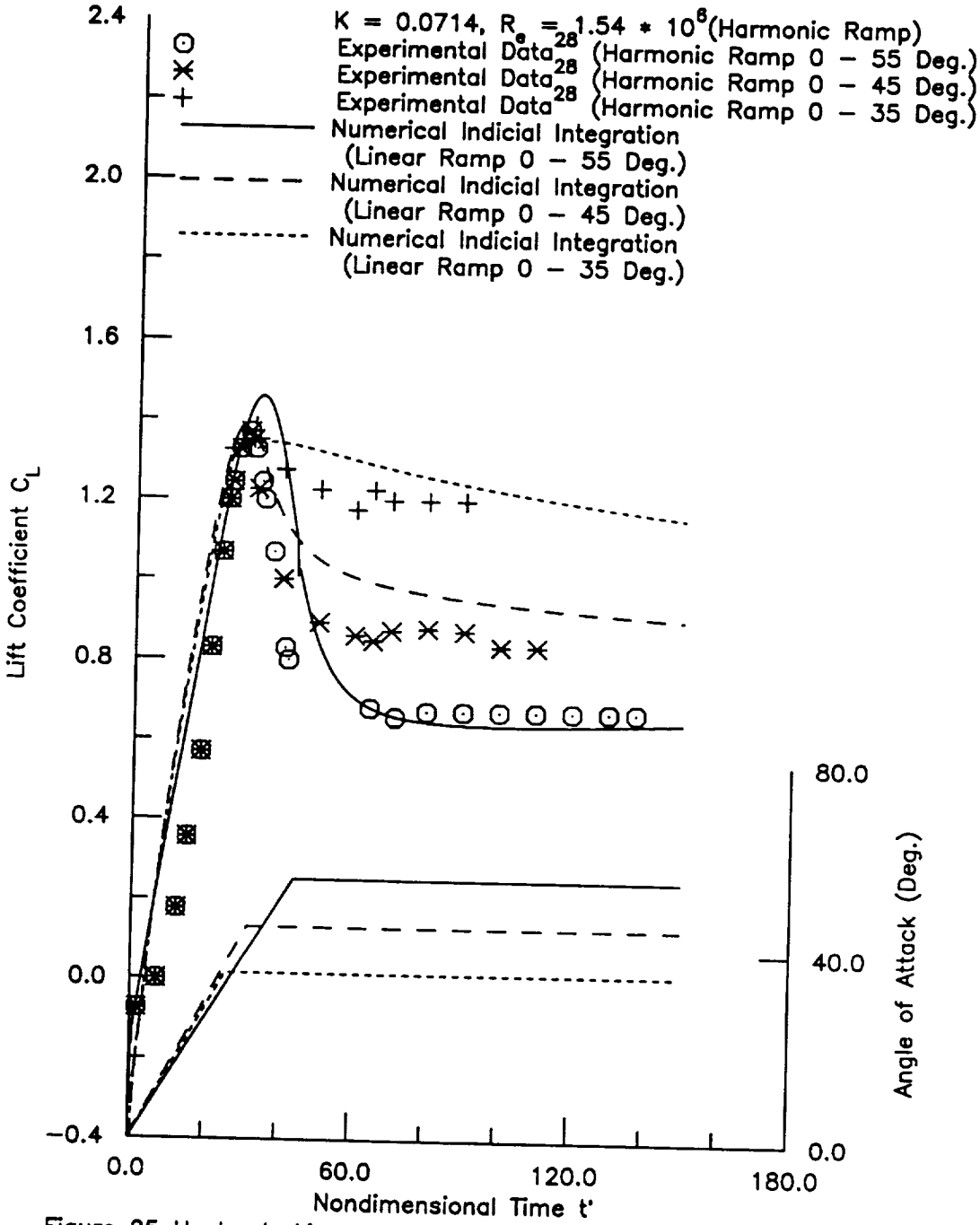

Figure 25 Unsteady Linear Ramp Lift Coefficients from Indicial Lift Model and Experiment of Harmonic Ramp motion for a 70–deg Delta Wing at Low Speed

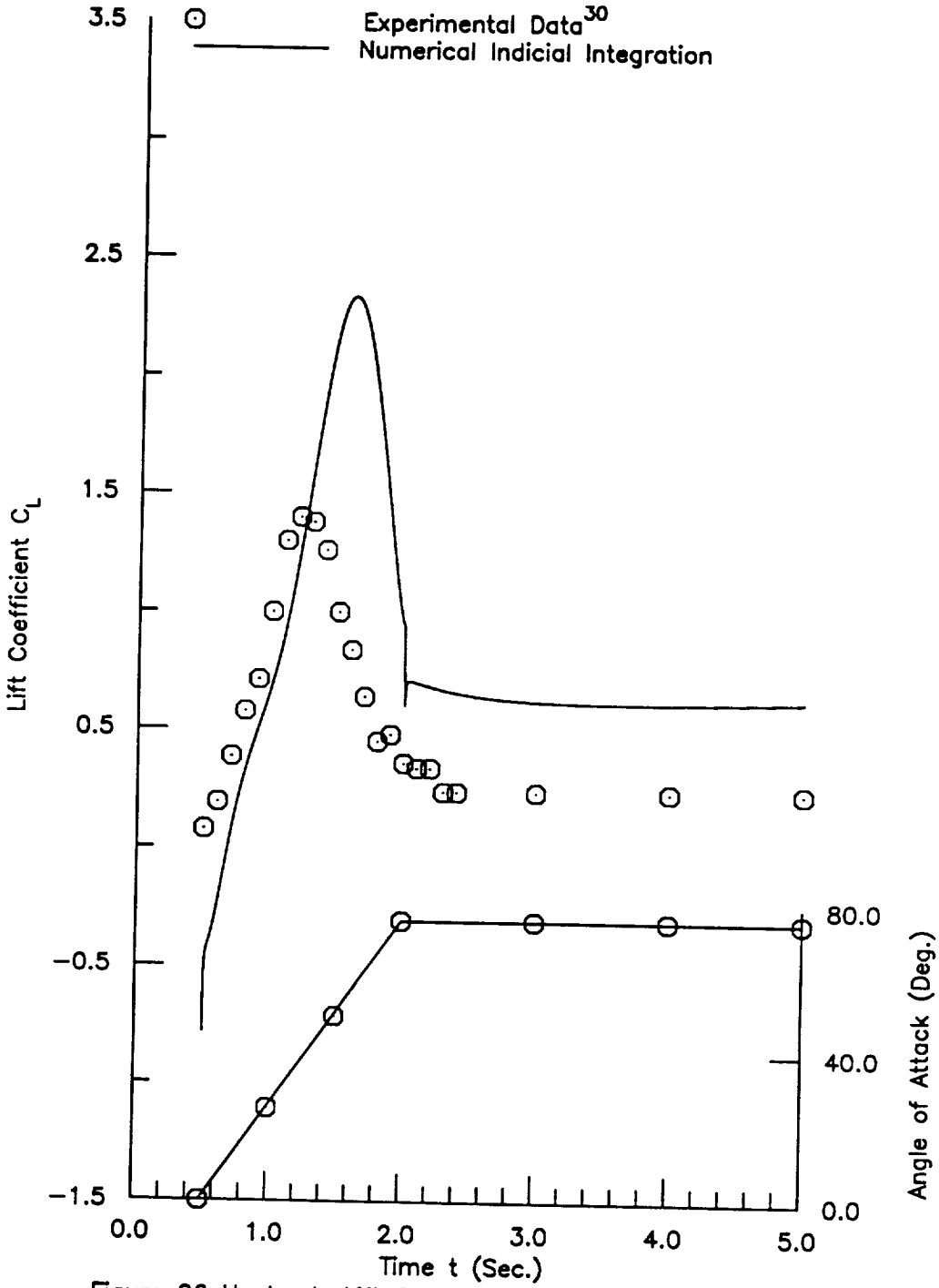

Figure 26 Unsteady Lift Coefficients from Indicial Lift Model and Experiment for a 70−deg Delta Wing in Harmonic Ramp Motion at Low Speed

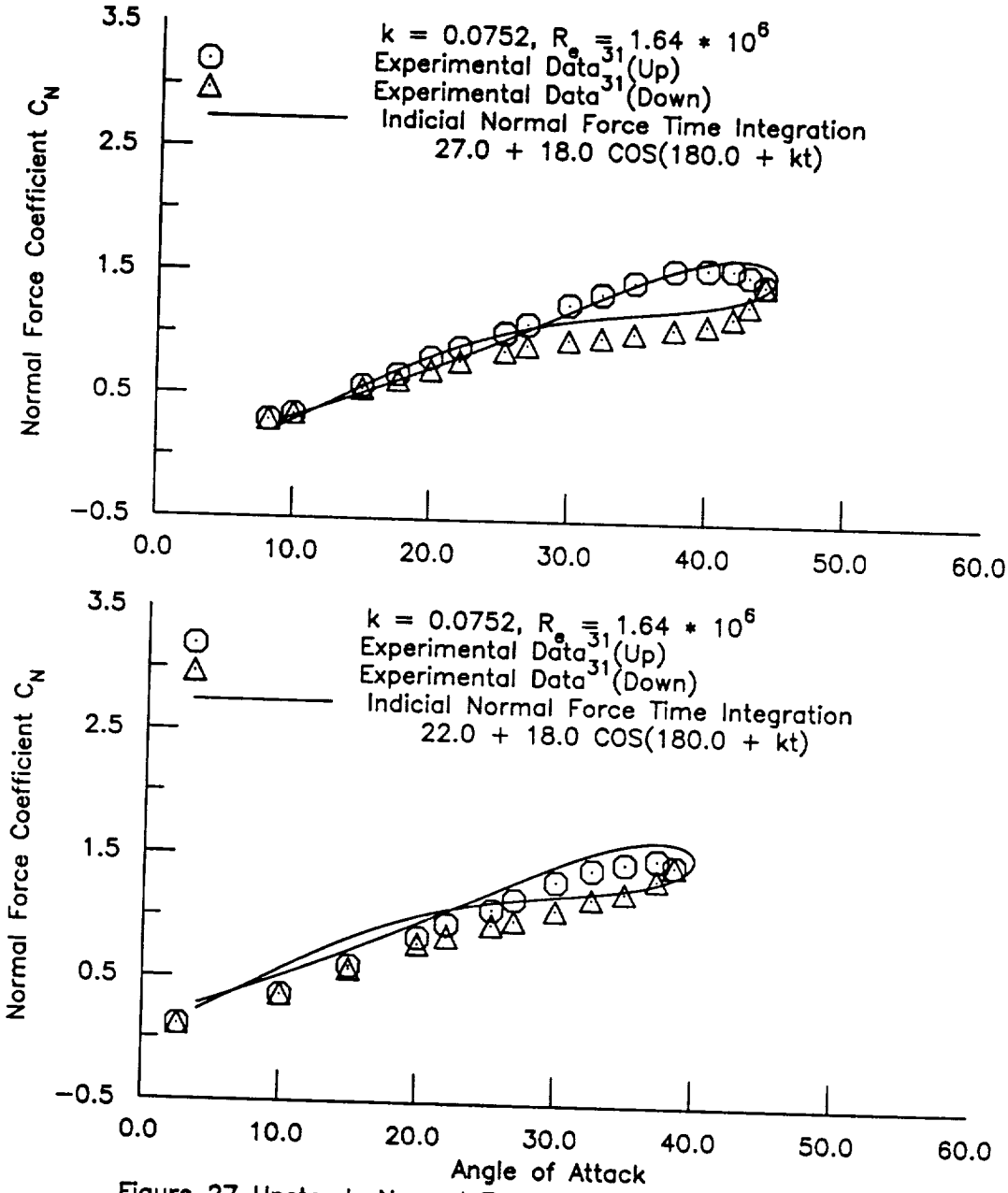

Figure 27 Unsteady Normal Force Coefficients from Indicial Normal Force Model and Experiment for a 70−deg Delta Wing at Low Speed and Various Mean Angles−of−Attack

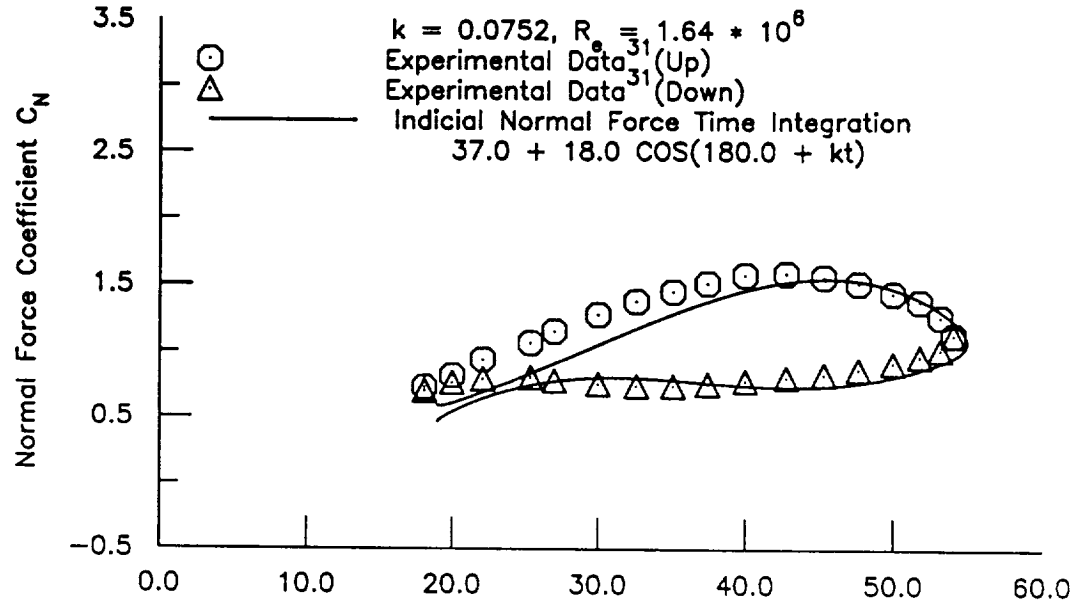

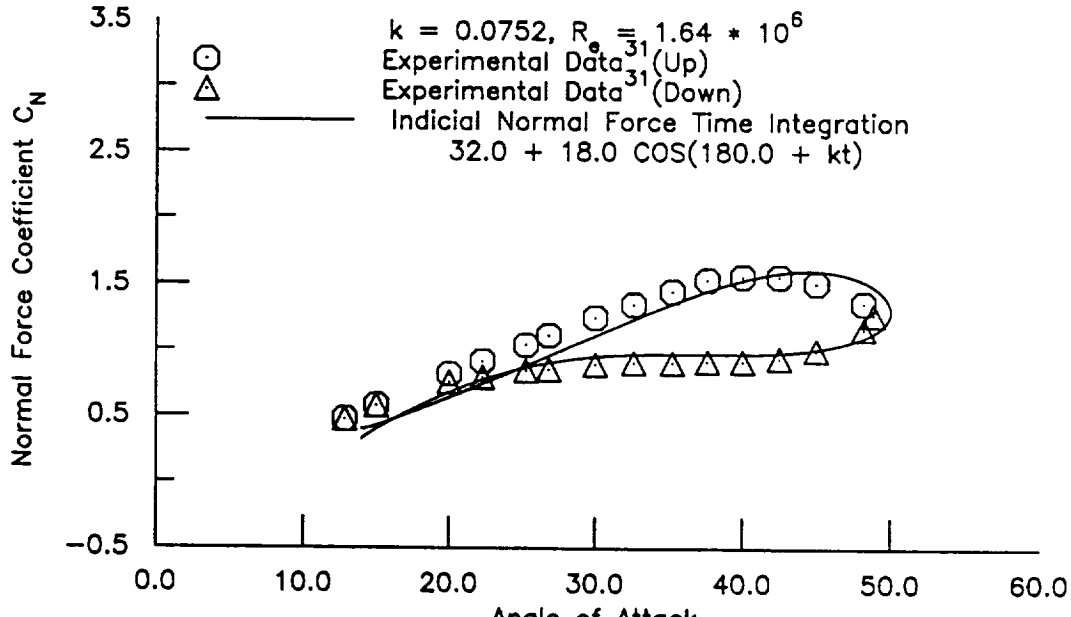

Figure 27 Concluded.

Table 1: Results for Linear Flow

2-D Linear Flow									
M	C_1	E_{11}	E_{21}	H_{11}	H_{21}	P_{11}	P_{21}	P_{31}	P_{41}
0.0	$2\pi/\beta$	0.5	0.0	1.0	0.4449	1.3170	0.2238	2.8422	0.0541
0.2	$2\pi/\beta$	0.3	0.0	1.0	0.6	0.0775	0.4196	0.1708	0.1322
0.4	$2\pi/\beta$	0.2651	0.2	1.0	1.4238	1.9738	0.3021	2.7280	0.0483
3-D Attached Flow									
M	C_1	E_{11}	E_{21}	H_{11}	H_{21}	P_{11}	P_{21}	P_{31}	P_{41}
0.0	1.6228	0.8	-0.4	1.0	0.7	0.3402	-0.007	5.6880	0.0009
0.2	1.5358	-1.0	-1.0	1.0	-0.3	-2.559	-0.088	1.3967	0.0009
0.4	1.4079	-0.8	-1.0	1.0	-0.3	-2.529	-0.208	1.1674	0.0009

$\beta^2 = 1 - M^2$

Table 2: Coefficients for C_L in Harmonic Motion

j	C_j	E_{1j}	E_{2j}	H_{1j}	H_{2j}	H_{3j}	H_{4j}	H_{5j}	H_{6j}
1	1.0	-0.3890	1.0617	0.7000	0.4626	none	none	none	none
2	1.0	0.2116	0.2500	-0.7000	0.5000	0.6000	none	none	none
3	1.0	-0.3683	0.1185	-0.9699	0.5337	0.9945	-1.0189	none	none
4	5.0	0.0250	-0.0625	-0.1000	0.4000	0.4000	1.0000	0.000	none
5	30.0	0.1855	0.0387	0.0961	0.5882	-0.0147	-0.0197	0.0009	0.0007
j	P_{1j}	P_{2j}	P_{3j}	P_{4j}	a_{1j}	a_{2j}	a_{3j}	a_{4j}	
1	-5.7882	-0.4526	5.5204	0.0297	-0.4021	-0.6464	-0.0374	-0.1437	
2	4.9467	-1.3874	15.2429	0.0010	-1.4369	1.7614	-0.0010	-0.0646	
3	3.5607	0.6534	4.3834	0.0406	0.8663	-0.0540	-0.0528	-0.1753	
4	24.4242	3.4119	21.3427	0.0010	3.5405	-2.3962	-0.0010	-0.0458	
5	6.1273	1.6037	1.2443	0.0248	1.5452	3.3789	-0.0256	-0.7780	

$C_{ave} = 0.6451$

Table 3: Coefficients for C_D in Harmonic Motion

j	C_j	E_{1j}	E_{2j}	H_{1j}	H_{2j}	H_{3j}	H_{4j}	H_{5j}	H_{6j}
1	1.0	-0.9559	-0.6614	0.3744	0.2473	none	none	none	none
2	1.0	0.3500	-0.2000	1.0	0.50	0.10	none	none	none
3	1.0	0.0178	-0.0855	0.3132	0.6458	0.0471	1.1550	none	none
4	1.0	0.3637	-0.0779	0.3273	1.2834	1.2561	-0.0228	-0.0165	none
5	15.0	-0.0525	-0.0163	0.1292	-0.1106	-0.0445	-0.0024	0.0010	0.0001
j	P_{1j}	P_{2j}	P_{3j}	P_{4j}	a_{1j}	a_{2j}	a_{3j}	a_{4j}	
1	-23.8955	-1.8567	7.2620	0.0043	-1.8712	-1.4193	-0.0044	-0.1333	
2	2.2992	1.2335	14.0822	0.0010	1.2674	-1.1041	-0.0010	-0.0700	
3	10.0916	4.2611	14.2989	0.0002	4.2885	-3.5827	-0.0002	-0.0697	
4	8.0642	1.9355	2.0652	0.0187	1.9340	1.9708	-0.0195	-4.6474	
5	5.5524	1.0617	7.3471	0.0284	2.0685	-1.3128	-0.0405	-0.0956	

$C_{ave} = 0.5113$

Table 4: Coefficients for C_m in Harmonic Motion

j	C_j	E_{1j}	E_{2j}	H_{1j}	H_{2j}	H_{3j}	H_{4j}	H_{5j}	H_{6j}
1	1.0	-1.2674	0.8828	-0.60	-0.6743	none	none	none	none
2	1.0	-0.5077	-0.3339	0.50	1.0376	0.9987	none	none	none
3	3.0	-0.3623	0.1131	0.1084	0.3632	0.9041	3.9701	none	none
4	10.0	-0.2541	0.0613	0.1581	0.70	0.40	0.00	0.00	none
5	10.0	-0.1987	0.03817	-0.7552	-0.9751	-0.9963	1.0089	0.0002	-0.0001
j	P_{1j}	P_{2j}	P_{3j}	P_{4j}	a_{1j}	a_{2j}	a_{3j}	a_{4j}	
1	0.8343	-0.2883	1.7085	0.03758	-0.3735	0.8618	-0.0404	-0.5449	
2	3.7401	0.9836	4.1175	0.05268	1.9091	-1.0008	-0.0772	-0.1656	
3	-7.5224	0.7289	3.9701	0.0366	1.6415	-3.5363	-0.0444	-0.2075	
4	-1.4207	1.0892	8.3962	0.0010	1.1094	-1.2786	-0.0010	-0.1181	
5	2.0289	1.0503	0.8991	0.0039	1.0498	1.2067	-0.0039	-1.1083	

C_{ave} = -0.3744

Table 5: Coefficients for C_N in Harmonic Motion

j	C_j	E_{1j}	E_{2j}	H_{1j}	H_{2j}	H_{3j}	H_{4j}	H_{5j}	H_{6j}
1	1.0	-1.0243	-0.3938	0.50	0.50	none	none	none	none
2	2.0	0.4337	0.2500	0.50	0.00	0.60	none	none	none
3	2.0	0.0339	0.0534	0.3322	0.3692	1.1193	-0.0587	none	none
4	15.0	0.025	-0.0625	-0.10	1.00	0.60	1.0	0.00	none
5	10.0	-0.1977	-0.0406	0.2942	0.0220	-0.0326	-0.0103	0.0018	0.0004
j	P_{1j}	P_{2j}	P_{3j}	P_{4j}	a_{1j}	a_{2j}	a_{3j}	a_{4j}	
1	-28.7136	-1.7155	9.4531	0.0049	-1.7368	-1.3006	-0.0052	-1.006	
2	14.7556	2.5230	15.4184	0.0010	2.5890	-1.6320	-0.0020	-0.0638	
3	14.2835	2.7413	18.0322	0.0010	2.8307	-2.0386	-0.0020	-0.0544	
4	12.6556	1.4290	13.1776	0.0010	1.4550	-0.4946	-0.0020	-0.0748	
5	-1.3764	1.2614	3.2283	0.02917	1.6546	-2.0809	-0.0326	-0.2772	

$C_{ave} = 0.8197$

Appendix A

Successive Fourier Analysis

The first step of "successive Fourier analysis" is to Fourier-analyze the response over one period. For simplicity, a Fourier series with three terms will be used to explain the procedure of the modeling. Then

$$C_L = A_0 + A_1 \cos\theta + A_2 \cos 2\theta + A_3 \cos 3\theta + B_1 \sin\theta + B_2 \sin 2\theta + B_3 \sin 3\theta \qquad \text{(A1)}$$

where

$$A_0 = \frac{1}{2\pi}\int_0^{2\pi} C_L \, d\theta$$

$$A_n = \frac{1}{\pi}\int_0^{2\pi} C_L \cos(n\theta) \, d\theta \qquad \text{(A2)}$$

$$B_n = \frac{1}{\pi}\int_0^{2\pi} C_L \sin(n\theta) \, d\theta$$

$n=1,2,3$ and $\theta=kt'$

Once the coefficients of A_0, A_n and B_n have been found, the next step is to split the coefficients into two groups by using the following formulas,

$$\cos n\theta = C(n,0)\cos^n\theta - C(n,2)\cos^{n-2}\theta \sin^2\theta + C(n,4)\cos^{n-4}\theta \sin^4\theta + \cdots\cdots\cdots\cdots$$

$$\sin n\theta = C(n,1)\cos^{n-1}\theta \sin\theta - C(n,3)\cos^{n-3}\theta \sin^3\theta - C(n,5)\cos^{n-5}\theta \sin^5\theta + \cdots\cdots\cdots\cdots \quad \text{(A3)}$$

where

$$C(n,m) = \frac{n!}{(n-m)!\ m!} \quad \text{and} \quad n! = 1*2*3*4******n$$

Therefore, the response of C_L becomes

$$\begin{aligned} C_L &= A_0 + A_1\cos\theta + A_2[\cos^2\theta - \sin^2\theta] \\ &\quad + A_3[\cos^3\theta - 3\cos\theta \sin^2\theta] \\ &\quad + B_1 \sin\theta + B_2[2\cos\theta \sin\theta] \\ &\quad + B_3[3\cos^2\theta \sin\theta - \sin^3\theta] \\ &= A_0 + [A_1 + A_2\cos\theta + A_3(\cos^2\theta - 3\sin^2\theta)]\cos\theta \\ &\quad + [B1 + 2B_2\cos\theta + B_3[3\cos^2\theta - \sin^2\theta]\sin\theta \\ &= A_0 + F(\cos\theta , \sin\theta)\cos\theta + G(\cos\theta , \sin\theta)\sin\theta \end{aligned}$$

Perform the Fourier analysis again for functions $F(\cos\theta , \sin\theta)$ and $G(\cos\theta , \sin\theta)$ by using Fourier series with the same terms as in the first

step. Then

$$F(\cos\theta,\sin\theta) = F_0 + FA_1 \cos\theta + FA_2 \cos2\theta + FA_3 \cos3\theta + FB_1 \sin\theta + FB_2 \sin2\theta + FB_3 \sin3\theta$$

$$G(\cos\theta,\sin\theta) = G0 + GA_1 \cos\theta + GA_2 \cos2\theta + GA_3 \cos3\theta + GB_1 \sin\theta + GB_2 \sin2\theta + GB_3 \sin3\theta$$

where

$$F_0 = \frac{1}{2\pi}\int_0^{2\pi} F\, d\,\theta \qquad G_0 = \frac{1}{2\pi}\int_0^{2\pi} G\, d\,\theta$$

$$FA_n = \frac{1}{\pi}\int_0^{2\pi} F\, d\,\theta \qquad GA_n = \frac{1}{\pi}\int_0^{2\pi} G\, d\,\theta$$

$$FB_n = \frac{1}{\pi}\int_0^{2\pi} F\, d\,\theta \qquad GB_n = \frac{1}{\pi}\int_0^{2\pi} G\, d\,\theta$$

$n = 1,2,3$

Using eq. (A3) again, then

$$F(\cos\theta,\sin\theta) = F_0 + FA_1 \cos\theta + FA_2 [\cos^2\theta - \sin^2\theta] + FA_3 [\cos^3\theta - 3\cos\theta \sin^2\theta] + FB_1 \sin\theta + FB_2[2\cos\theta \sin\theta] + FB_3 [3\cos^2\theta \sin\theta - \sin^3\theta]$$

$$G(\cos\theta,\sin\theta) = G_0 + GA_1 \cos\theta + GA_2 [\cos^2\theta - \sin^2\theta]$$

$$+ GA_3 [\cos^3\theta - 3\cos\theta \sin^2\theta]$$

$$+ GB_1 \sin\theta + GB_2[2\cos\theta \sin\theta]$$

$$+ GB_3 [3\cos^2\theta \sin\theta - \sin^3\theta]$$

Therefore

$$C_L = A_0 + \{F_0 + FA_1 \cos\theta + FA_2 [\cos^2\theta - \sin^2\theta]$$
$$+ FA_3 [\cos^3\theta - 3\cos\theta \sin^2\theta]$$
$$+ FB_1 \sin\theta + FB_2[2\cos\theta \sin\theta]$$
$$+ FB_3 [3\cos^2\theta \sin\theta - \sin^3\theta]\} \cos\theta$$
$$+ \{G_0 + GA_1 \cos\theta + GA_2 [\cos^2\theta - \sin^2\theta]$$
$$+ GA_3 [\cos^3\theta - 3\cos\theta \sin^2\theta]$$
$$+ GB_1 \sin\theta + GB_2[2\cos\theta \sin\theta]$$
$$+ GB_3 [3\cos^2\theta \sin\theta - \sin^3\theta]\} \sin\theta$$

All the terms associated with $\cos^n\theta$ on the right hand side of the above equation are divided by $(\alpha_0)^n$ and the terms associated with $\sin^n\theta$ are divided by $(-k\alpha_0)^n$. After rearrangement, the response of C_L becomes

$$C_L = A_0 + \{CC[0,0] + CC[1,0]\,\alpha + CC[2,0]\,\alpha^2 + CC[3,0]\alpha^3$$
$$+ DC[0,1]\,\dot{\alpha} + DC[1,1]\,\alpha\dot{\alpha} + DC[2,1]\,\alpha^2\dot{\alpha}$$
$$+ CC[0,2]\,\dot{\alpha}^2 + CC[1,2]\,\alpha\dot{\alpha}^2 + DC[0,3]\,\dot{\alpha}^3\}\,\alpha$$
$$+ \{CS[0,0] + CS[1,0]\,\alpha + CS[2,0]\,\alpha^2 + CS[3,0]\alpha^3$$

$$+ DS[0,1]\,\alpha + DS[1,1]\,\alpha\dot{\alpha} + DS[2,1]\,\alpha^2\dot{\alpha}$$

$$+ CS[0,2]\,\dot{\alpha}^2 + CS[1,2]\,\alpha\dot{\alpha}^2 + DS[0,3]\,\dot{\alpha}^3 \}\,\alpha \qquad \text{(A4)}$$

where

$$CC[n,m] = \frac{FA_{n+m}}{[\alpha_0^n\,(-k\alpha_0^m)]}, \qquad DC[n,m] = \frac{FB_{n+m}}{[\alpha_0^n\,(-k\alpha_0^m)]}$$

$$CS[n,m] = \frac{GA_{n+m}}{[\alpha_0^n\,(-k\alpha_0^m)]}, \qquad DS[n,m] = \frac{GB_{n+m}}{[\alpha_0^n\,(-k\alpha_0^m)]}$$

and the coefficients CC[n,m], DC[n,m], CS[n,m] and DS[n,m] are zeros for $n+m \geq 3$. Comparing with eq. (A1), it is obtained that

$$F_0 = A_0$$

$$F(\alpha, \dot{\alpha}) = CC[0,0] + CC[1,0]\,\alpha + CC[2,0]\,\alpha^2 + DC[0,1]\,\dot{\alpha} + DC[1,1]\,\alpha\dot{\alpha} + CC[0,2]\,\dot{\alpha}^2$$

$$G(\alpha, \dot{\alpha}) = CS[0,0] + CS[1,0]\,\alpha + CS[2,0]\,\alpha^2 + DS[0,1]\,\dot{\alpha} + DS[1,1]\,\alpha\dot{\alpha} + CS[0,2]\,\dot{\alpha}^2$$

Finally, collecting the same order terms together, then

$$C_L = A_0 + \{\, CC[0,0]\alpha + CS[0,0]\dot{\alpha} \,\}$$

$$+\{\, CC[1,0]\alpha^2 + DC[0,1]\alpha\alpha \quad +CS[1,0]\alpha\dot{\alpha} + DS[0,1]\,\dot{\alpha}^{\,2}\}$$

$$+\{\, CC[2,0]\alpha^3 + DC[1,1]\alpha^2\dot{\alpha} \;+ CC[0,2]\alpha\dot{\alpha}^{\,2} + CS[2,0]\alpha^2\dot{\alpha}$$

$$+DS[1,1]\alpha\dot{\alpha}^{\,2} + CS[0,2]\dot{\alpha}^{\,3}\,\} \qquad \text{(A5)}$$

Appendix B

Fourier Integration

of

Phase Function

By defining that $\psi_j(t')$ is the Fourier integration of phase function then

$$\psi_j(t') \equiv \frac{1}{2\pi\ i(jk)}\int_{-\infty}^{\infty} [1 - PD_j]\ e^{ijkt'}\ d(jk)$$

$$= \frac{1}{2\pi\ i(jk)}\int_{-\infty}^{\infty} [1 - \frac{P_{1j}(ik)^2 + P_{2j}(ik)}{P_{3j}(ik)^2 + ik + P_{4j}}]\ e^{ijkt'}\ d(jk) \qquad \text{(B1)}$$

$$= \frac{1}{2\pi\ i(jk)}\int_{-\infty}^{\infty} [1 - \frac{i(jk)\ a_{1j}}{i(jk) + ja_{3j}} - \frac{i(jk)\ a_{2j}}{i(jk) + ja_{4j}}]\ e^{ijkt'}\ d(jk)$$

By the characteristic of Fourier integral, the above equation can be inverted as

$$\frac{[1 - PD_j]}{i(jk)} = \frac{1}{2\pi}\int_{-\infty}^{\infty} \psi_j(t')\ e^{-ijkt'}\ dt' \qquad \text{(B2)}$$

$$= \frac{1}{2\pi}\int_{0}^{\infty} \psi_j(t')\ e^{-ijkt'}\ dt'$$

C-2

The low limit of the integral has been changed from negative infinity to zero due to the fact that there is no negative time. By introducing the new dummy variable r such that

$$r = i(jk)$$

then eq. (B2) becomes

$$\frac{[1 - PD_j(r)]}{r} = \frac{1}{2\pi}\int_0^{\infty} \psi_j(t') \, e^{-rt'} \, dt' \equiv \mathcal{L}\{\psi_j(t')\} \tag{B3}$$

Therefore, $\psi_j(t')$ is the inverse of the Laplace transform. i.e.

$$\psi_j(t') = \mathcal{L}^{-1}\left\{\frac{[1 - PD_j]}{r}\right\} = \mathcal{L}^{-1}\left\{\left[\frac{1}{r} - \frac{a_{1j}}{r + ja_{3j}} - \frac{a_{2j}}{r + ja_{4j}}\right]\right\} = 1 - a_{1j} \, e^{-ja_{3j}t'} - a_{2j} \, e^{-ja_{4j}t'} \tag{B4}$$

Appendix C

Newton's Method

for

Finding Phase and Reduced Frequency

As described in section 2.6, the governing equations for arbitrary motion are written as

$$F_1 = \alpha - \alpha_0 \cos(\phi + kt') = 0$$

$$F_2 = \alpha + \alpha_0 k \sin(\phi + kt') = 0$$

Let the Jacobian matrix be defined as

$$\begin{bmatrix} \frac{\partial F_1}{\partial k} & \frac{\partial F_1}{\partial \phi} \\ \frac{\partial F_2}{\partial k} & \frac{\partial F_2}{\partial \phi} \end{bmatrix} \qquad \text{(C1)}$$

where

$$\frac{\partial F_1}{\partial k}=\alpha_0 \sin(\phi + kt'), \qquad \frac{\partial F_1}{\partial \phi}=\alpha_0 \sin(\phi + kt')$$

$$\frac{\partial F_2}{\partial k}=\alpha_0 \sin(\phi + kt') + \alpha_0 k \cos(\phi + kt'), \qquad \frac{\partial F_2}{\partial \phi}=\alpha_0 k \cos(\phi + kt') \tag{C2}$$

The absolute value of the Jacobian becomes

$$\begin{aligned} |\text{Jacobian}| &= \frac{\partial F_1}{\partial k} * \frac{\partial F_2}{\partial \phi} - \frac{\partial F_1}{\partial \phi} * \frac{\partial F_2}{\partial k} \\ &= -\alpha_0^2 \sin^2(\phi + kt') \end{aligned} \tag{C3}$$

By Newton's method, the new values of unknowns k and ϕ are calculated as

$$\begin{bmatrix} k_{i+1} \\ \phi_{i+1} \end{bmatrix} = \begin{bmatrix} k_i \\ \phi_i \end{bmatrix} + \begin{bmatrix} \Delta k_i \\ \Delta \phi_i \end{bmatrix} \tag{C4}$$

where

$$\begin{bmatrix} \Delta k_i \\ \Delta \phi_i \end{bmatrix} = - [F_1 \quad F_2] * \frac{\text{Jacobian}^{-1}}{|\text{Jacobian}|} = - \frac{\begin{bmatrix} F_1 * \frac{\partial F_2}{\partial \phi} - F_2 * \frac{\partial F_1}{\partial \phi} \\ -F_1 * \frac{\partial F_2}{\partial k} + F_2 * \frac{\partial F_1}{\partial k} \end{bmatrix}}{|\text{Jacobian}|} \tag{C5}$$

The iteration will continue until both F_1 and F_2 reach 10^{-6}